THE STRATIGRAPHY AND METAMORPHISM OF THE SNYDER GROUP, LABRADOR

by

J. Alexander Speer

Dissertation submitted to the Graduate Faculty of the
Virginia Polytechnic Institute and State University
in partial fulfillment of the requirements for the degree of

DOCTOR OF PHILOSOPHY

in

Geological Sciences

APPROVED:

D. A. Hewitt, Chairman

J. R. Craig

L. Glover, III

M. C. Gilbert

P. H. Ribbe

S. A. Morse

April 1976

Blacksburg, Virginia

ACKNOWLEDGEMENTS

Field work and laboratory study for this research was supported in part by the Earth Sciences Section, National Science Foundation, NSF Grants GA-32124 and GA-41256X to S. A. Morse and GA-32267 and DES-22499 to D. A. Hewitt. The assistance of M. L. Hensley Dunn and A. R. Prunier in the field and D. A. Hewitt and S. A. Morse, as well as the other members of the advisory committee, J. R. Craig, M. C. Gilbert, L. Glover III, and P. H. Ribbe, for critically reviewing the manuscript, is appreciated.

TABLE OF CONTENTS

TABLE OF CONTENTS (continued)

Chapter 1

STRATIGRAPHY AND DEPOSITIONAL ENVIRONMENT OF THE SNYDER GROUP

Introduction

The Synder Group is a thin Proterozoic metasedimentary sequence, with minor intrusive rocks, that crops out on the coast of Labrador, Canada. It occurs within the central part of the Nain structural province as redefined by Taylor (1971) and lies between latitudes 57°04' and 57°10°N and longitudes 61°30' and 61°48'W. The rocks have undergone deformation and a deep seated contact metamorphism of the andalusite-sillimanite type as the result of the emplacement of the Kiglapait intrusion.

Wheeler (1942) first reported these rocks adjacent to the anorthositic rocks of the Kiglapait intrusion at the west end of the Kiglapait Mountains. Because of the well-preserved nature of the sedimentary features, the open folding of the group, and the lack of migmatites, Wheeler suggested that they were distinctly younger than the basement gneisses of the region. Morse (1961) first termed these rocks the Kiglapait Group, but they were subsequently renamed the Snyder Group (Morse, 1969).

The Snyder Group and Kiglapait intrusion lie at the north end of the Nain complex, the northern-most extent of the anorthositic and related rocks of the eastern Canadian Shield. The complex contains a series of rocks which range from anorthosites, troctolites, and norites to diorites and granites. Layered igneous intrusions, such as the Kiglapait intrusion, are numerous. The Nain complex is about 1.4 Gyr

(gigayears) old (Barton, 1974) and is bordered by granulites and gneisses of Kenoran age (2.6 Gyr; Barton and Barton, 1975).

Stratigraphy

General features

The greatest area of Snyder Group outcrop is on Snyder Island and in a narrow band up to 1.5 km wide on the adjacent mainland south southwest from Snyder Island as far as the Avakutakh River, a distance of 11 km (Figs. 1, 2). In addition, a series of tectonic fragments of the Snyder Group fringe the north shore of the Kiglapait Mountains as far east as Perry's Gulch (Umiakoviktannak), 12.5 km east of Snyder Island (Fig. 1). The largest of these is included in the more detailed geologic map of Figure 2 and contains the upper half of the lower quartzite, the iron formation, the quartzite marble, and fragments of the graphite-sulfide siltstone.

The Snyder Group is herein subdivided into five lithostratigraphic units that are defined for the first time. No formational names are proposed because of the lack of sufficient named geographic localities; alphabetical formational designations and informal lithologic names are used. The total thickness of the group is 239 m (785 ft.) and the Snyder Group outcrop is expanded to 355 m (1165 ft.) by intrusive rocks. In descending order the formations are as follows:

E formation:	upper quartzite	80 meters
D formation:	graphite-sulfide siltstone	14 meters
C formation:	quartzite marble	10 meters

Figure 1. Generalized geologic map of the northwest contact of the Kiglapait layered intrusion, Labrador.

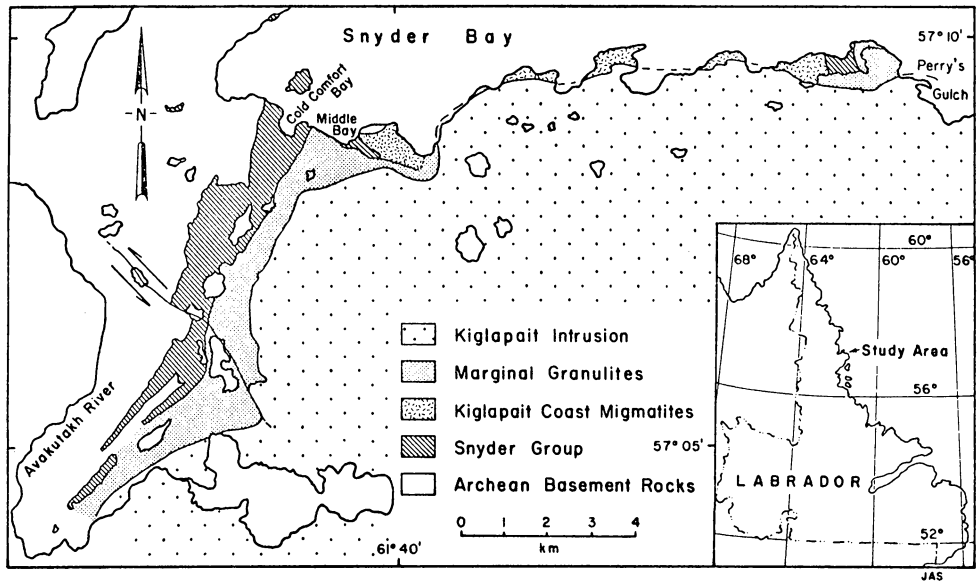
Snyder Bay
57° 10'
Perry's
Gulch
Cold Comfort
Bay
Middle
Bay
N
Avakutakh River
Kiglapait Intrusion
Marginal Granulites
Kiglapait Coast Migmatites
Snyder Group
Archean Basement Rocks
57° 05'
0 1 2 3 4
km
61° 40'
60°
68°
64°
60°
56°
Study Area
56°
LABRADOR
52°
JAS

B formation:	iron formation	15 meters
A formation:	lower quartzite	120 meters

The thicknesses are those of the three measured sections (X,Y,Z) located on Figure 3 and summarized in Figure 4. Measured sections are too few to ascertain the extent of any systematic regional change in thickness. Contacts between all formations are conformable, but an angular unconformity exists between the Snyder Group and Archean basement rocks, the Tikkegharsuk migmatites. All formations within the Snyder Group are apparently truncated by the marginal granulites of the Kiglapait intrusion.

Rocks of the lower quartzite are the most prevalent of the Snyder Group, occurring in all areas where the Snyder Group crops out. The presence of intrusive rocks has expanded the lower quartzite stratigraphic outcrop by 36 m to 156 m on section X. The next two younger formations, the iron formation and quartzite marble, occur in the core of a syncline on the east side of Snyder Island and on the west side of Cold Comfort Bay. They continue inland from the head of Cold Comfort Bay to an area 5 km south of Snyder Island. They are also exposed for a short distance on either side of the valley produced by the erosion of the Koghukulluk dike at the southern end of the Snyder Group. Smaller outcrops occur in the tectonic fragments of the Snyder Group along the north shore of the Kiglapait Mountains. Exposures on the west headland of Cold Comfort Bay contain an excellent exposure of the transition from lower quartzite to iron formation. The least weathered outcrops of quartzite marble are exposed in Cold Comfort Bay at low tide. The two uppermost formations, the

the graphite-sulfide siltstone and upper quartzite, extend from the east shore and bottom of Cold Comfort Bay inland to the area of 5 km south of Snyder Island. Locally, the graphite-sulfide siltstone is present in the tectonic fragments along the coast. Along its entire length, it is extensively intruded by dikes of mafic and ultramafic composition.

A formation, the lower quartzite

The lowermost formation of the Snyder Group consists of interbedded quartz arenite, arkosic arenite, metapelite, and quartz pebble conglomerate. Pebbles and cobbles of quartz monzonite and potassium feldspar are present in the conglomerate at or near the base of the formation, overlying with angular unconformity the Tikkegharsuk migmatites. The unconformity surface has up to 0.5 m of relief. The basal conglomerate is thin (10-15 cm), but persistent. It has a sandy matrix similar to overlying quartz arenite, with which it has a transitional contact, and is colored by biotite or chlorite. Conglomerate of two types also occurs at stratigraphically higher levels in the lower quartzite (Fig. 4): (1) quartz cobbles and pebbles in a pelitic matrix of quartz + micas + cordierite $\pm$ garnet $\pm$ orthopyroxene; and (2) the much less common occurrence of quartz pebbles with a finer matrix of originally coarse sand.

The fine- to coarse-grained quartzite consists of dominant, well-sorted, white quartz arenite with subordinate arkosic arenite common in the lower members. They are commonly spotted by 1-2 cm diameter concentrations or poikiloblasts of garnet, orthopyroxene, andalusite, micas, chlorite or cordierite, forming the spotted quartzite of Morse (1969). Where andalusite is unstable, clusters of sillimanite occur. Locally,

bands or veins of the stable aluminum silicate polymorph occur. In lower grade rocks, green quartzite is present, colored by amphibole, epidote or green biotite.

Two types of metapelites occur in the *A* formation. The most common type is composed of Al_2SiO_5 polymorphs, potassium feldspar, white mica, chlorite or cordierite, and can be distinguished by its pink to grey color, prominent slaty cleavage, and ease of weathering. This is the aluminous gneiss of Morse (1969). Subordinate amounts of a quartz-biotite-muscovite-garnet-cordierite $\pm$ orthopyroxene metapelite occur and show relict sedimentary textures.

Well-defined sedimentary bedding is common. Torrential crossbedding is abundant throughout the formation and has attitudes that indicate the direction of sedimentary transport was from the south. Trough crossbedding, occurring as festoons cut into previously deposited material, is common. Graded bedding, expressed by one less coarse grade in each successive increment upwards, is characteristic of the conglomerates and occasionally is present in the quartzites on a fine scale (5-10 cm). The graded bedding shows tops toward the east on the mainland and southeast on Snyder Island. Graded crossbedding, in which pebbles are aligned parallel to inclined strata and are increasingly coarser or more abundant down the length of the cross bed, is rare. It is in this type of bedding that heavy mineral layers composed of zircon, magnetite, and ilmenite are most commonly seen. The aluminous metapelites contain fine-grained, crossbedded quartzite lenses. Oscillation ripple marks preserved on the tops of a few beds have strike directions indicating

that the current by which they originated moved north-south. Individual amplitudes are less than 2 cm and wavelengths range from 3 to 15 cm.

Larger, symmetrical, ripple-like features with wavelengths of 30-60 cm and amplitudes of 3-6 cm occur on Snyder Island and the adjacent mainland. Each is overlain by a metapelite, suggesting that it may be a fold or compaction feature that forms at the surface separating two beds of unlike viscosity.

Individual beds of the lower quartzite are usually less than 1 m thick but nevertheless are quite extensive. One conglomeratic member can be traced from the coast of Snyder Bay southwestward a distance of 4 km. This particular member can be identified by its consistent occurrence just below the top of the lower quartzite, common occurrence of graded crossbedding, and presence of quartzite cobbles as well as quartz pebbles and cobbles.

B formation, the banded iron formation

The iron formation is a distinctive 15-20 m thick, brown colored unit lying stratigraphically above the lower quartzite. It consists of 1-30 mm bands of tan to white quartzites with minor iron silicates alternating with dark bands consisting largely of iron silicate with subordinate quartz. Three massive, tan quartzites up to 1.5 m thick occur in the iron formation. They consist of abundant quartz with a homogeneous distribution of iron silicates. They also contain fragments of bedded iron formation, a feature which is discussed below. About half a meter below the rhythmic banding of the iron formation there are dark pods consisting solely of orthopyroxene and grunerite in a medium-grained,

crossbedded quartzite. The pods are elongate, up to 1 m in length, and are 6-15 cm thick. The base of the iron formation (*B* formation) is defined by the appearance of these pods.

The most common iron silicates identified in thin section and by microprobe analyses in the *B* formation are inverted pigeonite (a mangonoan, calcian ferrohypersthene) and spessartine-almandine garnet. Manganoan grunerite, hornblende, manganoan hedenbergite, and biotite are also present. Accessory minerals include plagioclase, tourmaline, graphite, carbonate, pyrite, pyrrhotite, and ilmenite. Secondary iron and manganese oxides and hydroxides occur.

Microfaulting, contorted bedding, slump structures, and intraformational conglomerates of iron formation fragments are present. Most microfaults die out in a short distance and are thought to be of compactional origin, but a few are undoubtedly tectonic. Some folds are drag folds related to the formation of major synclines and anticlines. Other folds resulted from soft sediment deformation and occur in beds with a profusion of minor folds overlain and underlain by undeformed beds of similar lithology from which they are separated by decollement or erosional surfaces. The axial planes are at high angles to the major fold planes, unlike the drag folds. Rip-up clasts of the more quartz-rich layers varying from 10 to 50 mm in size occur at the base of the several massive quartzite beds. Embedded within these quartzites are large blocks, up to 40 cm, of highly contorted banded iron formation. Sedimentary features of a smaller scale than the fine banding have not survived metamorphic recrystallization.

C formation, the quartzite marble

The next youngest formation consists of quartz arenites interbedded with calcite marbles and calcsilicate rocks ranging from beds of marble to as much as 1 m thick with thin beds of quartzite to nearly massive quartzites with local pods of marble or calcsilicate rock. The marbles contain calcite, forsterite, and phlogopite with subordinate amounts of dolomite, spinel, chlorite, tremolite, diopside, titanite, graphite, and pyrrhotite. Local aggregates of apatite are found. Periclase, now pseudomorphed by brucite, was developed at high grades of metamorphism. The tan weathering marble is blue grey in color when fresh but took on a green color with serpentinization of the olivine. The pale green calcsilicate rocks and white quartz arenites contain differing proportions of quartz, tremolite, diopside, and phlogopite with local calcite, plagioclase, potassium feldspar, and epidote. Enstatite occurs in rocks of very high grade.

Fine-scale crossbedding of alternating layers of quartz and diopside or tremolite is present in the calcsilicate lenses suggesting that some of the original carbonate material was mechanically reworked. No other primary structures have been observed.

The iron formation contains some green, lime-rich bands below the contact with the quartzite marble. The mineralogy is characteristic of both formations and includes a manganoan chrysolite. However, the base of the *C* formation is placed where the fine banding of the *B* formation gives way to the massive bedding of the quartzites and marbles. Toward the top of the quartzite marble there are numerous lenses of graphite-

and sulfide-bearing hornfelses, similar to the rocks of the overlying *D* formation. The top of the *C* formation is taken at the first appearance of continuous beds of these hornfelses. There may be some variation in the member taken as the base of the *D* formation, but because the transition is small this is not a serious problem. The quartzite marble is 10 m thick in the Y section although it appears to vary laterally. The formation is expanded by tectonic thickening of the marbles in folds.

D formation, the graphite-sulfide siltstone

Within the upper 2 m of the quartzite marble occur lenses of sulfide- and graphite-bearing hornfelses that grade upward into a massive hornfels 14 m thick, interbedded with sporadic 2-3 cm layers of originally silt or fine-grained sand. The abundant graphite, dark color, and fine grain size are the features of this formation noted by Wheeler (1942). Petrographically the *D* formation is a fine grained, graphite- and sulfide-bearing quartzite with subordinate aluminum silicates, cordierite, biotite, muscovite, potassium feldspar, and plagioclase. The finely laminated hornfels is black when fresh and contains andalusite, sillimanite, cordierite, cummingtonite, and biotite porphyroblasts wherever the appropriate bulk composition is present. Abundant pyrrhotite, pyrite, and sphalerite with exsolved chalcopyrite occur as disseminated grains and in small veins. At high grades of metamorphism, the abundant graphite is recrystallized coarsely enough to define a weak schistosity parallel to bedding. The rocks of the *D* formation weather to a red-brown color, because of a thin gossan of secondary iron oxides

and hydroxides. Patches and streaks of pale yellow due to secondary sulfate minerals occur in moist areas.

E formation, the upper quartzite

The youngest formation of the Snyder Group consists of a sequence of quartzites. The base of the formation appears to grade transitionally up from the underlying graphite-sulfide siltstone. The quartzites are spotted with poikiloblasts of aluminum silicates, cordierite, biotite, and orthopyroxene. Rare pelitic rocks contain the chiastolite variety of andalusite. Locally arkoses are present. Disseminated sulfides, mainly pyrrhotite, sphalerite, and chalcopyrite, give the rocks a yellow brown to red brown color when weathered although the rocks are grey on freshly broken surfaces. Other minerals present include potassium feldspar, plagioclase, muscovite, and subordinate amounts of spinel, tourmaline, graphite, and ilmenite. Bedding is on the order of 10-50 cm thick and locally crossbedding is evident.

The upper quartzite is extensively injected by sills and dikes of basic rocks, half of its outcrop thickness of 160 m resulting from thickening by basic sills.

Depositional Environment

Several lines of evidence indicate that the lower quartzite had a shallow marine origin and was subject to much reworking by tidal currents and storms. (1) The very common trough and festoon types of crossbedding imply a confined unidirectional current flow characteristic of tidal, distributary, or fluvial channels. (2) The overwhelming

proportion of clean, well sorted quartz arenite in the section suggests a continually active, intensive sorting mechanism more efficient than might be expected in fluvial or distributary environments. (3) The continuous nature of the relatively thin beds over a distance of several kilometers also implies an unrestricted environment. (4) Frequent current action alternating with slack water and sediment reworking is also indicated by abundant crossbedding, ripple marks, graded bedding, and local flaser bedding. The several types of crossbedding that occur are torrential, trough, festoon, and low-angle planar crossbeds. Coarse material occurs associated with fining upwards sequences. (5) The maturity of sediments gradually increases upward, as reflected in the decrease of arkosic arenite upward from the basal members. This could be either a provenance control or a progressive increase in the duration of sediment transport or reworking. Considering the abundant potassium feldspar of the Archean basement rocks, the latter seems more probable.

The mineralogy, sedimentary textures, and extent of the two types of conglomerate suggest differing origins. The impersistent extent of the conglomeratic sandstone in lenticular beds with well-rounded pebbles suggests deposition of coarse, locally derived material in a restricted high energy environment. This may represent lateral or upward channel shifting. The persistent lateral extent of the thicker conglomeratic mudstones may be ascribed to the occasional influx of large amounts of coarser and muddier clastics. The numerous examples of upward fining cycles in these conglomerates are indicative of the waning of storm waves or flooding by the source.

The unusual composition of the aluminous metapelites and their sharp contacts are difficult to interpret. They are found throughout the lower quartzite. The lenticular bedding in which the isolated ripples are crossbedded implies an original fine grain for the majority of the sediment, and reworking by currents to winnow out the sand-size particles. They must have been covered or lithified relatively soon after deposition to protect them from the normally high energy environment of the lower quartzite. The lenticular bedding is a common feature of tidal and subtidal environments. It is uncertain whether the composition is originally detrital or caused perhaps by diagenesis of fine-grained clastic feldspars. Similar aluminous sediments in quartzites, containing gibbsite and kaolinite, have been reported by Chandler *et al.* (1969) who favored the latter interpretation for their rocks. The less aluminous pelites are scarce and their lenticular shape and sedimentary features indicate they were deposited in shallow depressions protected from current action.

The appearance of the iron formation - carbonate - siltstone sequence marks the advent of much quieter sedimentation. The fine lamination preserved in the iron formation and siltstone point toward a significant lack of current activity due either to a water depth below wave base or to a protected sedimentary environment. The area was prone to periodic disturbances as shown by the subaqueous slumping, rip-up clasts, and chaotic bedding of the iron-formation and crossbedding in the quartz marble. The slump and flow structures could be caused either by an unstable slope or by rapid current flow. However, their association with rip-up clasts and homogeneous beds containing blocks and pieces of

highly contorted, banded iron formation clearly records episodes of intraformational erosion and subsequent deposition. Such erosion would rework the unconsolidated iron formation into homogeneous rocks containing fragments of the more consolidated bands. The wide extent of these features points toward waves and currents generated during storms. It is thought that these formations represent sedimentary deposition in a protected environment infrequently reached by storms.

The exact implication of this sequence of quiet water sediments is unknown but some mutual relationship must exist because the contacts between the formations are very gradational. This led to sedimentary rocks and their metamorphic equivalents of unusual intermediate compositions. Even the lower quartzite clastic sedimentation and the largely chemical sedimentation of the iron formation must have overlapped. The contact between them shows medium-grained, crossbedded quartzites with pods of iron-manganese silicate minerals in what appear to be depositional troughs, indicating that the iron and manganese deposition process began early and the iron-manganese sediments were reworked during clastic sedimentation.

Considering the preservation of iron oxide minerals in other metamorphosed iron formations (Klein, 1973), the lack of these minerals in the Snyder Group iron formation would imply that it originally consisted largely of hydrated iron and manganese silicate minerals. No evidence was observed in the carbonate rocks to indicate whether they are biologic or chemical in origin. The graphite-sulfide hornfels was largely a clastic siltstone. The abundance of graphite in the formation would suggest that the site of deposition was nonoxidizing. The metal

sulfides of the *D* and *E* formation are thought to be synsedimentary because of their stratigraphically limited occurrence. Richard (1973) outlined the optimum site for synsedimentary sulfide deposits as organic-rich, fine-grained sediments with a contemporary volcanic association to act as a metal source. These conditions are met for the graphite-sulfide hornfels and to a lesser extent by the upper quartzite. The very presence of the sulfides attests to a source; whether it is associated with a particular igneous rock as a product of the aforementioned volcanic association or is nonvolcanic is speculative.

The reappearance of quartzites in the uppermost part of the Snyder Group indicates a return to more abundant sandy sediment supply and deposition. The crossbedding implies current activity.

In summary, the Snyder Group represents Proterozoic tidal or subtidal deposition, on an Archean basement, of largely quartz arenites with basal arkosic arenites. Rarely, pelitic compositions were also deposited and preserved. The high energy environment eventually gave way to quieter sedimentation manifested by the thin sequence of iron formation, carbonates, and graphitic siltstone. Subsequently, there was a return to coarser clastic sedimentation. Most of the outstanding sedimentary features preserved in the rocks were caused by reworking of the sediments by tidal currents or storm waves. Because the sedimentary rocks are a relatively thin sequence of shallow water sediments dominated by mature quartz arenites, it is suggested that the Snyder Group is a platform assemblage.

Intrusive Rocks

Five predeformational intrusive rocks have been distinguished in the immediate vicinity of the Snyder Group: the Snyder breccia, the Hill 1300 N amphibolite, the Hill 1100 gabbro, the Hill 800 ultramafic dike, and some metadiabases. The Snyder breccia is chemically a granodiorite (Barton and Barton, 1975) and it very closely corresponds in composition to an average Cenozoic andesite (Chayes, 1975). It is present as dikes and sills cutting both the Snyder Group and, to a lesser extent, the basement just below the basal contact and on the Tikkegharsuk Peninsula. It is characterized by a fine grain size, a light grey color, numerous angular and subrounded xenoliths of basement rocks, and locally by Snyder Group quartzite xenoliths. At low metamorphic grades, an original porphyritic texture is locally evident. At high grades of metamorphism a tan-colored metabasite containing xenoliths and large poikiloblastic pyroxenes is thought to be equivalent to the Snyder breccia.

The Hill 1300 N amphibolite (Fig. 2) appears to be a 10-15 m thick sill that has been intruded along the Snyder Group basement unconformity. It strikes roughly north-south and dips to the east at about 30°. The rock is uniformly coarse-grained and black in color. The metamorphic assemblage is hornblende and plagioclase with minor clinopyroxene and biotite.

The Hill 1100 gabbro (Fig. 2) is a locally discordant sill that truncates the lower stratigraphy at the southern end of the Snyder Group. At first glance the Hill 1100 gabbro appears to be a

coarse-grained, subophitic gabbro to leuconorite similar to many others of the Nain complex. Closer examination shows the minerals to be recrystallized and mimicking the original igneous textures. The present assemblage is plagioclase and hornblende with minor, and perhaps relict, orthopyroxene and clinopyroxene. Rarely is the core of a plagioclase megacryst not recrystallized. It is thought that this large dike was intruded into the country rocks as part of one of the gabbroic intrusions immediately to the south of the Snyder Group and that it was later metamorphosed by the Kiglapait intrusion with water introduced from the enclosing sedimentary rocks.

The Hill 800 ultramafic dike (Figs. 2, 3) is a Y-shaped dike that extends from the bottom of Cold Comfort Bay south under the hill and reappears on the other side. The metamorphic assemblages are olivine + orthopyroxene + cummingtonite, cummingtonite + orthopyroxene, and quartz + cummingtonite + orthopyroxene. The subordinate minerals are biotite, plagioclase, clinopyroxene, hornblende, and spinel. A faint layering and the diverse metamorphic mineral assemblages that occur over short distances within the dike are probably indicative of an original igneous layering. This dike may be related to the ultramafic dike mentioned by Berg (1974).

Lastly, there are a few metadiabase dikes of small size (less than 1 m thick) and extent, several of which are mapped in Figure 3.

The Snyder Group is intruded by a large variety of postdeformational igneous rocks. By far the most significant is the Kiglapait intrusion, a large layered intrusion of probable lopolithic form, described by Morse (1961, 1969) and the subject of other detailed studies

(Berg, 1971; Speer, 1973; Davies, 1974; Shirey, 1975). It acted as the heat source for much of the metamorphism and as the major cause of deformation of the Snyder Group. Between the Snyder Group and Kiglapait intrusion is a band of basic granulites mapped as the Outer Border Zone (OBZ) of the Kiglapait by Morse (1961, 1969). It is this unit that truncates the stratigraphy of the Snyder Group. Wheeler (1968) termed these and similar rocks at the margins of other Elsonian plutons as marginal granulites of uncertain origin. Arguments have been gathered for both igneous and metamorphic origins for these rocks.

The discussion has been intensified by Berg's (1974) discovery that a part of the OBZ consists of metasedimentary rocks that he assigns to an entirely new group overlying the Snyder Group. The mafic granulites are postulated to be metamorphosed hypabyssal sills and lava flows. This proposed group would occur above an erosional unconformity with the Snyder Group.

An interpretation favored here is that the basic granulites represent contamination of the basic magma by the country rocks as proposed by Wheeler (Morse, 1969) and similar to the model of Gribble and O'Hara (1967) for the development of partially melted country rocks associated with the basic gabbros and norites of north-east Scotland. Gribble and O'Hara envision intrusion of a basic magma into pelitic and granitic rocks leading to contact metamorphism and to partial melting of the country rocks adjacent to the intrusion. The basic magma near the contact would become contaminated by incorporation and digestion of the country rock, assimilation causing more rapid consolidation of the

contaminated magma. At some distance from the contact, the basic magma would crystallize unaffected by the events at its border.

This interpretation satisfies several features: (1) the chemical and petrographic evidence of Morse (1961, 1969) and Berg (1971) pointing to the igneous origin of the basic granulites; (2) the rather small volume of metasedimentary rocks and their discontinuous nature in the OBZ; (3) the continuous, even layering in the OBZ whereas the underlying Snyder Group east of Middle Bay has been faulted into a jumble of large and small blocks; (4) the fact that the contact of the Snyder Group with the OBZ does not represent a metamorphic maximum; and (5) the association of similar marginal granulites between the anorthositic plutons and granitic and pelitic country rocks locally around the Nain complex without the association of either of the Proterozoic metasedimentary groups.

Along the contact of the Snyder Group with the marginal granulites of the Kiglapait intrusion are several elongate bodies of igneous breccia which are in part the intermediate rocks mapped by Morse (1969). The matrix is cordierite-bearing granodiorite although some have quartz gabbro matrices. The xenoliths are upper quartzite of the Snyder Group, metabasites, and what appear to be border zone rocks of the Kiglapait intrusion. In the field the matrix of the border breccias appears texturally similar to the rocks of the upper quartzite. They can be most easily distinguished by the larger biotites of the granodiorites (5 mm as opposed to 2 mm) and the presence of xenoliths in larger outcrops. These border breccias may represent anatectic melts originating at

deeper levels that have migrated upwards along the Snyder Group-OBZ contact, as was similarly postulated by Morse (1969).

Other post-deformational rocks include cordierite- and andalusite-bearing granitic pegmatites on Snyder Island and the adjacent mainland; a granitic dike that crops out sporadically in an arc from the eastern head of Cold Comfort Bay inland about 2 km; and local diabase dikes. The most notable of the latter is the Koghukulluk dike, although no dike rock is evident in that part of the linear feature which contains the dike and extends into the Snyder Group.

Structure

The Snyder Group envelops the northwest corner of the Kiglapait intrusion in the form of a syncline gently plunging to the southeast with its core occupied by part of the intrusion. The core of the syncline would coincide with the trough between the north Tessialua and Wendy Bay radial ridges in the floor of the Kiglapait intrusion mentioned by Morse (1969). The eastern limb of the fold is poorly developed, the majority of the Snyder Group lying in the western limb. The western limb is elongate and is essentially a monoclinal sequence which strikes N 20 E and dips about SE 20-30° beneath the Kiglapait intrusion (Figs. 2, 5). The stratigraphy is eventually cut off by the Hill 1100 gabbro and the marginal granulites of the Kiglapait intrusion in a series of xenoliths and blocks (Figs. 1, 2). The tectonic blocks of the Snyder Group along the north coast of the Kiglapait Mountains east of Middle Bay (Fig. 1) represent the stringing out of the eastern limb. They are embedded in Tikkegharsuk migmatites which have been

Figure 5. Cross-sections perpendicular to strike on the Snyder Group from north (B-B') to south (E-E'). Lines of section are located on Figure 2. Symbols are the same as those of Figure 2.

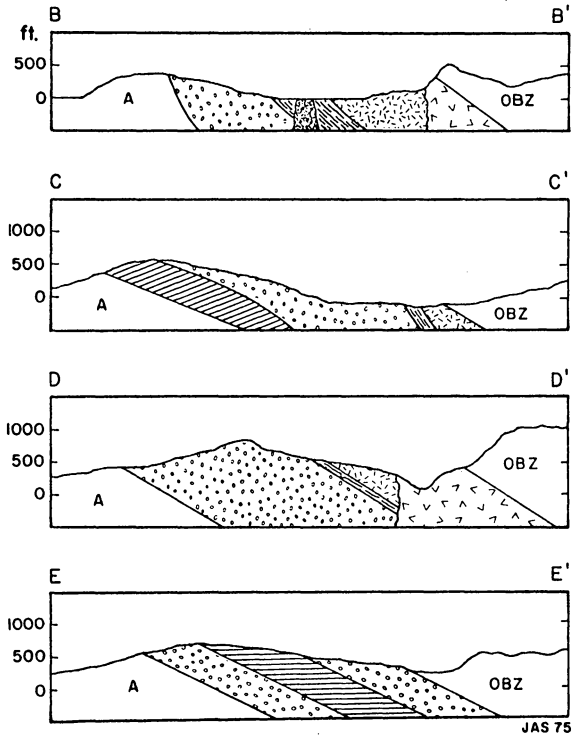
B
B'
ft.
500
0
A
OBZ
C
C'
1000
500
0
A
OBZ
D
D'
1000
500
0
A
OBZ
E
E'
1000
500
0
A
OBZ
JAS 75

anatectically rejuvenated in the contact aureole of the Kiglapait intrusion. They later were termed the Kiglapait Coast migmatites by Speer (1974) and were mapped as intermediate gneiss by Morse (1969), who similarly concluded that they were of rheomorphic origin. Small, upright, open folds within the syncline gently plunge nearly parallel to the major fold axis. These smaller folds are abundant in the trough of the syncline beginning on the west shore of Cold Comfort Bay and fanning around to the east side of Snyder Island (Fig. 3). The formational contacts undulate as they change to a more easterly strike.

There is a single large fault halfway along the west limb (Fig. 2). The left-lateral displacement amounts to 0.6 km on the Snyder Group and the fault plane is vertical. The fault occupies a northwest-southeast linear evident on air photographs, running from Laura Lake (61°55'W, 57°11'N) to Kiglapait Tessialua (61°42'W, 57°05'N). The fault does not appear to displace the Koghukulluk dike but may displace the marginal granulites of the Kiglapait intrusion (Berg, pers. comm.). Numerous other small faults with negligible displacement, on the order of 1-5 m, occur throughout the Snyder Group. These faults involve breakage of the more competent quartzite beds where they have slipped over the less competent pelitic beds during folding.

The deformation of the Snyder Group can be attributed almost entirely to the emplacement of the Elsonian plutons, the Kiglapait intrusion in particular. This does not preclude some gentle deformation during the Hudsonian orogeny but does argue against any significant deformation.

Age and Correlation

The Snyder Group unconformably overlies metamorphosed rocks of Archean age. K-Ar age dates for the metamorphism of the Archean rocks in the Nain province yield ages of 2.0 to 2.7 Gyr and average 2.3 Gyr (Taylor, 1972) denoting recrystallization during the Kenoran orogeny. Barton and Barton (1975) found a K-Ar age on hornblende of 2.6 Gyr within 15-20 km of the Snyder Group. The Snyder Group was intruded by the Snyder breccia after deposition and later by intrusive rocks of the Nain complex. The age of the Snyder breccia by Rb-Sr methods is 1.84 Gyr (Barton and Barton, 1975). The isotopic age of the Elsonian plutons of the Nain and Churchill provinces is 1.4 Gyr for the anorthosites (Emslie, 1964) and from 1.1 to 1.3 Gyr for the associated adamellites (Taylor, 1971; Barton, 1973; Krogh and Davis, 1973). The Kiglapait intrusion remains undated; however, K-Ar age dates of 1.48 Gyr for a border breccia and 1.1 Gyr for the Manvers granite (Beall *et al.*, 1963; Morse, 1969) are obtained for these igneous bodies cutting its margins. A Rb-Sr age of 1.27 Gyr has been obtained for the Manvers granite by Barton (1973). A K-Ar age of 1.28 Gyr on the Snyder breccia (Barton and Barton, 1975) dates the end of the metamorphism and is consistent with the dates on the igneous rocks. These radiometric ages would indicate that the deposition of the Snyder Group occurred after the Kenoran orogeny and before 1.84 Gyr for an Aphebian or Lower Proterozoic age (Stockwell, 1973). Its metamorphism by the Elsonian plutons would have begun at about 1.4 Gyr and would have dropped below a temperature low enough to prevent any significant argon loss at 1.28 Gyr.

In defining the Baffin Geosyncline in the northeastern Canadian Shield, Jackson and Taylor (1972) outlined a large central miogeosynclinal or shelf zone between the two enclosing mio-eugeosynclines, the Committee and Circum-Ungave Fold Belts. The Snyder Group would lie on the southern extension of this central zone on the coast of Labrador largely unaffected by the Hudsonian orogeny. Jackson and Taylor proposed that Aphebian rocks once may have extended from the Circum-Ungava Fold Belt as far east as the Archean exposed on the coast of Labrador. The Snyder Group would be an erosional remnant of this Aphebian cover. The lithologies of the Snyder Group and the Aphebian groups of the northeastern Canadian Shield show remarkable similarities of quartzites, iron formation, marbles, calcsilicates, and graphite- and sulfide-bearing siltstones. The last has been particularly stressed and is variously described as a rusty graphite quartz-rich gneiss or a sulfide facies iron formation. Such similarities do not provide a critical test of correlation but do point to similar environments of deposition.

There are many Aphebian supracrustal sequences in Labrador that could be fitted into the model of Jackson and Taylor (1972); among them are the Aillik (Gandhi *et al.*, 1969; Clarke, 1971), Croteau (Fahrig, 1957; Wanless and Loveridge, 1972), Mugford (Barton, 1975) and Snyder Groups. The Letitia (Brummer and Mann, 1961) and Ramah (Morgan, 1972; Knight, 1973) Groups are regarded as Aphebian in age but have not yet been radiometrically dated. The Croteau and Aillik Groups thicken southward towards the Grenville Front, suggesting that they are foreland sequences enclosing the southern end of the Baffin Geosyncline. The Ramah and Snyder Groups would be erosional outliers of the central zone.

The Mugford Group volcanics would be continental flood basalts with an extrusion age of 2.37 Gyr (Barton, 1975) overlying sedimentary rocks lithologically similar to other Aphebian sequences. In view of the great distances between the various Aphebian groups and the large interval of time in which they were deposited, direct correlation is probably too simple. Instead, they most likely indicate the location of certain depositional environments over a large time period during the Aphebian.

Knight (1974) has proposed a model correlating the Ramah and Mugford Groups with a reference to the Snyder Group. Based on his work in the Ramah Group (Knight, 1973), he envisions a southeastern transgression of shelf sediments across a peneplain of Archean rocks. The euxinic shales with iron sulfides, quartzites, cherts, and carbonates he mentions for the Ramah Group bear a resemblance to the Snyder Group, although the Snyder Group alone contains an iron formation. The southeastern transgression is interesting in light of the southern sediment source evidenced by the Snyder Group. The structural evidence advanced by Knight for the deformation during the Hudsonian is difficult to test because of the involvement of the Snyder Group in the emplacement of and metamorphism by the Nain complex.

Chapter 2

METAMORPHISM OF THE SNYDER GROUP IN THE KIGLAPAIT CONTACT AUREOLE

Introduction

This chapter considers the moderate pressure, upper greenschist to granulite facies metamorphism of the Snyder Group and Snyder breccia in the contact aureole of the Kiglapait intrusion. Emphasis is on the phase assemblages and phase compositions in order to outline reactions leading to the observed assemblages and deduce conditions during metamorphism. As the Kiglapait intrusion is one of a large number of plutons making up the Nain anorthosite complex, this study sheds light on the evolution of the country rocks and prevailing conditions at the time of emplacement of the intrusive rocks.

The contact aureole includes rocks of the Snyder Group as well as anorthositic rocks and the Tikkegharsuk migmatites (Fig. 6). The Tikkegharsuk migmatites have undergone deformation and anatexis during one or more Archean regional metamorphisms. They are biotite- and amphibole-bearing, suggesting amphibolite facies metamorphism. Textural and mineralogic evidence indicate they have undergone metamorphism and anatectic rejuvenation in the Kiglapait contact aureole. The contact-metamorphosed Tikkegharsuk migmatites have been termed the Kiglapait Coast migmatites by Speer (1974) who has mapped their extent and tentatively outlined their polymetamorphic nature. These were mapped as intermediate gneisses by Morse (1969) and were similarly concluded to be of rheomorphic origin.

Figure 6. Generalized geologic map of the northwest corner of the Kiglapait layered intrusion showing location of the metamorphic zones Ia, Ib, II, III.

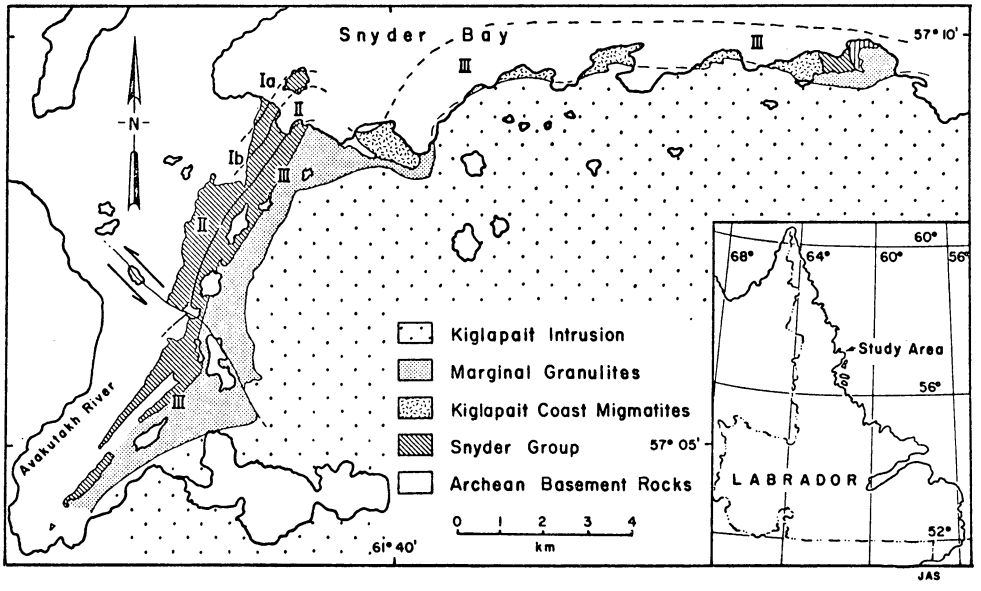
Snyder Bay
57° 10'
Ia
II
Ib
III
N
Avakutakh River
Kiglapait Intrusion
Marginal Granulites
Kiglapait Coast Migmatites
Snyder Group
Archean Basement Rocks
0 1 2 3 4
km
61° 40'
57° 05'
60°
68°
64°
60°
56°
Study Area
56°
LABRADOR
52°
JAS

The Snyder Group can be divided into three metamorphic zones based on the aluminum silicate distribution. Zone I contains andalusite; zone II is defined by the appearance of coarse sillimanite coexisting with andalusite; and zone III contains sillimanite alone. These divisions were chosen because of the abundance of aluminum silicates, their ease of mapping, and the insensitivity to changes in fluid pressure or composition. Zone I has been further subdivided on the basis of the assemblage chlorite + quartz in the metapelites and metabasites (zone Ia). Zone II is also characterized by the presence of cummingtonite in the metabasites. The boundary between zones II and III nearly coincides with the first appearance of orthopyroxene in the metabasites and metapelites.

As illustrated in Figure 6, the metamorphic zones have a clear spatial relation to the OBZ-IBZ contact of the Kiglapait intrusion. Metamorphic grade increases toward the Kiglapait. The map pattern of the isograds and their relation to the topography indicates that they are moderately dipping surfaces nearly paralleling the layering of the Kiglapait intrusion. Estimates of zone III thickness from the OBZ-IBZ contact and zone II thickness are 1 km and 0.7 km, respectively. The outer limit of zone I extends beyond the Snyder Group outcrop and cannot be distinguished from the effects of regional metamorphism in the basement.

A problem in terminology arises when we consider that the Snyder Group metamorphic rocks clearly represent a contact metamorphism, but that the mineral assemblages are equally representative of a low pressure regional metamorphic facies series. Using a mineralogic rather than

genetic definition of the metamorphic facies, the common low-pressure facies series of metamorphism, both regional and contact, is greenschist, amphibolite, granulite. In the Kiglapait contact aureole, zone Ia is equivalent to the greenschist facies, zone Ib and nearly all of zone II to the amphibolite facies, and the last part of zone II and zone III to the granulite facies.

Analytical Techniques

Insofar as possible, mineral assemblages were identified in the field. 192 samples of the 454 collected were thin-sectioned and mineral assemblages and textures studied in detail. Thin sections in which cordierite was suspected were stained for cordierite using the method of Boone and Wheeler (1968). Opaque mineral assemblages and their textures were determined by study of 85 polished sections in reflected light. Localities are shown in Figures 7 and 8. Correspondence between samples and localities are given in the sample catalog in the Appendix.

Mineral analyses were made on a three-channel ARL-EMX electron microprobe using well-characterized silicates, oxides, and sulfides as standards. The analyses were done at 15 kV with a beam current of 0.15 μA, pulse height selection, and a focused beam spot (10 μ). Preliminary work on polished thick sections showed little indication of inhomogeneity within mineral grains. Combined with the fact that the phases of interest occur in most cases as scattered, poikilitic porphyroblasts in an otherwise fine-grained, granoblastic matrix, analyses were done on mineral grains picked from a small volume of crushed rock and mounted in brass probe mounts with epoxy. 10-20 scattered 10-second point

counts were taken on several grains to insure that average compositions were obtained. As a token illustration of the validity of this procedure, two garnets each from SN 72134, SN 72149, SN 72176 were analyzed from core to rim in polished thick sections. Garnet was chosen for it is commonly zoned. Their analyses (Table 8) compare favorably and their homogeneity index (Boyd *et al.*, 1969; Boyd and Finger, 1975), as for all mineral analyses in this study, is 1-2 for major elements and 3-7 for minor elements (less than 2 weight %). A value in excess of 2-3 for a major element suggests inhomogeneity, whereas a value should be larger than 4-5 for a minor element to be considered inhomogeneous.

The data were converted to oxide weight percentages using the computer program EMPADR VII of Rucklidge and Gasparrini (1969). The Si and Al contents of the feldspars were obtained with the fixed stoichiometry feature of the program. Mineral formulas and components were calculated using the computer program SUPERRECAL of Rucklidge (1971). The program also calculates from the stoichiometry the amount of water present in hydrous minerals and adds it to the oxide weight percentages as calculated by EMPADR VII. The results are given in Tables 1 to 12 in the Appendix.

Pelite Petrology

Phase assemblages observed for the pelitic rocks are listed in the Appendix. Figures 9 and 10 graphically summarize the progressive phase assemblages and their compositions with increasing metamorphic grade. The graphical representation chosen is the AFM diagram suggested by Barker (1961) for pelitic rocks with ubiquitous potassium feldspar.

Figure 9. Progressive mineral changes in the pelitic rocks of the Snyder Group with increasing metamorphic grade.

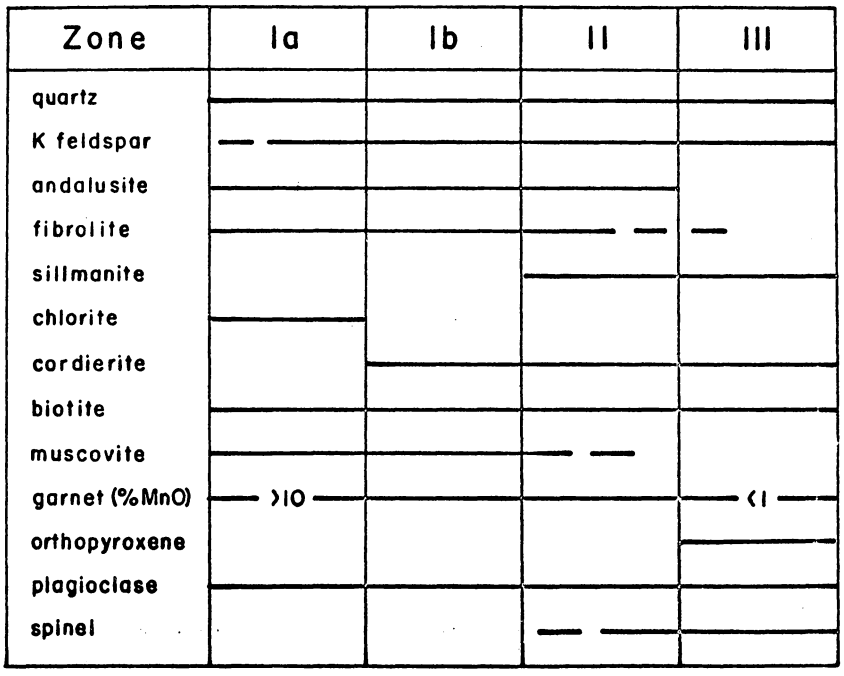
Zone
Ia
Ib
II
III
quartz
K feldspar
andalusite
fibrolite
sillmanite
chlorite
cordierite
biotite
muscovite
garnet (%MnO)
>10
<1
orthopyroxene
plagioclase
spinel

Figure 10. Summary AFM projections from K-feldspar of observed mineral assemblages in zone Ia(a), zone Ib(b), zone II(b,c), and zone III (c,d,e,f). Dashed lines from garnet or biotite indicate that phase in assemblates not showing it diagrammatically. Abbreviations: Bt, biotite; Cd, cordierite; Chl, chlorite; Ga, garnet; Opx, orthopyroxene; Sp, spinel; And, andalusite, Si, sillimanite.

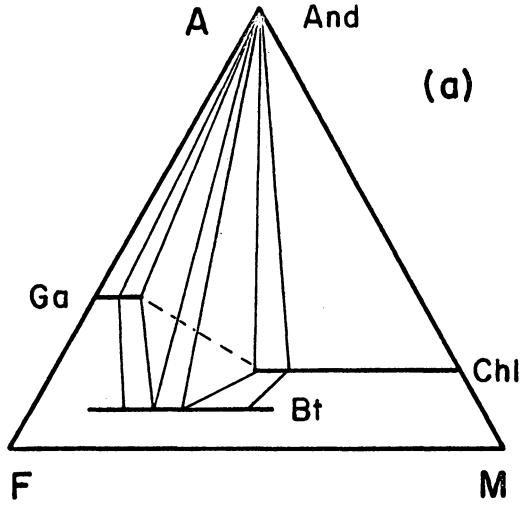
A
And
(a)
Ga
Chl
Bt
F
M

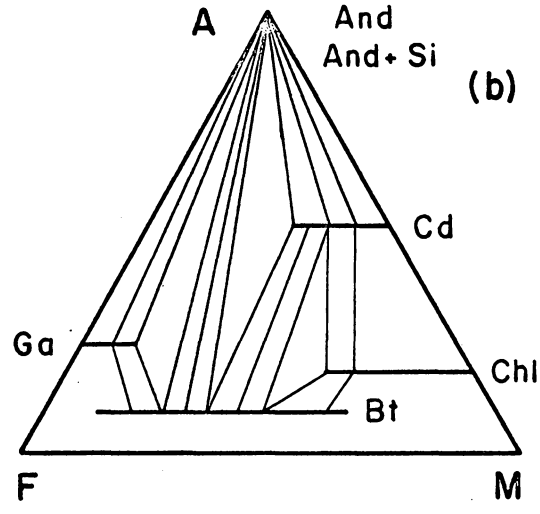
A
And
And + Si
(b)
Cd
Ga
Chl
Bt
F
M

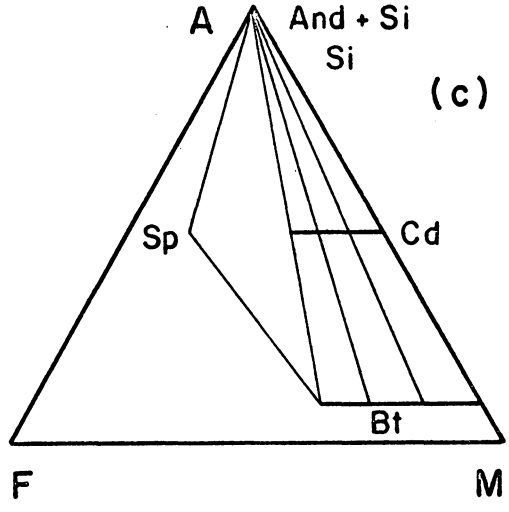
A
And + Si
Si
(c)
Sp
Cd
Bt
F
M

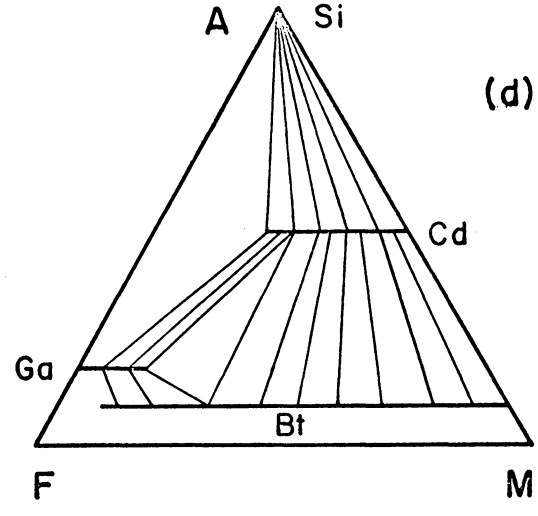
A
Si
(d)
Cd
Ga
Bt
F
M

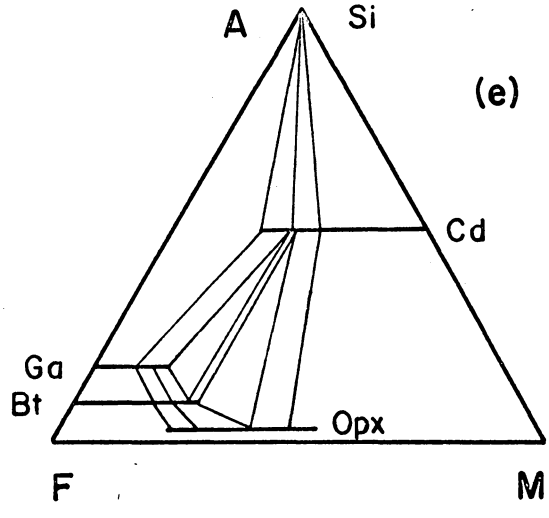
A
Si
(e)
Cd
Ga
Bt
Opx
F
M

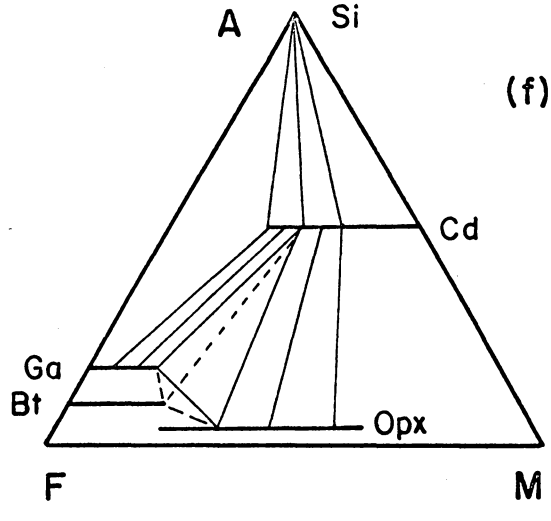
A
Si
(f)
Cd
Ga
Bt
Opx
F
M

Muscovite may or may not be present. The maximum number of phases in any assemblage projected on the graphical representation should be three. However, there are several instances where some pelites contain more phases than are permissible in equilibrium in this system and there are two different causes. Garnet, in particular, commonly appears in the stable zone Ia phase assemblage andalusite + biotite + chlorite + garnet. The presence of the garnet is believed to be caused by the presence of the additional component MnO. This is borne out by the high manganese content of the garnet (16 weight % MnO) and is shown schematically in Figure 10a by means of a dotted line to garnet. The second and more common cause of additional phases in the Snyder Group is that they represent multivariant reaction assemblages with the reactants and products coexisting over a limited range of intensive variables.

The aluminum silicate sequence with increasing metamorphic grade is andalusite-sillimanite. Andalusite is an abundant mineral in zones I and II and the pink porphyroblasts impart to the Snyder Group quartzites their most striking characteristic. It forms large, subhedral, poikilitic prophyroblasts that contain inclusions of quartz, potassium feldspar, muscovite, biotite, chlorite, sulfides, corundum, and spinel. In thin section, the normally colorless andalusites have small, pleochroic pink patches. Okrusch and Evans (1970) found an iron enrichment of similar pleochroic patches, but in this study no compositional differences were found. Andalusite in the sulfide-graphite hornfels and more pelitic rocks of the upper quartzite is developed as chiastolite. Andalusite appears at the lowest grade of metamorphism with no suggestion of the reaction leading to its appearance.

In zone I, sillimanite only occurs as fibrolite, intimately associated with biotite or along small shear planes. Beginning in zone II, sillimanite is developed as coarse, prismatic porphyroblasts, intergrown with andalusite, suggesting replacement of the andalusite by sillimanite. This suggestion is further substantiated by the sillimanite pseudomorphs after chiastolite. The aluminum silicates are still accompanied by fibrolite in zone II, but in zone III coarse, prismatic sillimanite is the only aluminum silicate polymorph.

The andalusite-sillimanite sequence establishes the pressure in the contact aureole as less than the aluminum silicate triple point [currently estimated to be at 5.1 kb and 610°C (M. C. Gilbert, pers. comm.)]. The occurrence of fibrolite in zone I poses the question as to whether or not the temperature and pressure conditions of the sillimanite phase field were reached within that zone. Its fine grain size, association in shear planes and intergrowths with biotite, and the lack of other minerals consistent with those pressures and temperatures suggest a special origin for the fibrolite. Chinner (1966) has also suggested that fibrolite may not be a reliable indiator of physical conditions. Greenwood (1972) points out that any solid-solid reaction having a small entropy change will be highly sensitive to small perturbations in free energy resulting from either disorder, solid solution, grain size, or surface energy.

As mentioned previously, almost all mineral assemblages contain potassium feldspar. Rocks containing muscovite but no potassium feldspar are rare and limited to zone Ia. The disappearance of muscovite would

mark the aluminum silicate-potassium feldspar isograd corresponding to the reaction:

$$\text{muscovite} + \text{quartz} \not\rightleftarrows Al_2SiO_5 + \text{K-feldspar} + H_2O \qquad (1)$$

The aluminum silicate polymorph can be either andalusite or sillimanite and the reaction assemblage occurs over a range of metamorphic conditions, muscovite persisting in some rocks to just outside zone III.

The assemblage muscovite + quartz + sillimanite indicates that the pressure conditions in the Kiglapait contact aureole were above the intersection of the andalusite-sillimanite transition and breakdown of muscovite + quartz (Fig. 12). Using the experimental data of Chatterjee and Johannes (1974) and Richardson *et al.* (1969) the intersection would occur at a pressure and temperature of 4.1 kb and 670°C. As the phengite and paragonite components and conditions of water pressure less than total pressure would lower the thermal stability of muscovite + quartz, this is a lower pressure estimate.

The breakdown of phengitic muscovite according to the reaction:

$$\text{phengite} = \text{muscovite} + \text{biotite} + \text{K-feldspar} + \text{quartz} + H_2O \qquad (2)$$

experimentally studied by Velde (1965) and the paragonite decomposition:

$$\text{paragonite} + \text{quartz} = \text{albite} + Al_2SiO_5 + H_2O \qquad (3)$$

determined by Chatterjee (1972) both indicate that the stability field of muscovite would be lowered with any chemical variation and could account for the temperature range of the univariant assemblage muscovite + quartz + Al_2SiO_5 + K-feldspar by means of a continuous reaction.

Analyzed muscovites (Table 7) are phengitic and show limited solid solution with paragonite. No systematic variation of phengite or paragonite content with increasing metamorphic grade is evident as would be expected if the variability in the muscovite composition were solely responsible for a continuous reaction. This suggests that variable fluid composition is the most likely cause.

Some idea of the fluid pressure variation can be obtained by noting that reaction (1) occurs at conditions of the zone Ia-Ib transition with temperatures of about 550°C. Calculation of fluid pressures for reaction (1) using the experimental data of Chatterjee and Johannes (1974) at 550°C and a total pressure of 4 kb yield a fluid pressure of less than 1 kb. As muscovite is also observed above the sillimanite isograd of zone II, a fluid pressure approaching total pressure is indicated.

Muscovites coexisting with plagioclase have higher paragonite contents than those without plagioclase (Fig. 11). Based on the experimental work of Chatterjee (1972), the paragonite contents of these muscovites would make the plagioclase-bearing assemblages the low temperature assemblages. No such feature is observed in the Snyder Group rocks because of the anorthite content of the plagioclase which permits the four phase assemblage Al_2SiO_5 + muscovite + alkali feldspar + plagioclase.

The assemblage andalusite + spinel + muscovite + corundum is observed in an andalusite crystal in zone Ia. The assemblage outside the andalusite is andalusite + chlorite + biotite + muscovite + K-feldspar + quartz. The texture would suggest that the assemblage inside the andalusite is effectively armored from that on the outside and therefore

Figure 11. Snyder Group muscovites (Table 7) plotted to show variations in paragonite (Na/Na+K) and phengite ($Fe+Mg+Ti/Al^{VI}+Fe+Mg+Ti$) contents. Triangles are muscovites coexisting with plagioclase.

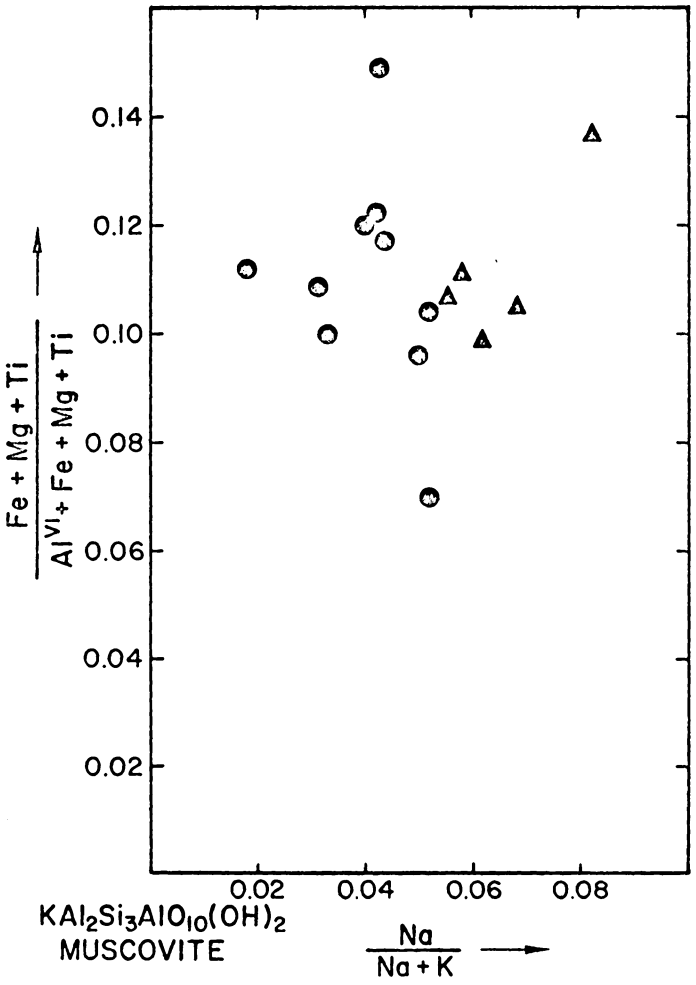
0.14
0.12
0.10
0.08
0.06
0.04
0.02
0.02
0.04
0.06
0.08
Fe + Mg + Ti
AlVI + Fe + Mg + Ti
Na
Na + K
KAl2Si3AlO10(OH)2
MUSCOVITE

Figure 12. Pressure ($P_{H_2O} = P_{Total}$)-temperature diagram showing experimentally determined and schematic mineral equilibria. Abbreviations in addition to those of Figure 10 are Qz, quartz; Mu, muscovite; Ky, kyanite. Aluminum silicate phase relations are from Richardson *et al.* (1969), breakdown of chlorite + muscovite + quartz from Hirschberg and Winkler (1968), and breakdown of muscovite + quartz from Chatterjee and Johannes (1974). High temperature, schematic phase relations involving cordierite are from Hensen (1971), and the reasons for their location in order to harmonize with the path of increasing metamorphism are discussed in the text. The isobaric line indicates the path of increasing metamorphic grade for the Snyder Group in the Kiglapait contact aureole.

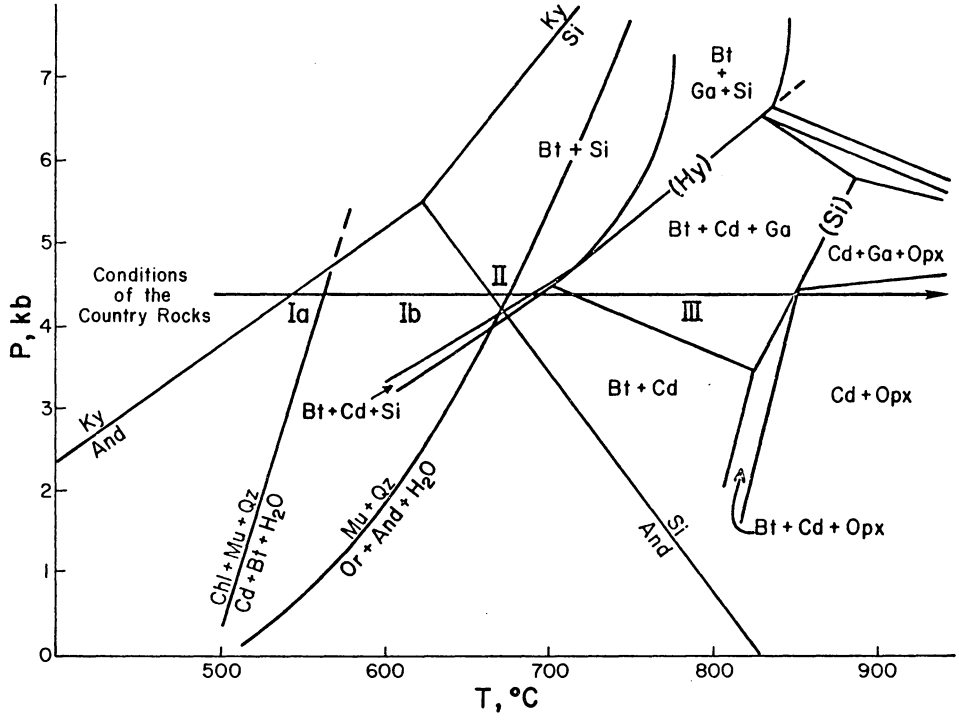
P, kb
T, °C
0
1
2
3
4
5
6
7
500
600
700
800
900
Ky
Si
Bt + Si
Bt
+
Ga + Si
(Hy)
(Si)
Bt + Cd + Ga
Cd + Ga + Opx
Conditions
of the
Country Rocks
Ia
Ib
II
III
Ky
And
Bt + Cd + Si
Bt + Cd
Cd + Opx
A
Bt + Cd + Opx
Chl + Mu + Qz
Cd + Bt + H2O
Mu + Qz
Or + And + H2O
Si
And

the two are not in equilibrium. The intersection of the ln f_{H_2O} vs. 1/T curves for these two univariant assemblages for P_{solid} = 4 kb, using the experimental data of Chatterjee and Johannes (1974), is at a temperature of 1148°C and a water fugacity of 121,000 bars, thus bearing out the contention that the two assemblages are not in equilibrium.

The small area of pelitic rocks in zone Ia, whose assemblages are represented in Figure 10a, are in the uppermost greenschist facies. The characteristic assemblage is chlorite + quartz. The appearance of cordierite (Fig. 10b), summarized by the reaction

$$\text{chlorite} + \text{muscovite} + \text{quartz} \rightleftarrows \text{cordierite} + \text{biotite} + H_2O \qquad (4)$$

marks the beginning of the amphibolite facies in zone Ib. Biotite is present below the isograd and while there is no textural evidence that biotite participated in the reaction, the lower octahedral aluminun contents (<.651) of the analyzed biotites coexisting with chlorite (SN 72135, 72200, 74327; Table 3) than those coexisting with cordierite (>.666) in zone I (SN 7215, 7256, 72131, 72151, 72179, 72193, 72194, 72215; Table 3) provides chemical evidence for the participation of biotite in the reaction. Ramsay (1972) has described the cordierite isograd in an Abukuma-type metamorphic aureole near Yellowknife, N. W. T., where the reaction is given by,

$$\text{chlorite} + \text{muscovite} + \text{biotite(1)} + \text{quartz} \; [+ \text{albite} + \text{ilmenite}] \rightleftarrows \text{cordierite} + \text{biotite(2)} + H_2O \qquad (5)$$

and where the biotite(2) is both more aluminous and sodic than biotite (1).

The last appearance of chlorite + muscovite + quartz is mapped as the boundary between zones Ia and Ib. The isograd is irregular, again pointing to variations in the temperature of reaction as the result of either differing water pressures or phase compositions. Interbedding of cordierite-bearing and chlorite + quartz assemblages on a scale of less than half a meter attest to such variations over small distances. Chlorites in zone Ia (Table 4) are ripidolites, using the nomenclature of Hey (1954), with Fe/(Fe + Mg) ratios of 0.5 to 0.75. Hirschberg and Winkler (1968) have experimentally determined reaction 4 to occur at temperatures of 505° to 550°C for the pressure interval 0.5 to 4.0 kb and a Fe/(Fe + Mg) range of 0.4 to 0.8. Seifert (1970) has shown that higher temperatures are required for the decomposition of chlorite in the Fe-free system. If the phase compositions are the cause of the variable temperature of reaction, systematic variations in chlorite and cordierite compositions with increasing metamorphic grade are to be expected. As no such variations are evident in the Snyder Group, it is suggested that variable water pressures have resulted in the smearing of the cordierite isograd.

Beginning in zone II there is an increase in frequency and abundance of cordierite with increasing metamorphic grade that points to additional cordierite-producing reactions. The nature of the reactions is evidenced in part by: (1) the collinearity of biotite-cordierite-Al_2SiO_5 on the AFM diagram (Fig. 10c); (2) the concurrent decrease in the modal amount of aluminum silicate and biotite; and (3) the frequent coronas of cordierite and hercynite armoring sillimanite (Fig. 13). This suggests that the reaction is:

Figure 13. Cordierite and spinel intergrowth armoring sillimanite as a result of the reaction biotite + Al_2SiO_5 ⇄ cordierite + spinel + K-feldspar + H_2O. A discontinuous rim of plagioclase envelops the cordierite and spinel. The matrix is K-feldspar + quartz + biotite + opaques. Sample SN 72111.

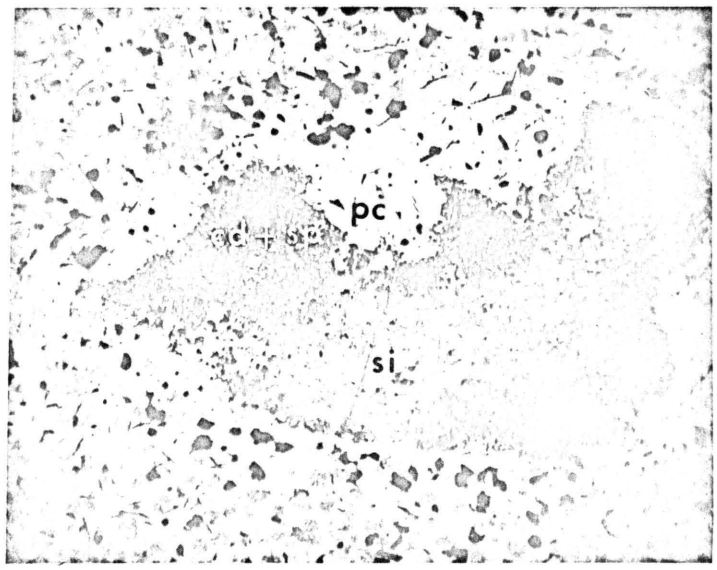
pc
si

$$\text{biotite} + Al_2SiO_5 + \text{quartz} \gtrless \text{cordierite} + \text{K-feldspar} + H_2O \quad (6)$$

Schreyer and Yoder (1961) have also interpreted some described occurrences of cordierite to have resulted from this reaction. The production of spinel in coronas is evidently the reaction:

$$\text{biotite} + Al_2SiO_5 \gtrless \text{cordierite} + \text{spinel} + \text{K-feldspar} + H_2O \quad (7)$$

wherein quartz is absent in the rock or excluded from the reaction because of the armoring of the sillimanite. The resulting spinel is a spinel-hercynite solid solution (SN 72111; Table 12). The assemblage is shown in Figure 10c, although the assemblage lacks excess quartz as required by these diagrams. Such coronas are common in the Nain area (J. H. Berg, E. P. Wheeler II, pers. comm.) and are also mentioned by Gable and Sims (1969) for the cordierite-bearing rocks of the Front Range of Colorado. This reaction contradicts the statement of Schreyer and Yoder (1961) that the reaction between biotite and sillimanite to produce cordierite will not take place in a silica-deficient environment or will cease as soon as the available quartz is used up.

Often encompassing the coronas of cordierite and hercynite are discontinuous rims of plagioclase. The exact origin of the plagioclase is uncertain as no calcium-bearing phases are reactants in reaction 7; nevertheless the texture clearly suggests that the plagioclase is a participant. It might result from remaining plagioclase that has contributed sodium to the alkali feldspar produced in reaction 7.

Garnet has a fairly widespread occurrence in zone III, in contrast to its restricted development in biotite-rich rocks in zones I and II. Garnet analyses (Table 6) show them to be almandine-rich

compositions, although the spessartine component is important at lower grades. Figure 14 summarizes the garnet compositions with increasing metamorphic grade. The greatest change in garnet composition is between zone I and II. Garnets of zone I contain from 14 to 40 mole percent spessartine + grossular; zone II, 7 to 13%, and zone III, 4 to 7%. The pyrope component is low, remaining between 4 and 16 mole percent for all zones.

The occurrence of the garnets is thought to be the result of two separate garnet-producing reactions. The first reaction would produce garnet as the result of the gradual decomposition of chlorite according to the reaction:

$$\text{chlorite} + \text{muscovite} + \text{quartz} \rightleftarrows \text{garnet} + \text{biotite} + H_2O \qquad (8)$$

The widespread almandine garnets of zone III can be envisioned as the result of the breaking of the biotite + Al_2SiO_5 tie line (Fig. 10b) by the garnet + cordierite tie line (Fig. 10d). The reaction is summarized by:

$$\text{biotite(1)} + Al_2SiO_5 + \text{quartz} \rightleftarrows \text{cordierite} + \text{garnet} + \text{biotite(2)} + \text{K-feldspar} + H_2O \qquad (9)$$

Manganese is selectively partitioned into the garnet in garnet-bearing assemblages. As increased manganese content stabilizes garnet at increasingly lower metamorphic grades (Hsu, 1968), production of garnet would occur over a range of metamorphic grade, the garnets showing a decrease in MnO content with progressive metamorphism. This behavior is observed for the unzoned Snyder Group garnets. Equilibrium

Figure 14. Garnet compositions (Table 6) on pyrope-almandine-grossular + spessartine triangles, (a) pelites, (b) iron formation, triangles, and metabasites, squares. Roman numerals indicate metamorphic zones in which the pelitic garnets occur.

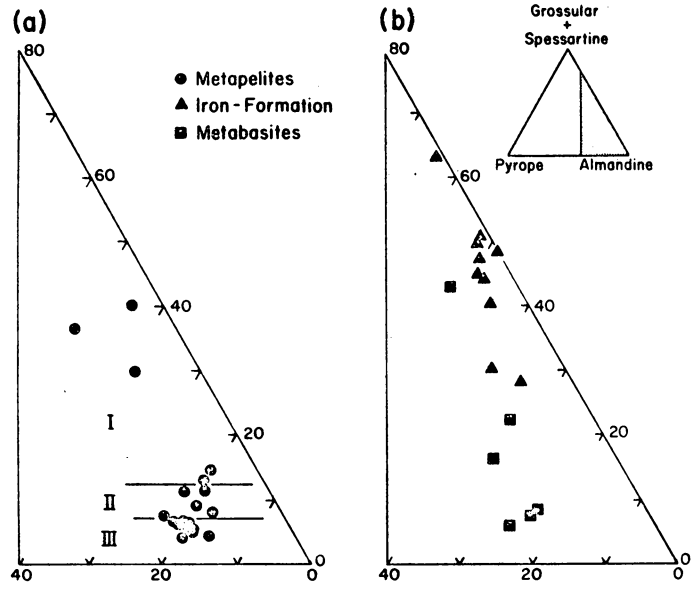
(a)
80
60
40
20
0
40
20
0
Metapelites
Iron-Formation
Metabasites
I
II
III
(b)
Grossular
+
Spessartine
Pyrope
Almandine
80
60
40
20
0
40
20
0

could have been favored in this case by either the extreme poikiloblastic texture of the garnets or the rather rapid advance of the thermal surfaces during metamorphism in relation to the nucleation of garnet so that garnets first nucleated at higher temperatures with increasing metamorphic grade.

The last silicate phase to appear in the prograde metamorphism of the pelitic rocks of zone III is orthopyroxene. It is ferrohypersthene, Fs_{52-69} (Table 11, Fig. 15), and as a whole contains greater amounts of aluminum, 2.45-4.01 weight percent, than the other analyzed Snyder Group pyroxenes. The calcium content is also much lower. Orthopyroxene is produced by the reaction:

$$\text{biotite} + \text{quartz} \rightleftarrows \text{orthopyroxene} + \text{K-feldspar} + H_2O \qquad (10)$$

and is illustrated by the Figure 10d to Figure 10e transition. In many cases there is coexisting garnet and analyses of the coexisting ferromagnesian phases show the garnet-biotite-orthopyroxene to be nearly collinear on the AFM diagram (Fig. 10e) which suggests that the reaction:

$$\text{biotite(1)} + \text{quartz} \rightleftarrows \text{orthopyroxene} + \text{garnet} + \text{biotite(2)} + H_2O \qquad (11)$$

also contributes to the production of orthopyroxene.

The sequence cordierite-garnet-orthopyroxene can be understood in terms of the theoretical treatments of Hess (1969) and Hensen (1971). Starting with Hess's (1969) invariant point involving the phases Al_2SiO_5-biotite-cordierite-garnet-orthopyroxene, Hensen (1971) further amplified the relations below the invariant point in anticipation of his experimental work on garnet-cordierite pairs coexisting with either

Figure 15. The pyroxenes of the Kiglapait contact aureole (Table 11) projected onto the pyroxene quadrilateral on the triangular Ca-Mg-Fe plot. The line at the bottom is for olivine compositions (Table 8). Tie lines connect coexisting mineral pairs. Symbols: triangles, marbles and calcsilicates; open diamonds, metapelites, circles, metabasites; squares, iron formation.

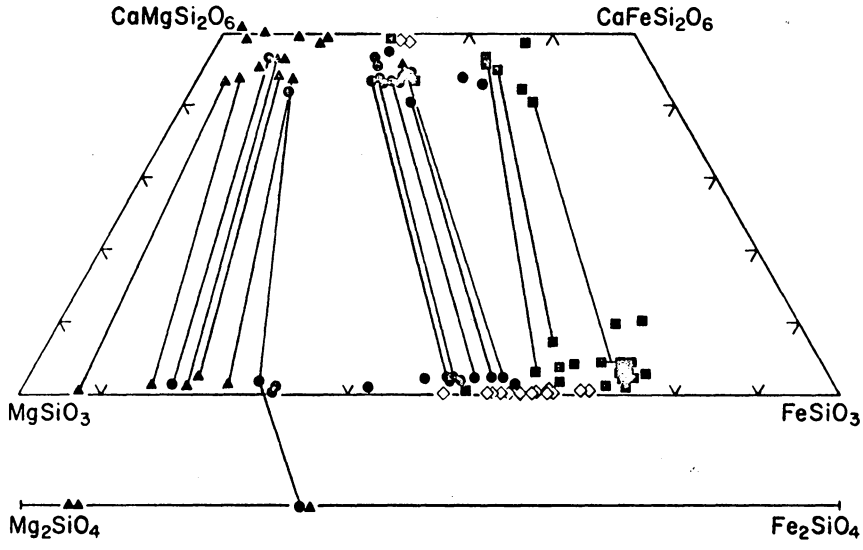
$CaMgSi_2O_6$
$CaFeSi_2O_6$
$MgSiO_3$
$FeSiO_3$
Mg_2SiO_4
Fe_2SiO_4

sillimanite or orthopyroxene (Hensen and Green, 1971, 1972, 1973) and of the complication of the anhydrous reactions by the biotite + quartz breakdown. His results are summarized in his Figure 9 (Hensen, 1971) which is reproduced in Figure 12 for some intermediate composition. The configuration and placement of the diagram changes with changes in bulk rock and fluid chemistry.

The placement in P-T space of the applicable parts of Hensen's (1971) phase diagram on Figure 12 with respect to the path of increasing metamorphism can be fixed by several observations. (1) In the contact aureole, the first appearance of almandine by reaction 9 occurs just after the appearance of cordierite by reaction 6. This indicates that the biotite + garnet + sillimanite field lies above the pressure conditions in the aureole of 4 to 5 kb. (2) Biotite + cordierite assemblages interlayered with biotite + cordierite + garnet assemblages point to a smearing of the boundary between these two fields as a result of bulk compositional differences. The path of increasing temperature passes through this broadened boundary. (3) Placement of the reaction boundaries with respect to temperature is governed by the cordierite-producing reaction taking place after the appearance of sillimanite and the disappearance of muscovite + quartz in zone II.

The assemblage of specimen SN 7282 of andalusite + sillimanite + garnet + cordierite + biotite + muscovite + potassium feldspar + quartz would place the univariant phase boundary (Hy) of Figure 12 at the intersection of the andalusite-sillimanite transition and the breakdown of muscovite + quartz at 670°C and 4.1 kb. The temperature and pressure

of SN 7282 can also be obtained from the compositions of the coexisting garnet and cordierite, which are related by the reaction:

$$3 \text{ cordierite} \rightleftarrows 2 \text{ garnet} + 4 \text{ sillimanite} + 5 \text{ quartz} \qquad (12)$$

The temperatures and pressures for this reaction according to Currie (1971), Hensen and Green (1973), and Hutcheon *et al.* (1974) are respectively 675°C, 4.8 kb; 760°C, 6.5 kb; and 767°C, 4.5 kb. The points for the method of Currie (1973) and Hutcheon *et al.* (1974) were calculated using a computer program supplied by I. Hutcheon. Only the point of Currie (1971) falls reasonably close to the intersection of the andalusite-sillimanite transition and breakdown of muscovite + quartz. As pointed out by Currie (1974), the calibrations of Hensen and Green (1973) and Hutcheon *et al.* (1974) encounter difficulties in andalusite-bearing assemblages. While the numbers obtained for pressure and temperature are useful for estimates, the calibrations of the cordierite-garnet geothermometer and geobarometer are uncertain due to the inconsistent results of the several workers. Accordingly, the boundary (Hy) has been placed at higher temperatures in Figure 12 than the intersection of the andalusite-sillimanite transition and the breakdown of muscovite + quartz as representative of the majority of the phase assemblages. Sample SN 7282 contains both manganiferous garnet (3.00 wt. %) and cordierite (1.02 wt. %) which allows the assemblage to stabilize at somewhat lower temperatures (Weisbrod, 1973).

Shortly after these reactions, orthopyroxene appears as would be predicted from the phase diagram as a result of the decomposition of biotite + quartz outlined in reaction 10. The coexistence of biotite

+ orthopyroxene + cordierite + garnet + K-feldspar (Fig. 10e,f) is only possible on the univariant phase boundary (Si) of Figure 12. Compositional data on garnet-cordierite pairs coexisting with orthopyroxene and the experimental work of Hensen and Green (1973) allow an approximate location of the intersection of this boundary by the path of increasing metamorphism at between 840-860°C and a pressure of 4 kb.

The highest temperature assemblages predicted from Hensen's (1971) work would be cordierite + garnet + orthopyroxene or cordierite + orthopyroxene (Fig. 10f). The cordierite + orthopyroxene assemblage dominates in the Snyder Group which suggests that the path of increasing metamorphism passes below the cordierite + orthopyroxene and cordierite + garnet + orthopyroxene field boundary for the majority of rock compositions. The compositions of a garnet + cordierite pair in a rare cordierite + garnet + orthopyroxene assemblage at this grade (NC 7449) yield a temperature of 950°C and a pressure of 4 kb (Hensen and Green, 1973).

Biotite is in equilibrium with a number of phase assemblages at all metamorphic grades and is an ever-present reactant and product in reactions 5, 6, 9, 10, and 11. These differing mineral assemblages and reactions are reflected in the biotite chemistry and a noticeable decrease in modal amounts of biotite. Biotite analyses are given in Table 3. As illustrated by Figure 16, their compositional variability is large, lying along a diagonal band from phlogopite to siderophyllite. No trend with increasing metamorphic grade is evident in this type of diagram, but is revealed in the series of histograms for Al^{VI}, Ti, and Fe/(Fe + Mg) contents for different metamorphic zones in Figure 17.

Figure 16. Biotite compositions of Table 3 projected onto the phlogopite-annite-eastonite-siderophyllite field.

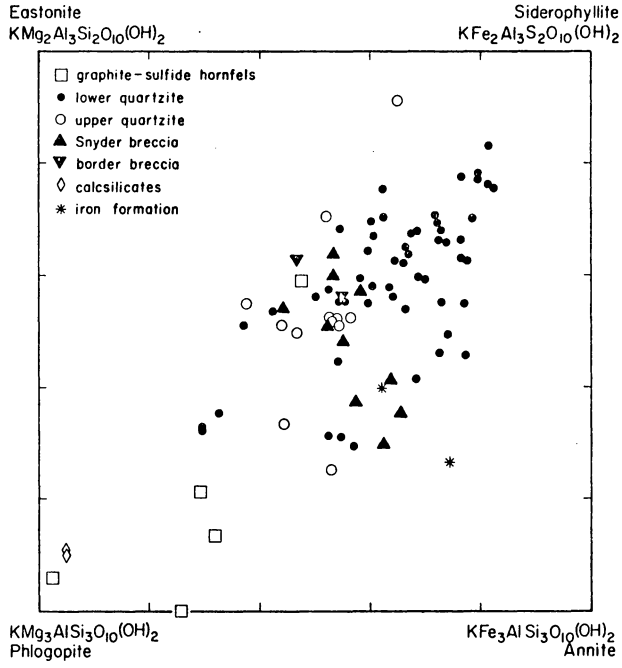
Eastonite
$KMg_2Al_3Si_2O_{10}(OH)_2$
Siderophyllite
$KFe_2Al_3S_2O_{10}(OH)_2$
graphite-sulfide hornfels
lower quartzite
upper quartzite
Snyder breccia
border breccia
calcsilicates
iron formation
$KMg_3AlSi_3O_{10}(OH)_2$
Phlogopite
$KFe_3AlSi_3O_{10}(OH)_2$
Annite

Figure 17. Histograms of pelitic Snyder Group biotites showing variation of Fe/(Fe+Mg), Ti, and octahedral Al (Al^{VI}) contents by metamorphic zones in the Kiglapait contact aureole. The letters refer to the zone III metamorphic mineral assemblages: A, sillimanite or cordierite + spinel; B, garnet + cordierite; C, orthopyroxene + cordierite $\pm$ garnet.

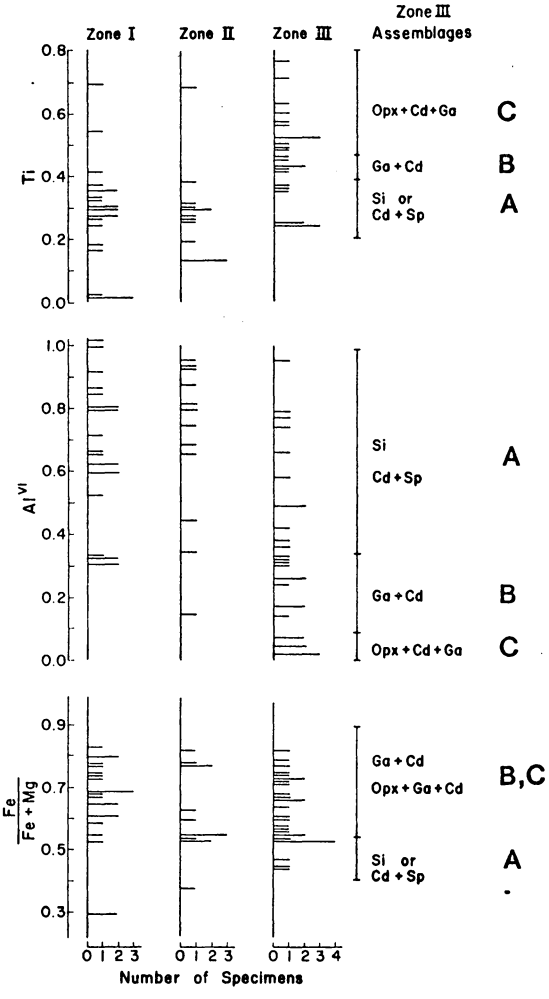
Zone I
Zone II
Zone III
Zone III Assemblages
Ti
0.8
0.6
0.4
0.2
0.0
Opx + Cd + Ga
C
Ga + Cd
B
Si or Cd + Sp
A
Al^{VI}
1.0
0.8
0.6
0.4
0.2
0.0
Si
Cd + Sp
A
Ga + Cd
B
Opx + Cd + Ga
C
$\frac{Fe}{Fe + Mg}$
0.9
0.7
0.5
0.3
Ga + Cd
Opx + Ga + Cd
B,C
Si or Cd + Sp
A
0 1 2 3
0 1 2 3
0 1 2 3 4
Number of Specimens

While the ranges for the different zones are comparable, the average octahedral aluminum content may decrease slightly as one passes from zone I and II to zone III. A similar slight increase is noted for the titanium content and no such trend is apparent for Fe(Fe + Mg).

Closer examination of the zone III biotite octahedral aluminum contents showed they could be divided into three groups according to the coexisting mineral phases in order of decreasing Al^{VI} in the biotites. They are:

A. Sillimanite or cordierite + spinel intergrowths armoring sillimanite.

B. Garnet + cordierite.

C. Orthopyroxene + cordierite $\pm$ garnet.

In turn, this division can be applied to the Ti and Fe/(Fe + Mg) histograms where group A exhibits the lowest Ti and Fe/(Fe + Mg) contents, group C the highest, and B intermediate or overlapping ranges with C.

In light of the above discussion, the increasing high grade metamorphic assemblages are A, B, C, the biotite becoming less aluminous and more iron- and titanium-rich with increasing metamorphic grade. Experimental work has shown that the increased thermal stability of biotite is favored by increased magnesium (Wones and Eugster, 1965) and aluminum contents (Rutherford, 1973). The obvious contradiction in these two results is probably a result of the influence of the coexisting phases orthopyroxene, garnet, and cordierite. Cordierite would be of particular importance for it is both more aluminous and magnesian than the other phases and would serve to deplete these components from the other phases.

Biotite is continually reacting to produce phases which contain very little Ti and as the biotite becomes less modally abundant in the rocks, Ti becomes concentrated in the residual biotite. Hess (1969) points out that biotite still occurs under conditions of high grade metamorphism, even though it would be expected to disappear, and may be present only because of particular bulk compositions. Its presence as an extra phase in the Snyder Group may result from the additional component TiO_2, biotites containing up to 7 weight percent TiO_2. Because of this, tie lines to biotite in Figure 10f are dashed.

As evidenced by the interlayering of hydrous and anhydrous mineral assemblages and the irregular nature of dehydration reaction isograds, fluid pressures were variable over distances of less than half a meter. Variation in mineral chemistry would have affected the temperatures of reaction but as there is no systematic change in mineral chemistry with metamorphic grade, it was not the sole factor. For the most part, water pressure was less than total pressure as illustrated by the common decomposition of muscovite + quartz to produce andalusite and K feldspar by reaction 1. At temperatures of the zone Ia-Ib transition (550°C) this reaction would proceed at water pressures of about 1 kb. As this decomposition has occurred at both lower temperatures in zone Ia and higher temperatures as denoted by the appearance of sillimanite in zone II, a range of water pressures from less than 1 kb to nearly 4 kb is indicated. The hydrous assemblages are invariably rocks with originally fine grain size, the silt- and mudstones of the graphite-sulfide siltstone, the matrix of the conglomerates, and the pelitic members of the lower and upper quartzites.

The broader question of whether pore fluid, which would have been mostly water resulting from dehydration reactions, was absorbed by the Kiglapait magma or expelled outward before the advancing isothermal surfaces can best be answered by knowing the origin of the Outer Border Zone. If the OBZ is part of the Kiglapait intrusion, then it represents the contaminated gabbroic magma which absorbed the water. If the OBZ is a metavolcanic sequence as suggested by Berg (1974), then any water must have been driven down the thermal gradient.

Pelite Mineralogy

Aluminum silicates

Zone II, defined by the coexistence of andalusite and sillimanite, is nearly a kilometer wide on the surface and ∿0.7 km thick perpendicular to the isograd surfaces. Whether andalusite + sillimanite associations represent multivariant equilibrium assemblages or overstepping of the univariant andalusite-sillimanite transition has been considered by many authors (Chinner, 1966; Strens, 1968; Albee and Chodos, 1969; Chinner *et al.*, 1969; Althaus, 1969; Fyfe, 1969; Okrusch and Evans, 1970; Dodge, 1971; Greenwood, 1972). With these possibilities in mind the aluminum silicates in the contact aureole were examined in more detail.

In zone II the percentage of andalusite of total silicate shown in Figure 18 remains greater than 99% until nearly halfway across the zone and then decreases to 0%. The difficulty in recognizing trace amounts of andalusite or the consumption of aluminum silicates in the

Figure 18. Variation of the andalusite to sillimanite ratio in terms of modal percent andalusite/andalusite + sillimanite across zone II, as a fraction of the thickness. Zone II is defined as the appearance of andalusite + sillimanite and is estimated to be 0.7 km thick.

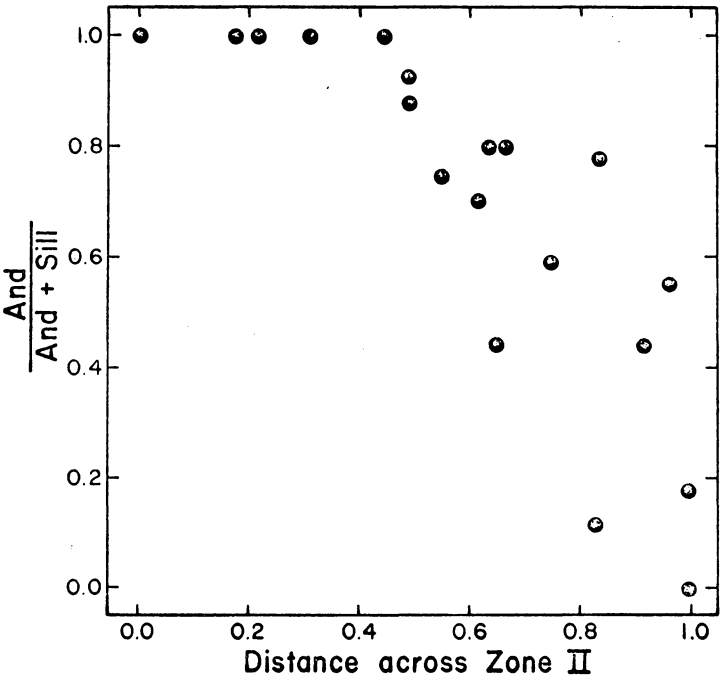
1.0
0.8
0.6
0.4
0.2
0.0
And / And + Sill
0.0
0.2
0.4
0.6
0.8
1.0
Distance across Zone II

cordierite-producing reaction 6 may account for the absence of a similar long, gradual trailing off of andalusite.

Qualitative scans of the aluminum silicates indicated that iron was the only element besides aluminum and silicon detectable in more than trace amounts. The homogeneity index of less than 4 indicates that the variation of iron content within the same Al_2SiO_5 polymorph is negligible. Results obtained are given in Table 1. Figure 19 shows the number of atoms of iron for either andalusite and sillimanite in the formula $Al_{2-n}Fe_nSiO_5$ as a function of the metamorphic zones. The ranges of iron contents for the two aluminum silicates overlap; however, the iron content of zone III sillimanites is distinctly lower than zone I andalusites. For the coexisting aluminum silicates of zone II, the ranges again overlap but the iron content of the andalusite is higher than that of the coexisting sillimanite. The only exceptions are the very iron-poor aluminum silicates, which occur in sulfide-rich rocks, where there is a tendency toward equal partitioning. A similar trend was also noted by Okrusch and Evans (1970) both for their rocks and those of Albee and Chodos (1969) and Chinner *et al.* (1969). The iron content of the Snyder Group andalusites and, to a lesser extent, sillimanites is considerably greater than those found by Chinner *et al.* (1969), Albee and Chodos (1969), or Okrusch and Evans (1970). It is typical of the generally iron-rich nature of Snyder Group minerals.

As noted, the aluminum silicates of the Snyder Group show a consistent iron enrichment of the andalusites. The distribution of iron between coexisting aluminum silicates of zone II is shown graphically in Figure 20. The magnitude of this enrichment, given by the

Figure 19. Iron content of the Snyder Group aluminum silicates (Table 1) expressed as n_{Fe} where n is $Al_{2-n}Fe_nSiO_5$ by metamorphic zones in the Kiglapait contact aureole. Symbols: open circles, andalusite; open triangles, sillimanite; filled circles, andalusite from sulfide-rich rocks; filled triangles, sillimanite from sulfide-rich rocks.

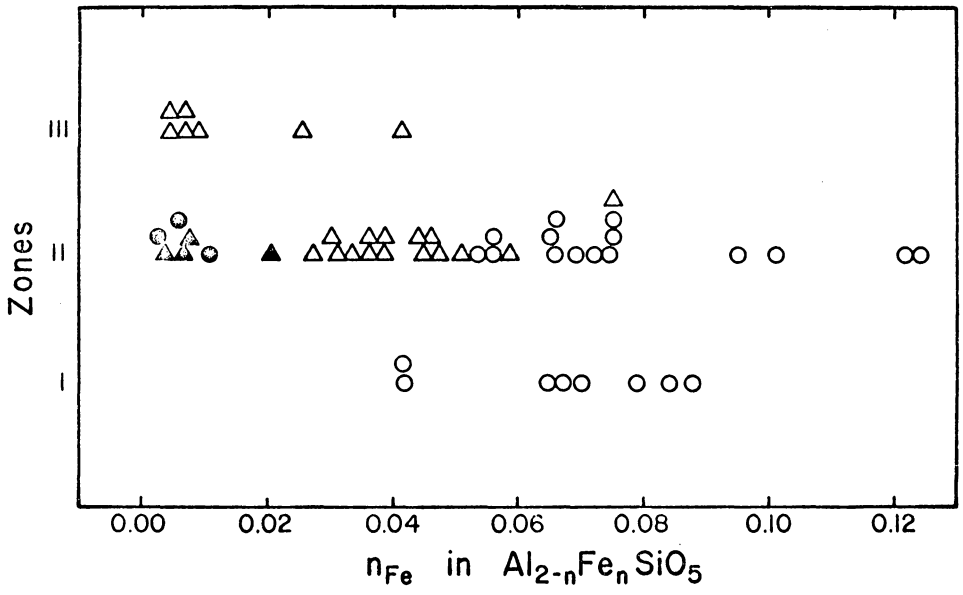
Zones
III
II
I
0.00
0.02
0.04
0.06
0.08
0.10
0.12
n_{Fe} in $Al_{2-n}Fe_nSiO_5$

Figure 20. Iron content of coexisting Snyder Group aluminum silicates (Table 1) expressed as n_{Fe}, where n_{Fe} is $Al_{2-n}Fe_nSiO_5$. Number within the square is the percentage of modal sillimanite/sillimanite + andalusite for each coexisting aluminum silicate pair. Numbers with each line segment are the distribution coefficients for that particular slope.

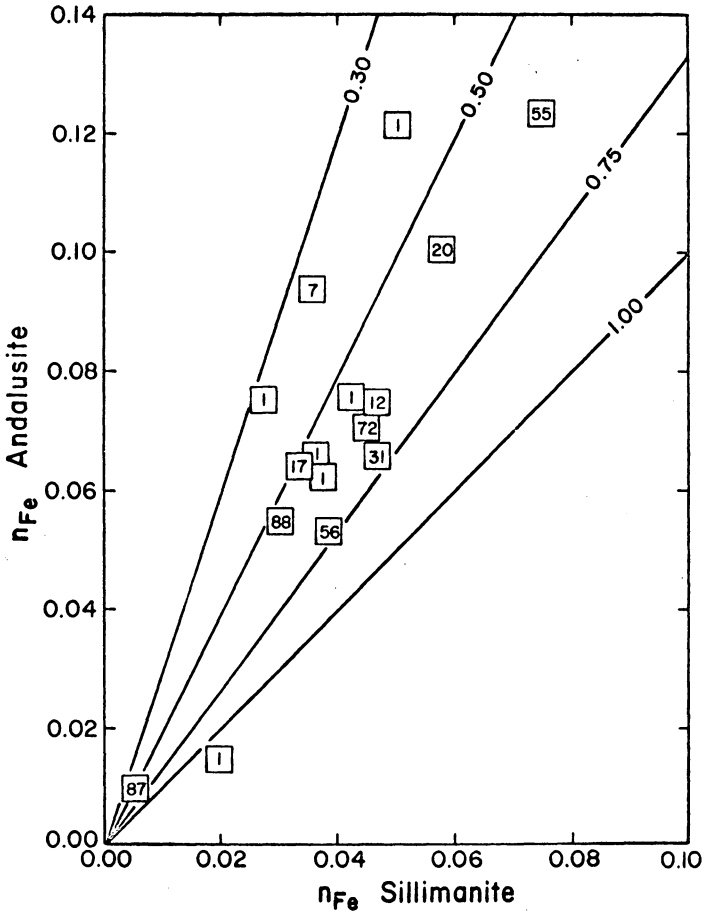
0.14
0.12
0.10
0.08
0.06
0.04
0.02
0.00
0.00
0.02
0.04
0.06
0.08
0.10
n_{Fe} Andalusite
n_{Fe} Sillimanite
0.30
0.50
0.75
1.00
1
55
20
7
1
1
12
72
1
17
1
31
88
56
1
87

distribution coefficient n_{Fe}andalusite/n_{Fe}sillimanite, is not constant but varies between 0.3 and 0.8. Aluminum silicate pairs show generally increasing coefficients with increasing metamorphic grade as reflected in the increasing sillimanite percentage of total aluminum silicate. This changing distribution coefficient with temperature is what could be expected for the equilibrium distribution of a component (Fe) between two crystalline solutions such as andalusite and sillimanite (Saxena, 1973). Difficulties in this treatment arise from working only on the extreme iron-poor compositional end of the crystalline solutions, with the compositional uncertainty of small amounts of iron, and the uncertainty in the qualitative estimate of temperature based on the modal fraction of sillimanite.

In zone II, the replacement of chiastolite andalusite by sillimanite and the intimate intergrowth of andalusite and sillimanite suggests that the andalusite-sillimanite transition is taking place by polymorphic transformation. The simple mineralogies of most rocks involved offer little in the way of other intermediate reactions leading to the appearance of the sillimanite. Production of sillimanite by the breakdown of muscovite + quartz is uncommon as most muscovite decomposed in the andalusite field. The width of zone II, the systematic increase of sillimanite at the expense of andalusite across the zone, and the systematic iron partitioning between the andalusite and sillimanite are features consistent with a multivariant andalusite + sillimanite phase field. Metastable persistence of andalusite could be expected to behave in a more arbitrary manner. Several causes may contribute to an existence of a multivariant phase field for an otherwise simple

polymorphic transformation. Because the free energy and entropy differences of the andalusite-sillimanite transition are very small, the stability relations in terms of temperature and pressure may be greatly altered by minor element partitioning, grain size, surface energy, strain energy, and order-disorder of Al-Si in sillimanites.

Feldspars

Potassium feldspar is very abundant in the Snyder Group quartz and arkosic arenites. Some of it is the result of prograde metamorphism from the breakdown of muscovite + quartz, but most are original detrital grains. Most of the potassium feldspars are colorless except for pink detrital grains and those of zone III. Optically, potassium feldspar varies texturally consisting of grid-twinned microcline with or without string microperthite, orthoclase with or without string microperthite, and sanidine. Compositionally (Table 7) it has a restricted compositional range of Or_{75} to Or_{97}. As the exsolution is very fine, these represent bulk compositions. Figure 21 shows the metasedimentary feldspars on the An-Ab-Or compositional triangle with tie lines drawn to coexisting plagioclases. It is evident that there is little ternary solid solution as would be expected for coexisting feldspars under metamorphic conditions of several hundred degrees (Seck, 1971). Some feldspar compositions may be largely inherited from their detrital precursors.

Examination by single crystal methods of 13 Snyder Group specimens revealed cryptoperthites of both triclinic and monoclinic potassium feldspar with sodium-rich plagioclase. The data are summarized on an

Figure 21. Compositions of plagioclase and potassium feldspars of the Snyder Group metapelites in the Or-Ab-An system with tie lines to co-existing feldspars. Symbols: circles, quartzites; squares, graphite-sulfide siltstone; triangles, iron formation. Not all of the potassium feldspars of Table 10 are plotted.

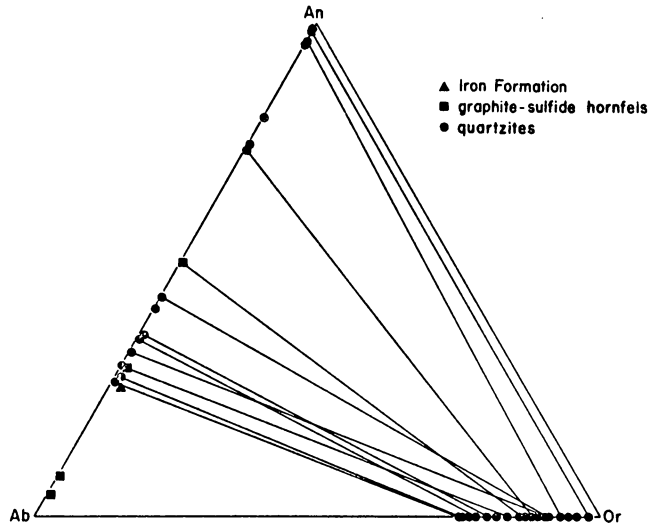
An
Ab
Or
▲ Iron Formation
■ graphite-sulfide hornfels
● quartzites

$\alpha^*\gamma^*$ plot (Fig. 22). The potassic phase ranges from high or low sanidine to nearly maximum microcline, with no systematic variation either with metamorphic grade or with composition. For the monoclinic specimens, the diffraction maxima consist of a central spot with monoclinic geometry from which short diffuse streaks extend along row lines. Long exposure x-ray photographs revealed the diffuse streaks to be part of diffuse layer lines which extend entirely along lattice rows. While formally considered to be monoclinic, alkali feldspars showing diffuse streaks consist of triclinic unit cells irregularly and periodically twinned on the albite and pericline laws. The α^* and γ^* angles of the albite-twinned phase are consistent with low plagioclases whose An and Or contents are less than 10 mole percent. The coexisting potassium phase is nearly pure potassium feldspar as determined from a^*, α^*, and γ^*. These compositions determined by reciprocal lattice parameters are subject to considerable uncertainty because of possible coherent strain of the lattices. In summary, the observations on the potassium feldspars are consistent with a series of transformations of the original microcline, orthoclase, or sanidine towards an assemblage of epitaxial maximum microcline and low sodium plagioclase arrested at various stages of size development as the result of difficult kinetics of exsolution.

The potassium feldspars coexisting with plagioclase show a widening of the compositional range with increasing metamorphic grade (Fig. 23). This can be interpreted as a result of the narrowing of the solvus with the plagioclase feldspars with increasing temperature. Particularly, K-rich alkali feldspars may reflect inherited compositions of detrital grains. Application of experimentally determined solvi of

Figure 22. Lattice angles α^* and γ^* for sodic and potassic phases in cryptoperthites from the lower and upper quartzites of the Snyder Group. End points and reference compositions are from Smith (1974).

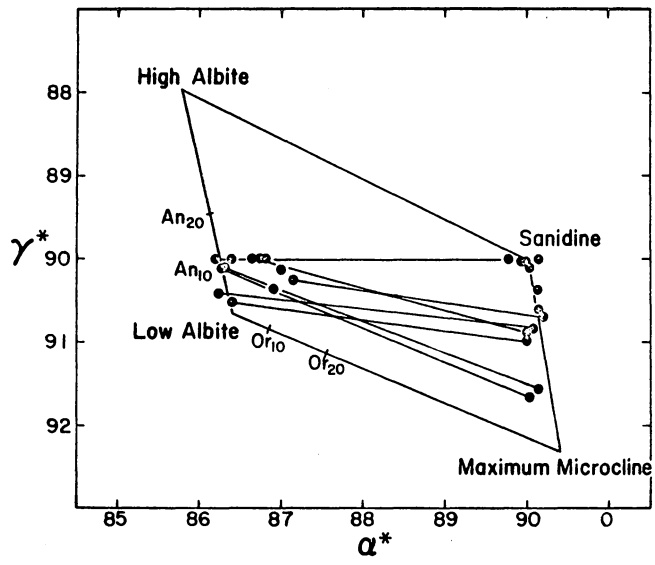
High Albite
Sanidine
Low Albite
Maximum Microcline
An20
An10
Or10
Or20
88
89
90
91
92
γ*
85
86
87
88
89
90
0
α*

Figure 23. Histograms of Snyder Group potassium feldspar compositions (Table 10) by metamorphic zones.

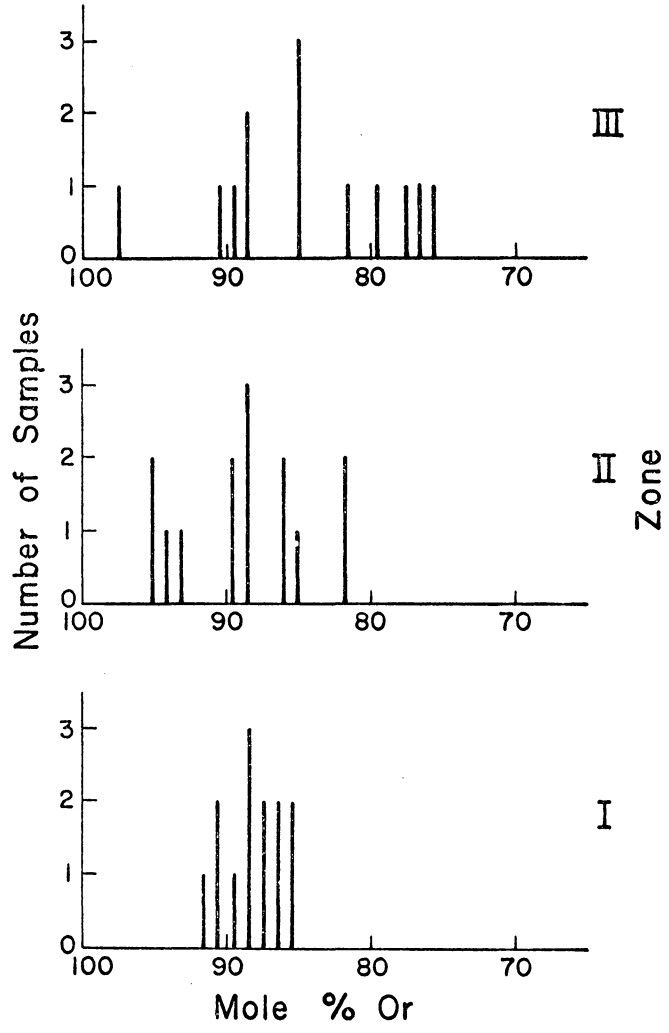
3
2
1
0
100
90
80
70
III
II
I
Zone
Number of Samples
Mole % Or

alkali feldspars at 5 kb is difficult as the coexisting plagioclases are labradorites to anorthites and would yield erroneously low temperatures. The nearest approach to common experimental conditions are the zone I potassium feldspars that coexist with oligoclase. Using the 5 kb schematic subsolidus phase diagram of Martin (1974), the potassium feldspar compositions of zone I would indicate temperatures of 500° to 550°C, in fair agreement with temperatures thought to prevail at that grade.

Changes in plagioclase compositions with metamorphic grade are less well documented. Extinction angles on a-sections of zones I and II plagioclases indicate they are oligoclases and andesines. Plagioclases of zone III are generally bytownites and anorthites.

Opaque minerals

In the lower quartzite, ilmenite is the dominant opaque accessory mineral, occurring as homogeneous anhedral to subhedral grains and less frequently as euhedral grains. Magnetite and ilmenite, containing lenses of exsolved hematite, are present as anhedral grains and are less abundant. Weathered ilmenite is commonly replaced by hematite and rutile in the form of irregular mats. Magnetite contains intergrowths of ilmenite in a trellis microtexture. Occasionally, beads of dark green hercynite form at the ilmenite-magnetite boundaries. In the higher grades of metamorphism, green hercynite rims the magnetite. Pyrite occurs as subhedral to euhedral grains frequently surrounded by colloform aggregates of secondary iron oxides. Pyrrhotite is anhedral and contains intergrowths of chalcopyrite

and pentlandite. The pyrrhotite alters to marcasite in the more weathered specimens. Chalcopyrite more commonly occurs as separate grains also surrounded by secondary iron oxides.

In the graphite-sulfide hornfels and upper quartzite, graphite and pyrrhotite are the abundant opaque minerals and can make up to 10 percent of the rocks. Cubes of pyrite occur in the most pyrrhotite-rich rocks and may be of secondary origin. Sphalerite containing intergrowths of chalcopyrite is common in the graphite-sulfide hornfels. An analyzed sphalerite (SN 7201) contained 9.89 weight percent iron. Ilmenite, chalcopyrite, and magnetite are present in small amounts. Alteration of the sulfides to secondary iron oxides is common.

Textural evidence suggests that most of the ilmenite and magnetite were originally of detrital origin. During the contact metamorphism and subsequent retrograde metamorphic reequilibration, magnetite was preserved, showing that conditions of oxygen fugacity remained between those of the magnetite-hematite and magnetite-quartz-fayalite buffers.

The analyzed sphalerite (SN 7201) coexists with pyrite and pyrrhotite. Scott and Barnes (1971) have shown that sphalerite buffered by pyrite and pyrrhotite becomes less iron-rich with increasing pressure and is a potential geobarometer. Scott (1973) has shown that below 600°C sphalerite is nearly only pressure dependent and that 17 mole percent FeS in sphalerite corresponds to a pressure of 3 ± 1 kb. As the specimen occurs at the sillimanite isograd with a temperature estimate of 670°C at 4 kb total pressure, a lower pressure would be indicated according to the work of Scott (1973). Discrepancy in the

pressure estimates given by the silicates and sulfides probably results from reequilibration of the sulfides during retrograde metamorphism.

The distribution of iron sulfides in the Snyder Group shows both pyrite and pyrrhotite the iron sulfides at the lower grades of metamorphism, whereas pyrrhotite is the dominant or sole iron sulfide at higher grades. This would be consistent with the idea of desulfurization, analogous to dehydration and decarbonization, during progressive metamorphism. Observations by Neumann (1950), Muraro (1966), Antun (1967), and Han (1968) support this phenomena, and both French (1968) and Carpenter (1974) have even considered an isograd based on the prograde appearance of pyrrhotite.

Noting the common occurrence of pyrite and pyrrhotite together at a number of metamorphic grades and the alternating pyrite and pyrrhotite-bearing beds in the Snyder Group, it appears that the fluid phase with respect to sulfur is buffered by the local mineral assemblage. It would be unlikely for the two iron sulfides to exist over a considerable temperature range if the sulfur fugacity were externally controlled. Evidently the temperatures of zone III exceeded the ability of the mineral assemblages studied to buffer the fluid composition so that pyrite was still stable.

Metaigneous Rocks

The only metaigneous rock found at all metamorphic grades is the Snyder breccia and consequently it is the most studied. Barton and Barton (1975) reported it to be chemically a granodiorite and it corresponds very closely to a Cenozoic andesite (Chayes, 1975).

Other metabasites include the Hill 1300 N amphibolite, the Hill 1100 gabbro, the Hill 800 ultramafic and some metadiabases. The progressive mineral changes of the Snyder breccia are summarized in Figure 24. Other metabasites at similar grades show similar mineral assemblages.

The metabasites occurring in zone Ia and in the basement rocks show the mineral assemblage green actinolitic hornblende + chlorite + biotite + epidote + plagioclase + quartz, which is characteristic of greenschists. Muscovite, or at somewhat higher grades, potassium feldspar, may be present. Epidote and chlorite are minor. The plagioclase is an oligioclase or andesine. Titanite occurs as granular grains surrounding ilmenite. Large, subhedral apatites with cloudy cores are common and probably reflect the original mineralogy.

Just before zone Ib, chlorite disappears, which marks the beginning of the amphibolite facies. Epidote is still present in minor amounts. Plagioclase is usually andesine; however, some rocks contain labradorite. The Snyder breccia locally contains calcic clinopyroxene. Liou *et al.* (1974) have shown that chlorite disappears for a basaltic composition between 550° and 575°C for the pressure interval 2 to 5 kb. These temperatures are compatible with the estimated conditions for the appearance of cordierite in zone Ib reviewed in the section on metapelites.

With advancing metamorphism, cummingtonite appears in the lower part of zone II. The cummingtonite is colorless, well-twinned, and forms continuous rims on a pleochroic green, untwinned hornblende that contains exsolution lamallae of cummingtonite. Its occurrence as rims on the hornblende suggests that the hornblende is not part of the

Figure 24. Progressive mineral changes in the metaigneous rocks intruding the Snyder Group with increasing metamorphic grade.

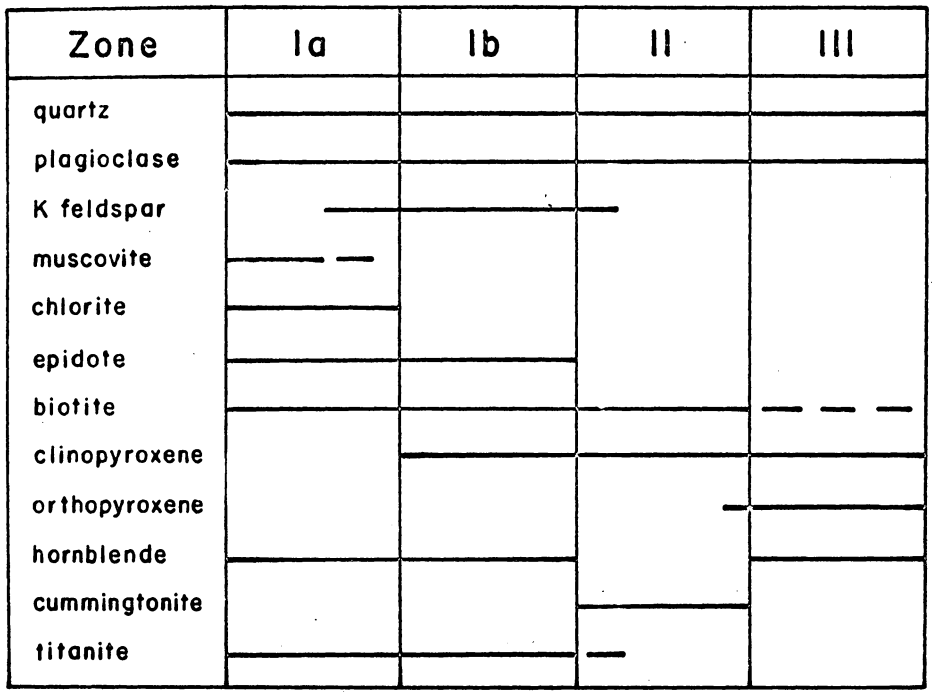
Zone
Ia
Ib
II
III
quartz
plagioclase
K feldspar
muscovite
chlorite
epidote
biotite
clinopyroxene
orthopyroxene
hornblende
cummingtonite
titanite

equilibrium assemblage. The associated plagioclase is labradorite. Epidote has disappeared by this time.

Toward the upper part of zone II, orthopyroxene appears, marking the beginning of the granulite facies. Clinopyroxene is abundant. The plagioclase is bytownite or anorthite. The amphibole is a brown hornblende and, like biotite, may or may not be present.

According to the nomenclature proposed by Leake (1968), the calcic amphiboles in the Snyder breccia would be magnesio- and ferro-hornblendes with some actinolitic and ferro-actinolitic hornblendes. One amphibole from the Hill 1300 amphibolite (SN 47231) would be termed a magnesian hastingsitic hornblende. The subcalcic amphiboles of zone II are cummingtonites. Analyses are given in Table 2 and their projected atomic percentages of Ca, Fe, and Mg are plotted in Figure 25. The calcic amphiboles of zones I and II are pleochroic in colors of green, whereas those of zone III are brown. No obvious change in chemistry is noted to explain the color change.

Biotite is ubiquitous and occurs as anhedral to subhedral, randomly oriented plates either disseminated or in segregations. The pleochroic colors are variable in shades of brown or red-brown; biotites pleochroic in shades of green are restricted to zone I. Biotite analyses are given in Table 3. As illustrated by Figure 16, biotites of the Snyder breccia lie for the most part in the annite quadrant.

Garnets infrequently occur in zones II and III in metaigneous rocks other than the Snyder breccia. Analyses (Table 6) show them to be almandine-spessartine garnets with slightly higher pyrope contents than garnets of the metapelites (Fig. 14).

Figure 25. The amphibole quadrilateral showing the compositions of the amphiboles in the Kiglapait contact aureole (Table 2). Tie lines connect coexisting amphibole pairs. Symbols: triangles, marbles and calc-silicates; diamonds, metapelites; circles, metabasites; squares, iron formation.

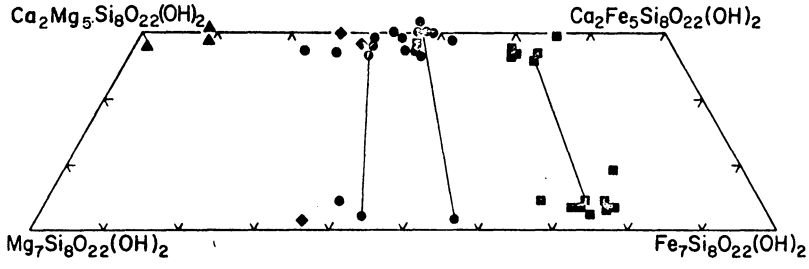
$Ca_2Mg_5Si_8O_{22}(OH)_2$
$Ca_2Fe_5Si_8O_{22}(OH)_2$
$Mg_7Si_8O_{22}(OH)_2$
$Fe_7Si_8O_{22}(OH)_2$

The oxides ilmenite and magnetite are the common accessories of the metabasites. Magnetite occurs at low grades as clusters of euhedral crystals and inclusions in recrystallized plagioclase phenocrysts. Locally, magnetite shows trellis intergrowths of ilmenite. Ilmenite commonly shows hematite intergrowths and inclusions of apatite. The sulfides pyrrhotite, pyrite, and chalcopyrite are ubiquitous and may be altered to secondary marcasite, hematite, or goethite. Pyrrhotite was observed to contain intergrowths of pentlandite. The Hill 800 layered dike contains chalcopyrite-bornite grains. Graphite is observed in some metabasites.

The pyroxenes of metaigneous rocks have a large compositional range owing to the diverse bulk compositions. The majority of analyses are for pyroxenes of the Snyder breccia. These show a narrow range of Fe/Mg ratios: Fs_{21-27} for the clinopyroxenes and Fs_{51-60} for the orthopyroxenes (Fig. 15). The clinopyroxenes in zones Ib and II generally contain less wollastonite component than those of zone III coexisting with orthopyroxene. The pyroxenes of zone III in the Snyder breccia possess a texture resembling the spinifex texture of ultrabasic rocks. The pyroxenes are elongate, poikilitic, and are arranged in branching or radiating orientations. Inclusions are plagioclase and quartz. The orthopyroxenes are tan, clinopyroxenes brown to black. The coexisting pyroxenes of zone III show well-developed, very fine exsolution lamellae or orthopyroxene in clinopyroxene and clinopyroxene in orthopyroxene.

An expression for the equilibrium temperatures in terms of the compositions of coexisting orthopyroxene and clinopyroxene has been

developed by Wood and Banno (1973) and critically evaluated for granulite facies rocks by Hewins (1975). Temperatures were calculated for the Snyder breccia (Table 13) using a computer program written by Hewins (1975) using the assumptions of Wood and Banno (1973) on site occupancies, their equation number 27, and the compositional data for coexisting pyroxenes of Table 11. The estimated temperature obtained for the initial appearance of coexisting pyroxenes is 809°C (SN 72126). Estimated temperatures for the two-pyroxene assemblages of the Snyder breccia in zone III are between 841° and 866°C. These rocks are interlayered with the pelitic garnet-cordierite-orthopyroxene assemblages for which temperatures of between 840° and 860°C are obtained using the experimental curves of Hensen and Green (1973). The similarity of temperatures from the two methods is somewhat remarkable. There is also good agreement of these granulite facies temperatures with those obtained by Hewins (1975) for other localities. The remaining temperatures in Table 13, which are greater than 950°C, are for various two-pyroxene metamorphic assemblages of Snyder Group xenoliths in the Kiglapait Coast migmatites, very close to the Kiglapait IBZ contact. NC 7425 is just a few meters from the contact.

Iron Formation

Quartz-inverted pigeonite-spessartine-almandine garnet form the dominant mineral assemblage of the iron formation. Grunerite or manganoan grunerite is important at the lowest grades of metamorphism. Changes in the progressive metamorphic mineral assemblages (Fig. 26)

Figure 26. Progressive mineral changes in the iron formation of the Snyder Group with increasing metamorphic grade.

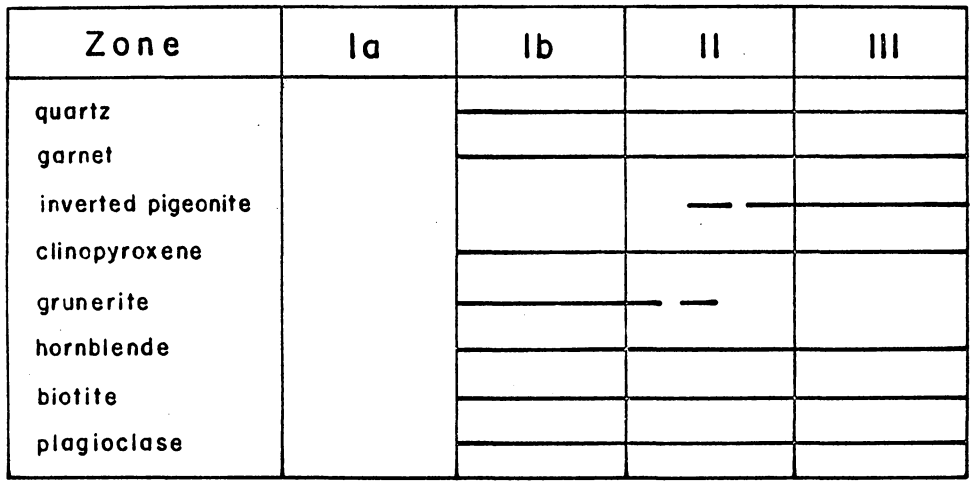
Zone
Ia
Ib
II
III
quartz
garnet
inverted pigeonite
clinopyroxene
grunerite
hornblende
biotite
plagioclase

are rather limited, consisting mainly of the dehydration of the remaining grunerite to produce pyroxene by the reaction:

$$\text{amphibole} \rightleftarrows \text{pyroxene} + \text{quartz} + H_2O \qquad (13)$$

Using the reactions in the metapelites as a guide, the reaction temperature must be between 600° and 650°C. Popp (1975) estimates this reaction temperature to lie between 710° and 765°C at 2 kb for amphiboles on the $Mg_7Si_8O_{22}(OH)$-$Fe_7Si_8O_{22}(OH)_2$ join experimentally studied at conditions of the quartz-magnetite-fayalite buffer. The lower temperatures in the Snyder Group likely result from either the manganese content of the natural phases or conditions of water pressure less than total pressure, or both. Minor ferro-actinolite or ferrohornblende, manganoan augites and hedenbergites, biotite, plagioclase, carbonate, graphite, and tourmaline are developed only as accessories.

Important retrograde metamorphic effects are the exsolution and inversion of original pigeonite into much or all of the now present manganoan ferrohypersthene (Table 10) and the formation of hydrous silicates, mostly grunerite, at the expense of the prograde minerals. The orthopyroxenes are unusually large, up to 2 cm, in comparison to other metamorphic minerals in the iron formation and are often flattened perpendicular to the banding, constituting the entire dark band of the iron formation. These large orthopyroxene grains contain two sets of Ca-pyroxene exsolution lamellae. The thicker, earlier lamallae have diverse orientations, having formed along the (001) of several preexisting pigeonite grains which have inverted into the single large ferrohypersthene grain. The thinner, later lamellae are parallel to

(100) of the ferrohypersthene, having exsolved from the ferrohypersthene after it had inverted from the pigeonite. The orthopyroxenes exhibit a range of calcium contents (Table 10, see Fig. 15), reflecting the development of the exsolution of the pyroxenes probed. The group of pyroxenes with low calcium contents represents the composition of the orthopyroxenes, the exsolution lamellae being avoided, while the pyroxenes with the higher calcium contents are orthopyroxenes where very fine, abundant exsolution lamellae were unavoidable and thus represent the original pigeonite composition before unmixing and inversion. The pigeonites contained between 3 and 4 weight percent CaO, corresponding to 7 to 9 atom percent wollastonite; the manganese component varied between 8 to 12 atom percent and ferrosilite between 59 and 65. The orthopyroxene contains from 0.9 to 4.9 wollastonite, 4.8 to 15.9 manganese component, and 49.9 to 70.9 ferrosilite. The fine size of the exsolved Ca-pyroxenes made them impossible to analyze with the microprobe.

Some pyroxene grains retain the optical properties of pigeonite, having small positive 2V's. Closer examination of these grains revealed a very fine lamellar texture. They are most likely inverted pigeonites on a very fine scale.

Pyrrhotite is the dominant opaque mineral and occurs as small, spheroidal grains. Very minor amounts of ilmenite, magnetite, chalcopyrite, and graphite also occur. Besides some secondary iron oxides associated with the above phases, secondary manganese oxides in veins were also observed. On the whole, opaque accessories are rare in the iron formation.

The garnet + pigeonite assemblage of the Snyder Group iron formation is quite different than the pigeonite + magnetite assemblage of the Biwabik iron formation (French, 1968; Bonnischen, 1961, 1975; Morey *et al.*, 1972), and pigeonite + olivine + magnetite of the Gunflint iron formation (Simmons *et al.*, 1975) produced by the contact metamorphism of the Duluth Complex at pressures of 2 to 4 kb and a temperature maximum somewhat greater than 800°C. The differences are apparently the result of bulk composition. The Snyder Group iron formation is a silicate iron formation not containing the abundant oxide minerals found in the others and has a higher aluminum content which is contained in the garnet. Davidson and Mathison (1973) have found that garnet forms in the iron formations of the Quairading district of Australia with high aluminum contents under granulite facies metamorphism. Morey *et al.* (1972) have made similar arguments for the local distribution of garnet in the Biwabik iron formation. The occurrence of garnet rather than the oxidized assemblage spinel + quartz could depend on lower oxygen fugacities.

Calcareous Rocks

Three types of calcareous rocks of the Snyder Group quartzite-marble are distinguished on the basis of their major mineralogies: (1) marbles, (2) quartz + diopside-bearing calcsilicates, and (3) enstatite-bearing calcsilicates. They form segregated layers in the quartzite marble as a result of the original sedimentary structures and the metamorphism. Mineral changes with progressive metamorphism are shown in Figure 27.

Figure 27. Progressive mineral changes in the calcareous rocks of the Snyder Group with increasing metamorphic grade.

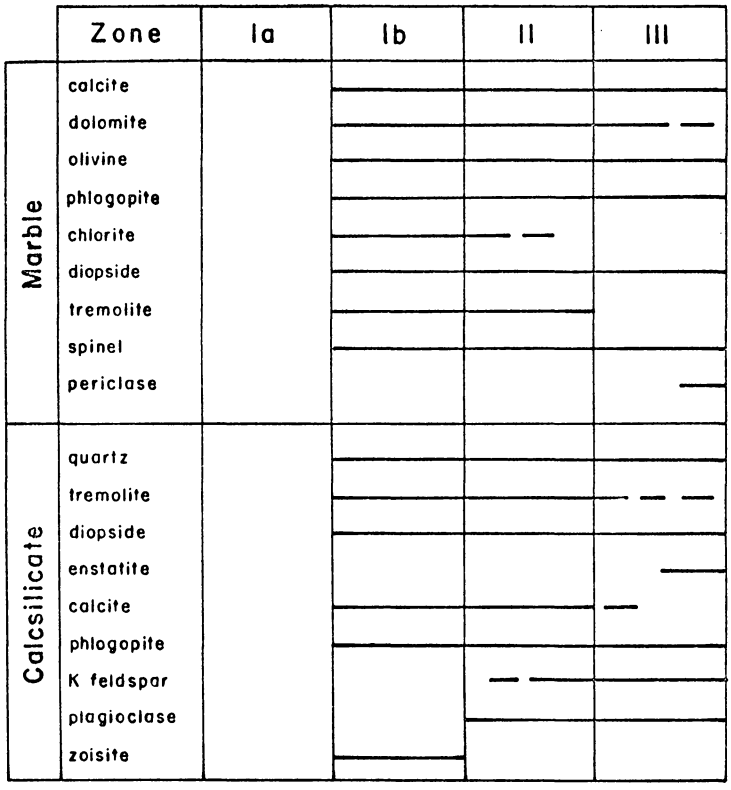
Zone
Ia
Ib
II
III
Marble
calcite
dolomite
olivine
phlogopite
chlorite
diopside
tremolite
spinel
periclase
Calcsilicate
quartz
tremolite
diopside
enstatite
calcite
phlogopite
K feldspar
plagioclase
zoisite

The marbles contain both calcite and dolomite, with calcite being the more abundant. Only in zone I does dolomite have an abundance comparable to calcite. Subhedral olivine and diopside are the important silicates and are present at all metamorphic grades in the marbles. Analyses of the olivine (Table 8) in the marbles show it to be forsterite. Olivine in the rocks transitional to the iron formation is more intermediate in composition and is manganiferous (SN 72128, Table 8). The clinopyroxenes (Table 11) are diopsides and occasionally augites. Spinel, chlorite, phlogopite, and tremolite are present in varying amounts. Brucite pseudomorphs after originally octahedral periclase are present at high grades. Accessories include titanite, apatite, pyrrhotite, graphite, and chalcopyrite. The pyrrhotite is occasionally rimmed by magnetite or marcasite. Olivine is frequently serpentinized with networks of magnetite or pyrrhotite threaded through the serpentine. The abundance of chlorite and spinel indicates that the marbles are aluminous. The presence of potassium in some rocks causes the appearance of phlogopite at the expense of chlorite.

The quartz-diopside calcsilicates make up a large proportion of the quartzite marble. They are generally banded, consisting of differing proportions of randomly oriented quartz and diopside and may contain small amounts of tremolite, phlogopite, potassium feldspar, plagioclase, carbonate, titanite, epidote or ilmenite. Oriented intergrowths of tremolite on corroded diopside are common at high grade, indicating that most or all of the amphibole is secondary in these rocks. Diopsides of zone III are exsolved with lamellae of orthopyroxene.

The calcareous rocks on Snyder Island represent the lowest grade metamorphism of these rocks, the beginning of the amphibolite facies. Already diopside, forsterite, and spinel have appeared and tremolite is disappearing. The phase assemblage forsterite + diopside + tremolite + calcite + dolomite suggests conditions of either of the invariant points, 1 (Fig. 28). The appearance of these phases at temperatures of about 550°C, based on the associated pelitic assemblages, is possible only under conditions of low X_{CO_2} or fluid pressures less than total pressures. The contention that conditions were those of the water-rich invariant point, 1, is further substantiated by the presence of epidote + diopside + tremolite assemblages, which indicates conditions on the low X_{CO_2} side of the reaction:

$$\text{zoisite} + CO_2 \rightleftarrows \text{anorthite} + \text{calcite} + H_2O \qquad (14)$$

The calculated position for this reaction (Johannes and Orville, 1974) in Figure 28 is for the zoisite composition $Ca_2Al_3Si_3O_{12}(OH)$ which passes almost through the water-rich invariant point, 1. Substitution of iron for aluminum will move the reaction to higher X_{CO_2} values. The existence of dolomite rather than periclase + calcite would place a lower limit on X_{CO_2} of greater than 0.01.

With increasing metamorphic grade, tremolite disappears in the marbles and in quartz + diopside-bearing calcsilicates by zone III as the result of the completion in different rocks of one of the following reactions:

$$\text{tremolite} + \text{dolomite} \rightleftarrows \text{forsterite} + \text{calcite} + \text{vapor} \qquad (15)$$

$$\text{tremolite} + \text{calcite} \rightleftarrows \text{diopside} + \text{forsterite} + \text{vapor} \qquad (16)$$

Figure 28. Isobaric T-X_{CO_2} diagram for siliceous carbonates at P_{CO_2} + P_{H_2O} = 4000 bars. Reaction curves are labeled and the numbered invariant points indicate the five-mineral assemblages: (1) calcite + dolomite + tremolite + diopside + forsterite; (2) quartz + calcite + dolomite + tremolite + diopside. The T-X equilibria are calculated from equilibrium constants obtained from the equations of Skippen (1971, 1974) and Johannes and Orville (1974). The breakdowns of calcite + quartz and dolomite were calculated from the data of Greenwood (1967) and Harker and Tuttle (1955) respectively. Ideal mixing of water and carbon dioxide was assumed. Values for water fugacity were obtained from Burnham *et al.* (1969) and fugacity coefficients for carbon dioxide from Burnham and Wall (1974). Locations of the invariant points are derived from the intersections of the calculated reactions. The reactions shown are only a few of the many reactions possible in the system.

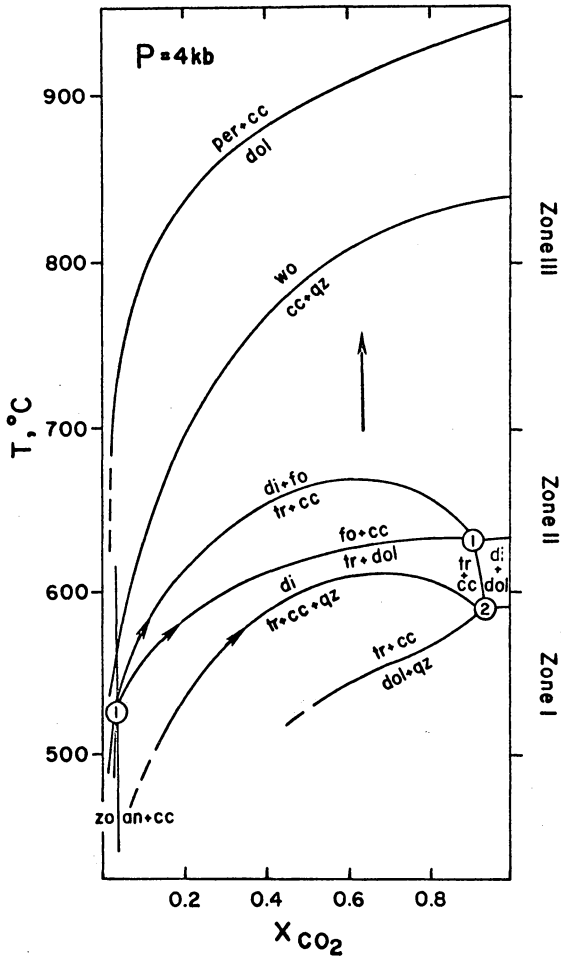
P=4kb
900
800
700
600
500
T, °C
per+cc
dol
wo
cc+qz
di+fo
tr+cc
fo+cc
tr+dol
di
tr+cc+qz
tr+cc
dol+qz
tr
+
cc
di
+
dol
1
2
1
zo an+cc
0.2
0.4
0.6
0.8
X CO2
Zone III
Zone II
Zone I

$$\text{tremolite} + \text{calcite} + \text{quartz} \rightleftarrows \text{diopside} + \text{vapor} \qquad (17)$$

The persistence of tremolite in the calcsilicates in zone I and II is the result of either being part of an unreactive assemblage (*i.e.*, one of the reactants is not present) or by buffering of the decomposition reactions during progressive metamorphism. In P-T-X_{CO_2} space, the equilibrium conditions for such a buffered reaction are on a divariant surface and the paths of metamorphism follow the surfaces as long as the divariant assemblage is present. Thus, with increasing metamorphism of these rocks, the X_{CO_2} of the vapor phase is increasing, the composition of the vapor being controlled by the reacting solids until one of the reactants is used up. The presence of minor tremolite in the temperature conditions of zone II, about 675°C, suggests that some assemblages were able to buffer the fluids to compositions near their thermal maxima.

The water-rich nature of the vapor in open fissures of the zone I calcareous rocks is indicated by the calcite + wollastonite + diopside + epidote $\pm$ garnet vein assemblage located in the marbles and metabasites on the northeast corner of Snyder Island. The production of wollastonite by the reaction:

$$\text{calcite} + \text{quartz} \rightleftarrows \text{wollastonite} + \text{vapor} \qquad (18)$$

can proceed at those temperatures only at low X_{CO_2}. Figure 28 shows reaction 18 to pass close to the postulated conditions of these rocks at the invariant point, 1. The low X_{CO_2} is also attested to by the presence of epidote according to reaction 14. Much of the material in the larger veins was supplied by reaction with the enclosing metabasites as evidenced by zoning with the wall rocks and inclusions.

Chlorite also disappears by zone III, most likely as the result in different rocks of any of the following reactions:

chlorite + calcite $\rightleftarrows$ diopside + forsterite + spinel + vapor (19)

chlorite + calcite $\rightleftarrows$ tremolite + forsterite + spinel + vapor (20)

chlorite $\rightleftarrows$ forsterite + spinel + vapor (21)

Based on their occurrence in the Snyder Group, these reactions appear to take place over the same temperature range as those leading to the disappearance of tremolite. Similarly, the persistence of chlorite is most likely a result of buffering of the reactions.

In zone III within 0.25 km of the IBZ contact, euhedral periclase appears as a result of the decomposition of the dolomite of a dolomitic marble:

dolomite $\rightleftarrows$ periclase + calcite + vapor (22)

The periclase has since retrograded to brucite. The estimated temperature of reaction from the two-pyroxene geothermometer of associated metabasites is greater than 950°C. This high estimate for the temperature of reaction indicates the fluid present was CO_2 rich (Fig. 28). Conditions for the breakdown of dolomite exceed those for calcite + quartz, yet wollastonite has not been found in the quartzite marble of zone III. The lack of wollastonite is the result of inappropriate bulk composition. The marbles do not contain quartz, and the quartz + diopside-bearing calcsilicates contain only rare calcite that was used up in diopside-producing reactions at lower grades.

The enstatite + diopside and enstatite + diopside + tremolite-bearing calcsilicates are restricted to blocks and boundinaged layers embedded in the Kiglapait Coast migmatites. The clinopyroxenes are diopsides, the orthopyroxenes enstatites and bronzites (Table 11). Coexisting pyroxene pairs are shown in Figure 15. Small amounts of plagioclase, phlogopite, carbonate, quartz, and potassium feldspar are present. The quartz + potassium feldspar assemblage has a granophyric texture which may represent an interstitial quenched melt rather than enstatite-quartz equilibrium.

The mineralogy and occurrence of the enstatite-bearing calcsilicates suggest they are calcareous rocks that have undergone extensive metamorphic differentiation. There is little evidence of the reactions leading to the present assemblages, but most likely involve the dehydration of tremolite and decarbonization of the carbonate. The small amount of micrographic intergrowth of quartz and potassium feldspar is interesting in light of Luth's (1967) experimental studies on the stability of phlogopite and may represent the melting of phlogopite according to the reaction:

$$3 \text{ tremolite} + 1 \text{ phlogopite} \not\geq 9 \text{ diopside} + 9 \text{ enstatite} + 1 \text{ melt (potassium feldspar)} \quad (23)$$

For the magnesium end-members, the melt would be of potassium feldspar composition. Excess SiO_2 in the form of quartz could be generated by deficiencies of potassium in the phlogopite and aluminum going into the pyroxenes. The small amount of melt could migrate from the

calcsilicates to the enclosing migmatites. Temperature estimates on this reaction would be about 950°C (Luth, 1967).

Partial Melting in the Contact Aureole

In zone III, the border breccias and Kiglapait Coast migmatites are interpreted as having crystallized from partial melts. The border breccias are for the most part cordierite-bearing granodiorites. One is a quartz gabbro. They contain xenoliths of Snyder Group rocks and rocks of the marginal granulites of the Kiglapait intrusion. Otherwise they are internally structureless and appear to have been emplaced at their present level. The Kiglapait Coast migmatites are biotite- and orthopyroxene-bearing granodiorites exhibiting varied migmatitic textures. The dark portions consist of orthopyroxene-cordierite-plagioclase-biotite assemblages. Embedded within the Kiglapait Coast migmatites are xenoliths or blocks of Snyder Group lithologies, mafic, and ultramafic rocks. The Kiglapait Coast migmatites are partial melts that have not migrated from their site of origin.

These anatectic melts lie within a kilometer of the Inner Border Zone of the Kiglapait intrusion. Clinopyroxene-orthopyroxene (NC 7411, 7416, 7425, 7447; Table 13) and garnet-cordierite (NC 7449) pairs indicate temperatures greater than 950°C. In the calcareous rocks of the Snyder Group xenoliths, enstatite and periclase appear. At these temperatures a silicate melt could be generated with little water (Tuttle and Bowen, 1958). The Kiglapait Coast migmatites attest to generation of significant volumes of melt from the Tikkegharsuk migmatites and the presence of orthopyroxene attests to relatively

anhydrous conditions. In that part of the Snyder Group, which crops out from Cold Comfort Bay south-southwestward to the Avakutakh River, there is no evidence of *in situ* partial melting. Temperatures are estimated to be 850°C and less, and water pressures must have been small enough to prevent the generation of partial melts. By contrast, the Snyder Group lithologies preserved on the north coast of the Kiglapait Mountains are quartzites and calcite and periclase marbles. The lack of more granitic and pelitic members of the Snyder Group would suggest they underwent partial melting under conditions of the north coast and migrated from the more refractory members into the surrounding Kiglapait Coast migmatites.

Cordierite-bearing granitic rocks have been suggested to represent partial melting of pelitic materials (Flood and Shaw, 1973). Preliminary experimental work by Green (1976) suggests that cordierite-bearing granitic rocks were generated at less than 25 km depth (∿6 kb), whereas garnet-bearing rocks were derived at depths greater than 25 km. This is consistent with the pressure estimates in the aureole. Models for the production of anatectic melts (Brown and Fyfe, 1970) suggest that granodiorite magmas are generated at greater depths and higher temperatures than granitic magmas. In the Kiglapait contact aureole, it was the extremely high temperatures that were responsible for the granodiorites.

Summary

Experimental data applicable to the metapelites and metabasites show that the Snyder Group was subject to temperatures of 550° to

1000°C at a load pressure of about 4 kb. Water pressures varied from less than 1 kb to nearly 4 kb. The sequence of metamorphic facies is greenschist, amphibolite, granulite. This isobaric line of progressive metamorphism is shown on the phase diagram in Figure 12. The Snyder breccia at distances up to 6 km from the contact of the Kiglapait intrusion has mineral assemblages similar to those of zone Ia. As these rocks are too distant to be considered a part of the contact aureole, the country rocks were probably undergoing a regional thermal metamorphism in the low-pressure greenschist facies at the time of the emplacement of the Elsonian plutons. The lower temperature limit of the greenschist facies is usually taken at between 300° and 400°C with an upper limit of about 550°C (Winkler, 1967), the estimated temperature of the zone Ia-Ib boundary. A K-Ar age date on a hornblende from the basement rocks of 2.6 Gyr 15-20 km from the Kiglapait intrusion (Barton and Barton, 1975) similarly points to a lack of significant regional metamorphism during the emplacement of the Elsonian plutons.

Positioning of the zone boundaries shows the Kiglapait intrusion to be the heat source with mineral zoning in the aureole showing falling temperatures away from the intrusion. The upper metamorphic temperature limit of 1000°C is reasonable in view of the ambient temperature of the country rocks and the Kiglapait intrusion's basaltic composition, size, and magmatic convection during crystallization. The configuration of the zonal boundaries, metamorphic assemblages, and mineral geothermometers indicates that the Inner Border Zone, rather than the Outer Border Zone contact, acted as the intrusion margin. Metamorphic textures produced by incomplete metamorphic reactions

indicate radiation of the isothermal surfaces from the margin as a monotopic progressive metamorphism. Lack of penetrative deformation textures suggests the metamorphism to be static.

REFERENCES

Albee, A. L. and Chodos, A. A. 1969. Minor element content of co-existent Al_2SiO_5 polymorphs. *Am. J. Sci. 267*, 310-316.

Althaus, E. 1969. Experimental evidence that the reaction of kyanite to form sillimanite is at least bivariant. *Am. J. Sci. 267*, 273-277.

Antun, P. 1967. Sedimentary pyrite and its metamorphism in the Oslo region. *Norsk Geo. Tidsskr. 47*, 211-235.

Barager, W. R. A. 1974. The Seal Lake and Croteau volcanic rocks of Labrador. *In* Author's Abstracts, Geol. Assoc. Can. - Min. Assoc. Can., Ann. Meeting, 1974, p. 5.

Barker, F. 1961. Phase relations in cordierite-garnet-bearing Kinsman Quartz Monzonite and the enclosing schist, Lovewell Mountain Quadrangle, New Hampshire. *Am. Mineral. 46*, 1166-1176.

Barton, J. M. 1973. Progress of isotopic and geochemical investigations, Coastal Labrador, 1973. *In* Nain Anorthosite Project, Labrador, Field Rep. 1973, S. A. Morse (ed.), Univ. Massachusetts Contrib. 13, 19-28.

Barton, J. M., Jr. 1975. The Mugford Group Volcanics of Labrador: age, geochemistry, and tectonic setting. *Can. J. Earth Sci. 12*, 1196-1208.

Barton, J. M., Jr. and Barton, E. S. 1975. Age and geochemical studies of the Snyder breccia, coastal Labrador. *Can. J. Earth Sci. 12*, 361-370.

Beall, G. H., Hurley, P. M., Fairbairn, H. W., and Pinson, W. H., Jr. 1963. Comparison of K-Ar and whole-rock Rb-Sr dating in New Quebec and Labrador. *Am. J. Sci. 261*, 571-580.

Berg, J. H. 1971. The petrology of the outer and inner border zones of the Kiglapait layered intrusion. Unpubl. M.S. thesis, Franklin and Marshall College, Lancaster, Pa., 133p.

Berg, J. H. 1974. New stratigraphic sequence above the Snyder Group. *In* Nain Anorthosite Project, Labrador, Field Rep. 1973, S. A. Morse (ed.), Univ. Massachusetts Contrib. 13, 27-33.

Bonnischen, B. 1968. Metamorphic pyroxenes and amphiboles in the Biwabik Iron Formation, Dunka River Area, Minnesota. *Mineral. Soc. Am. Spec. Pap. 2*, 217-239.

Bonnischsen, B. 1975. Geology of the Biwabik Iron Formation, Dunka River Area, Minnesota. *Econ. Geol. 70*, 319-340.

Boone, G. M. and Wheeler, E. P., 2nd. 1968. Staining for cordierite and feldspars in thin section. *Am. Mineral. 53*, 327-331.

Boyd, F. R., Finger, L. W., and Chayes, F. 1969. Computer reduction of electron probe data. *Carnegie Inst. Washington Year Book 67*, 210-215.

Boyd, F. R. and Finger, L. W. 1975. Homogeneity of minerals in mantle rocks from Lesotho. *Carnegie Inst. Washington Year Book 74*, 519-525.

Brown, G. C. and Fyfe, W. S. 1970. The production of granitic melts during ultrametamorphism. *Contr. Mineral. Petrol. 28*, 310-318.

Brummer, J. J. and Mann, E. L. 1961. Geology of the Seal Lake Area, Labrador. *Geol. Soc. Am. Bull. 72*, 1361-1382.

Burnham, C. W., Holloway, J. R., and Davis, N. F. 1969. Thermodynamic properties of water to 1000°C and 10,000 bars. *Geol. Soc. Am. Spec. Pap. 132.*

Burnham, C. W. and Wall, V. J. 1974. Fugacity coefficients for carbon dioxide in the range to 10 kb, 1000°C. Written communication, 1974 NATO Advanced Study Institute on Volatiles in Metamorphism.

Carpenter, R. H. 1974. Pyrrhotite isograd in southeastern Tennessee and southwestern North Carolina. *Geol. Soc. Am. Bull. 85*, 451-456.

Chandler, F. W., Young, G. M., and Wood, J. 1969. Diaspore in Early Proterozoic quartzites (Lorrain Fm.) of Ontario. *Can. J. Earth Sci. 6*, 337-340.

Chatterjee, N. D. 1972. The upper stability limit of the assemblage paragonite + quartz and its natural occurrences. *Contr. Mineral. Petrol. 34*, 288-303.

Chatterjee, N. D. and Johannes, W. 1974. Thermal stability and standard thermodynamic properties of synthetic $2M_1$-muscovite $KAl_2[AlSi_3O_{10}(OH)_2]$. *Contr. Mineral. Petrol. 48*, 89-114.

Chatterjee, N. D. and Froese, E. 1975. A thermodynamic study of the pseudobinary join muscovite-paragonite in the system $KAlSi_3O_8$-$NaAlSi_3O_8$-Al_2O_3-SiO_2-H_2O. *Am. Mineral. 60*, 985-993.

Chayes, F. 1975. Statistical petrology. *Carnegie Inst. Washington Year Book 74*, 542-550.

Chinner, G. A. 1966. The significance of the aluminum silicates in metamorphism. *Earth-Sci. Rev. 2*, 111-126.

Chinner, G. A., Smith, J. V., and Knowles, C. R. 1969. Transition metal contents of Al_2SiO_5 polymorphs. *Am. J. Sci. 267-A*, 96-113.

Cipriani, C., Sassi, F. P., and Scolari, A. 1971. Metamorphic white micas: definition of paragenetic fields. *Schweiz. Mineral. Petrog. Mitt. 51*, 259-302.

Clarke, A. M. S. 1971. Structure and lithology of a part of the Aillik Series, Labrador. *Geol. Assoc. Can., Proc. 24*, 107-117.

Currie, K. L. 1971. The reaction 3 cordierite = 2 garnet + 4 sillimanite + 5 quartz as a geological thermometer in the Opinicon Lake region, Ontario. *Contr. Mineral. Petrol. 33*, 215-226.

Currie, K. L. 1974. A note on the calibration of the garnet-cordierite geothermometer and geobarometer. *Contr. Mineral. Petrol. 44*, 35-44.

Davidson, L. R. and Mathison, C. I. 1973. Manganiferous orthopyroxenes and garnets from metamorphosed iron formations of the Quairading district, western Australia. *Neues Jahrb. Mineral. Mh.*, 47-57.

Davies, H. M. 1974. Apatite and volatiles in the Kiglapait layered intrusion, Labrador. Unpubl. M.S. thesis, Univ. Massachusetts, Amherst, Mass., 46p.

Dodge, F. C. W. 1971. Al_2SiO_5 minerals in rocks of the Sierra Nevada and Inyo Mountains, California. *Am. Mineral. 56*, 1443-1450.

Emslie, R. F. 1964. Potassium-Argon age of the Michikamau anorthosite intrusion, Labrador. *Nature 202*, 172-173.

Fahrig, W. F. 1957. Geology of certain Proterozoic rocks in Quebec and Labrador. *Roy. Soc. Canada, Spec. Publ. No. 2*, 112-113.

Flood, R. H. and Shaw, S. E. 1973. A cordierite-bearing granite suite from the New England batholith, N.S.W., Australia. *Contr. Mineral. Petrol. 52*, 157-164.

French, B. M. 1968. Progressive contact metamorphism of the Biwabik iron-formation, Mesabi Range, Minnesota. *Minn. Geo. Surv. Bull. 45*, 103p.

Fyfe, W. S. 1969. Some second thoughts on Al_2O_3-SiO_2. *Am. J. Sci. 267*, 291-296.

Gable, D. J. and Sims, P. K. 1969. Geology and regional metamorphism of some high grade cordierite gneisses, Front Range, Colorado. *Geol. Soc. Am. Spec. Pap. 128.*

Gandhi, S. S., Grasty, R. L., and Grieve, R. A. F. 1969. The geology and geochronology of the Makkovik area, Labrador. *Can. J. Earth Sci. 6*, 1019-1035.

Green, T. H. 1976. Experimental generation of cordierite- or garnet-bearing granitic liquids from a pelitic composition. *Geology 4*, 85-88.

Greenwood, H. J. 1967. Wollastonite: stability in H_2O-CO_2 mixtures and occurrence in a contact-metamorphic aureole near Salmo, British Columbia, Canada. *Am. Mineral. 52*, 1669-1680.

Greenwood, H. J. 1972. Al^{IV}-Si^{IV} disorder in sillimanite and its effect on phase relations of the aluminum silicate minerals. *Geol. Soc. Am. Mem. 132*, 553-571.

Gribble, C. D. and O'Hara, M. J. 1967. Interaction of basic magma with pelitic materials. *Nature 214*, 1198-1201.

Guidotti, C. V. 1973. Compositional variation of muscovite as a function of metamorphic grade and assemblage in metapelites from N.W. Maine. *Contr. Mineral. Petrol. 42*, 33-42.

Han, Tsu-Ming. 1968. Ore mineral relations in the Cuyana sulfide deposit, Minnesota. *Mineral. Deposita 3*, 109-134.

Harker, R. I. and Tuttle, O. F. 1955. Studies in the system CaO-MgO-CO_2. Part I. The thermal dissociation of calcite, dolomite, and magnetite. *Am. J. Sci. 253*, 209-224.

Hensen, B. J. 1971. Theoretical phase relations involving cordierite and garnet in the system MgO-FeO-Al_2O_3-SiO_2. *Contr. Mineral. Petrol. 33*, 191-214.

Hensen, B. J. and Green, D. H. 1971. Experimental study of cordierite and garnet in pelitic compositions at high pressures and temperatures. I. Compositions with excess alumino-silicate. *Contr. Mineral. Petrol. 33*, 309-330.

Hensen, B. J. and Green, D. H. 1972. Experimental study of cordierite and garnet in pelitic compositions at high pressures and temperatures. II. Compositions without excess alumino-silicate. *Contr. Mineral. Petrol. 35*, 331-354.

Hensen, B. J. and Green, D. H. 1973. Experimental study of cordierite and garnet in pelitic compositions at high pressures and temperatures. III. Synthesis of experimental data and geological applications. *Contr. Mineral. Petrol. 38*, 151-166.

Hess, P. C. 1969. The metamorphic paragenesis of cordierite in pelitic rocks. *Contr. Mineral. Petrol. 24*, 191-207.

Hewins, R. H. 1975. Pyroxene geothermometry of some granulite facies rocks. *Contr. Mineral. Petrol. 50*, 205-209.

Hey, M. H. 1954. A new review of the chlorites. *Mineral. Mag. 30*, 277-292.

Hirschberg, A. and Winkler, H. G. F. 1968. Stabilitätsbeziehungen zwischen Chlorit, Cordierit und Almandin bei der Metamorphose. *Contrib. Mineral. Petrol. 18*, 17-42.

Hsu, L. C. 1968. Selected phase relationships in the system Al-Mn-Fe-Si-O-H: a model for garnet equilibria. *J. Petrol. 9*, 40-83.

Hutcheon, I., Froese, E., and Gordon, T. M. 1974. The assemblage quartz-sillimanite-garnet-cordierite as an indicator of metamorphic conditions in the Daly Bay Complex, N.W.T. *Contrib. Mineral. Petrol. 44*, 29-34.

Jackson, G. D. and Taylor, F. C. 1972. Correlation of major Aphebian rock units in the Northeastern Canadian Shield. *Can. J. Earth Sci. 9*, 1650-1669.

Johannes, W. and Orville, P. M. 1974. Experimental determination of an isobaric invariant point and associated reactions involving anorthite in the system CaO-K_2O-Al_2O_3-SiO_2-CO_2-H_2O. Written communication, 1974 NATO Advanced Study Institute on Volatiles in Metamorphism.

Klein, Cornelis, Jr. 1973. Changes in mineral assemblages with metamorphism of some banded Precambrian iron-formations. *Econ. Geol. 68*, 1075-1088.

Knight, I. 1973. The Ramah Group between Nachvak Fjord and Bears Gut, Labrador. *In* Report of Activities, Pt. A: April to October 1972, *Geol. Surv. Can. Pap. 73-1*, Pt. A, 156-161.

Knight, I. 1974. The Ramah Group-Mugford Group-Snyder Group--a correlation in Labrador and a possible link between the Labrador Trough and western Greenland. *In* Author's Abstracts, Geol. Assoc. Can. - Min. Assoc. Can., Ann. Meeting, 1974, p. 50.

Krogh, T. E. and Davis, G. L. 1973. The significance of inherited zircons on the age and origin of igneous rocks--an investigation of the ages of the Labrador adamellites. *Carnegie Inst. Washington Year Book 72*, 610-613.

Leake, B. E. 1968. A catalog of analyzed calciferous and subcalciferous amphiboles together with their nomenclature and associated minerals. *Geol. Soc. Am. Pap. 68.*

Liou, J. G., Kuniyoshi, S., and Ito, K. 1974. Experimental studies of the phase relations between greenschist and amphibolite in a basaltic system. *Am. J. Sci. 274*, 613-632.

Luth, W. C. 1967. Studies in the system $KAlSiO_4$-Mg_2SiO_4-SiO_2-H_2O: I, inferred phase relations and petrologic applications. *J. Petrol. 8*, 372-416.

Martin, R. F. 1974. Controls of ordering and subsolidus phase relations in the alkali feldspars. *In* W. S. MacKenzie and J. Zussman (eds.), *The Feldspars*, Manchester Univ. Press, Manchester, p. 313-336.

Morey, G. B., Papike, J. J., Smith, R. W., and Weiblen, P. W. 1972. Observations on the contact metamorphism of the Biwabik Iron Formation, East Mesabi District, Minnesota. *Geol. Soc. Am. Memoir 135*, 225-263.

Morgan, W. C. 1972. Ramah Group and Proterozoic-Archean relationships in northern Labrador. *In* Report of Activities, Pt. A, April to October 1972, *Geol. Surv. Can. Paper 72-1*, Pt. A, 125-128.

Morse, S. A. 1961. Geology of the Kiglapait layered intrusion, coast of Labrador, Canada. Unpubl. Ph.D. thesis, McGill Univ., Montreal, Quebec, 319p.

Morse, S. A. 1969. The Kiglapait layered intrusion, Labrador. *Geol. Soc. Am. Memoir 112*, 204p.

Muraro, T. W. 1966. Metamorphism of zinc-lead deposits in southeastern British Columbia. *Can. Inst. Mining Met., Special Volume 8*, 239-241.

Neumann, H. 1950. Pseudomorphs of FeS after pyrite in the Balachulish slates. *Mineral. Mag. 29*, 234-238.

Okrusch, M. and Evans, B. W. 1970. Minor element relationships in co-existing andalusite and sillimanite. *Lithos 3*, 261-268.

Popp, R. K. 1975. Iron-magnesium amphiboles: synthesis and stability with respect to temperature, pressure, oxygen fugacity, and sulfur fugacity. Unpubl. Ph.D. thesis, Virginia Polytechnic Institute and State University, Blacksburg, Virginia, 122p.

Ramsay, C. R. 1974. The cordierite isograd in Archean meta-sediments near Yellowknife, N.W.T., Canada--variations on an experimentally established reaction. *Contrib. Mineral. Petrol. 47*, 27-40.

Richard, D. T. 1973. Limiting conditions for synsedimentary sulfide ore formation. *Econ. Geol. 68*, 605-617.

Richardson, S. W., Gilbert, M. C., and Bell, P. M. 1969. Experimental determination of kyanite-andalusite and andalusite-sillimanite equilibria; the aluminum silicate triple point. *Am. J. Sci. 267*, 259-272.

Rucklidge, J. C. 1971. Specifications of Fortran program SUPERRECAL. Dept. of Geology, Univ. of Toronto.

Rucklidge, J. and Gasparrini, E. L. 1969. Specifications of a computer program for processing electron microprobe analytical data. Dept. of Geology, Univ. of Toronto.

Rutherford, M. J. 1973. The phase relations of aluminous iron biotites in the system $KAlSi_3O_8$-$KAlSiO_4$-Al_2O_3-Fe-O-H. *J. Petrol. 14*, 159-180.

Saxena, S. K. 1973. *Thermodynamics of Rock-forming Crystalline Solutions.* Springer-Verlag, New York, 188p.

Schreyer, W. and Yoder, H. S. 1961. Petrographic guides to the experimental petrology of cordierite. *Carnegie Inst. Washington Year Book 60*, 147-152.

Scott, S. D. 1973. Experimental calibration of the sphalerite geobarometer. *Econ. Geol. 68*, 466-474.

Scott, S. D. and Barnes, H. L. 1971. Sphalerite geothermometry and geobarometry. *Econ. Geol. 66*, 653-669.

Seck, H. A. 1971. Koexistierende Alkali-feldspate und Plagioklase in System $NaAlSi_3O_8$-$KAlSi_3O_8$-$CaAl_2Si_2O_8$-H_2O bei temperaturen von 650°C bis 900°C. *Neues Jahrb. Mineral. Abh. 115*, 315-395.

Seifert, F. 1970. Low-temperature compatibility relations of cordierite in haplo-pelites of the system K_2O-MgO-Al_2O_3-SiO_2-H_2O. *J. Petrol. 11*, 73-100.

Shirey, S. B. 1975. Sulfides and sulfur content of the Kiglapait layered intrusion, Labrador. Unpubl. M.S. thesis, Univ. Massachusetts, Amherst, Mass.

Simmons, E. C., Lindsley, D. H., and Papike, J. J. 1974. Phase relations and crystallization sequence in a contact-metamorphosed rock from the Gunflint Iron Formation, Minnesota. *J. Petrol. 15*, 539-565.

Skippen, G. B. 1971. Experimental data for reactions in siliceous marbles. *J. Geol. 79*, 451-481.

Skippen, G. 1974. An experimental model for low pressure metamorphism of siliceous dololomitic marble. *Am. J. Sci. 274*, 487-509.

Smith, J. V. 1974. *Feldspar Minerals.* I. Crystal structure and physical properties. II. Chemical and textural properties. Springer-Verlag. Heidelberg. 627 and 690pp.

Speer, J. A. 1974. The contact aureole of the Kiglapait intrusion. *In* Nain Anorthosite Project, Labrador, Field Rep. 1974, S. A. Morse (ed.), Univ. Massachusetts Contrib., 17-26.

Speer, J. A. and Ribbe, P. H. 1973. The feldspars of the Kiglapait intrusion, Labrador. *Am. J. Sci. 273A*, 468-478.

Stockwell, C. H. 1973. Revised Precambrian time scale for the Canadian Shield. *Geol. Surv. Can. Pap. 72-52.*

Strens, R. G. J. 1968. Stability of Al_2SiO_5 solid solutions. *Mineral. Mag. 36*, 839-849.

Sutton, J. S., Marten, B. E., Clark, A. M. S., and Knight, I. 1972. Correlation of the Precambrian supracrustal rocks of coastal Labrador and southwestern Greenland. *Nat. Phys. Sci. 238*, 122-123.

Taylor, F. C. 1971. A revision of Precambrian structural provinces in northeastern Quebec and northern Labrador. *Can. J. Earth Sci. 8*, 579-584.

Taylor, F. C. 1972. The Nain province. *In* Variations in tectonic styles in Canada. *Geol. Assoc. Can. Sp. Pap. 11*, 436-452.

Tuttle, O. F. and Bowen, N. L. 1958. Origin of granite in the light of experimental studies in the system $NaAlSi_3O_8$-$KAlSi_3O_8$-SiO_2-H_2O. *Geol. Soc. Am. Memoir 74*, 153p.

Velde, B. 1965. Phengite micas: synthesis, stability and natural occurrence. *Am. J. Sci. 263*, 886-913.

Wanless, R. K. and Loveridge, W. D. 1972. Rubidium-strontium isochron age studies, report 1. *Geol. Surv. Can. Pap. 72-23.*

Weisbrod, A. 1973. Cordierite-garnet equilibrium in the system Fe-Mn-Al-Si-O-H. *Carnegie Inst. Washington Year Book 72*, 515-518.

Wheeler, E. P., II. 1942. Anorthosite and associated rocks about Nain, Labrador. *J. Geol. 50*, 611-642.

Wheeler, E. P., II. 1968. Minor intrusives associated with the Nain anorthosite. *In* Anorthosites and Related Rocks, I. W. Isachsen (ed.), *New York State Mus. and Sci. Serv. Memoir 18*, 189-206.

Winkler, H. G. F. 1967. *Petrogenesis of Metamorphic Rocks.* Springer-Verlag, 237p.

Wones, D. R. and Eugster, H. P. 1965. Stability of biotite: Experiment, theory and application. *Am. Mineral. 50*, 1228-1278.

Wood, B. J. and Banno, S. 1973. Garnet-orthopyroxene and orthopyroxene-clinopyroxene relationships in simple and complex systems. *Contr. Mineral. Petrol. 42*, 109-124.

APPENDIX

SNYDER GROUP SAMPLE CATALOGUE

ABBREVIATIONS FOR ROCK UNITS ARE:

SNYDER GROUP

LQQ	LOWER QUARTZITE QUARTZITE AND ARKOSES
LQP	LOWER QUARTZITE PELITE
LQA	LOWER QUARTZITE ALUMINOUS PELITE
IFM	IRON FORMATION
QMM	QUARTZ MARBLE MARBLE
QMC	QUARTZ MARBLE CALC SILICATE ROCK
SHF	SULFIDE GRAPHITE HORNFELS
UQQ	UPPER QUARTZITE QUARTZITE

OTHER

SBX	SNYDER BRECCIA
UQP	UPPER QUARTZITE 2 PYROXENE GABBRO (SNYDER BRECCIA)
LDY	LAYERED DYKE ON HILL 800
HAM	HILL 1300N AMPHIBOLITE
HGA	HILL 1100S GABBRO
MDY	OTHER METAMORPHOSED DYKES
EDY	ELSONIAN DYKES
OBZ	OUTER BORDER ZONE OF THE KIGLAPAIT INTRUSION
BBX	BORDER BRECCIA
KCM	KIGLAPAIT COAST MIGMATITES

SP #	ST#	UNIT
7200	1	LQP

7201 2 SHF P
ASSEMBLAGE BIOT EP? QTZ SPHL

7202 2 SHF

7203 2 SHF

7204 2 QMC

7205 2 QMM

7206 2 QMM TS
ASSEMBLAGE CC CPX AMPH
ASSEMBLAGE CC PHLOG CL

7207 2 QMM P TS
ASSEMBLAGE CC OL CHL AMPH PHLOG

7208 3 IFM

7209 3 IFM

7210 4 LQC

7211 5 SBX P TS
ASSEMBLAGE BIOT HBL EP KSP PC QTZ TIT AP CC
MODE 18.60 35.40 0.006 0.006 40.40 2.00 2.40

7212 6 LQA

7213 6 SBX

7214 7 LQA

7215 8 LQA P TS

7218 10 LQA

7219 12 LDY P TS
ASSEMBLAGE BIOT AMPH PC OPX SP

7220 14 QMC P TS
ASSEMBLAGE QTZ CC AMPH CPX
ASSEMBLAGE QTZ CC AMPH CPX
ASSEMBLAGE CC AMPH CL PHLOG

7221 15 SHF

7222 16 UQP P TS
ASSEMBLAGE OPX PC QTZ BIOT HBL

7223 17 SHF

7224 18 IFM

7225 19 LQA P TS
ASSEMBLAGE QTZ KSP CORD AND SILL FIB BIOT MUSC
ASSEMBLAGE QTZ CORD BIOT

7226 20 LQA

7227 21 QMC
ASSEMBLAGE CC PHLOG CL AMPH

ASSEMBLAGE CC PHLOG CPX AMPH
ASSEMBLAGE CC CPX AMPH

7228 22 SHF

7229 23 SHF P TS
ASSEMBLAGE SILL CORD FIB KSP MUSC

7230 24 LDY

7231 25 LDY

7232 26 HAM

7233 27 ???

7234 29 UQP

7235 29 UQQ

7236 30 LQC P

7237 31 LQA P TS
ASSEMBLAGE SILL AND MUSC BICT CORD QTZ KSP
MODE 13.99 5.25 1.90 4.77 5.40 8.43 56.23 4.93

7238 CS SBX

7239 CS LQQ

7240 CS LQQ

7241	CS LQP ASSEMBLAGE QTZ BIOT GAR AND MUSC CHL PC	P TS
7242	CS LQC	P
7243	CS LQQ	
7244	CS LQQ	
7245	CS SBX	
7246	CS LQC	
7247	CS LQQ	
7248	CS LQA	
7249	CS LQA	
7250	CS LQA	
7251	CS LQQ	
7252	CS SBX	
7253	CS LQQ	
7254	CS LQC	
7255	CS SBX	
7256	CS LQQ	P TS

ASSEMBLAGE QTZ KSP AND FIB MUSC BIOT CORD

7257 CS LQQ

7258 CS SBX P TS
ASSEMBLAGE HBL PC BIOT QTZ EP CHL KSP? AP TIT CC
MODE 27.46 56.78 11.18 0.006 TR 0.001 X 3.73

7259 CS LQQ

7260 CS LQA

7261 CS SBX

7262 CS LQQ

7263 CS LQQ

7264 CS LQA

7265 CS SBX TS
ASSEMBLAGE PC BIOT CUMM HBL CPX EP QTZ KSP CC CHL

7266 CS IFM P TS
ASSEMBLAGE QTZ GRUN HBL BIOT CPX OPX? GAR CC

7267 CS IFM P TS
ASSEMBLAGE QTZ GRUN BIOT GAR CC PX?

7268 CS SBX P TS
ASSEMBLAGE CUMM HBL BIOT CPX OPX QTZ PC KSP CC ALLANITE
MODE 5.64 22.71 12.13 2.39 45.56 12.13 0.001

7269 2 QMM

7270 2 QMM

7271 2 IFM

7272 39 LQP P

7273 40 LQA P TS

	ASSEMBLAGE	KSP	QTZ	AND	FIB	SILL	BIOT	CHL	CORD
MODE		37.16	34.35	4.81	9.71	2.08	2.25	4.49	3.53	1.60

7274 41 LQA P TS

	ASSEMBLAGE	AND	FIB	SILL	CORD	BIOT	KSP	QTZ	MUSC
MODE		1.48	6.06	1.61	6.93	1.24	65.09	12.62	4.08	0.009

7275 42 LQA P TS

	ASSEMBLAGE	AND	FIB	SILL	CORD	QTZ	KSP	BIOT	MUSC
MODE		4.79	8.18	1.07	3.06	49.21	31.59	0.20	TR	1.74

7276 43 HAM

7277 44 LQQ

7278 45 LQA P TS

	ASSEMBLAGE	QTZ	KSP	PC	AND	FIB	SILL	CORD	MUSC	BIOT
MODE		2.77	61.08	1.83	6.87	4.32	0.005	17.85	3.33	0.005	0.009

7279 46 LQA

7280 46 HAM

7281 47 LQQ P TS
ASSEMBLAGE QTZ KSP AND SILL FIB MUSC BIOT CHL
MODE 26.05 40.80 8.85 0.005 13.10 4.30 2.10 4.30

7282 1 LQQ P TS
ASSEMBLAGE QTZ KSP PC AND SILL CORD MUSC BIOT GAR
MODE 0.01 27.13 0.007 10.85 0.009 3.18 23.26 31.44 0.003

7283 49 SHF P

7284 52 QMM P TS
ASSEMBLAGE CC OL AMPH PHLOG CHL SP

7285 52 QMC P TS
ASSEMBLAGE CC PHLOG CPX AMPH CHL KSP QTZ PC
ASSEMBLAGE CC OL PHLOG CPX AMPH

7286 53 MDY

7287 54 LQA P

7288 55 LQA P TS
ASSEMBLAGE AND SILL FIB QTZ KSP BIOT MUSC CORD
MODE 3.92 4.36 5.66 13.39 29.30 8.71 12.42 19.06 3.05

7289 57 LQQ P TS
ASSEMBLAGE QTZ KSP SILL AND FIB MUSC CORD BIOT
MODE 14.59 42.33 3.49 2.51 1.70 0.16 33.09 0.89 1.21

7290 58 LQQ

7291 61 LDY

7292 62 BBX

7293 63 BBX

7294 64 UQP

7295 65 UQP

7296 66 SHF P TS
ASSEMBLAGE SILL BIOT CORD? QTZ MUSC PC TIT ZIR

7297 66 UQP

7298 66 UQQ

7299 67 QMC P TS
ASSEMBLAGE QTZ CPX AMPH KSP CC PC

72100 68 MDY

72101 69 QMC P TS

72102 70 QMC

72103 75 HGA

72104 79 HGA

72105 85 LQQ

72106 85 MDY

72107 86 IFM P TS
ASSEMBLAGE QTZ PC GAR HBL CPX AP CPX

72108 88 MDY

72109 89 LQQ P TS
ASSEMBLAGE SILL AND PC QTZ KSP BIOT CORD?
MODE 5.56 4.53 8.42 38.39 37.44 0.87 2.70 1.11 1.11

72110 97 EDY

72110 97 UQQ

72111 98 UQQ
ASSEMBLAGE QTZ KSP PC CORD BIOT SILL SP

72112 99 UQQ

72113 101 KCM

72114 103 MDY TS

72115 103 MDY

72116 103 MDY

72117 102 SBX P TS
ASSEMBLAGE BIOT HBL QTZ +PC EP TIT AP
MODE 6.57 31.87 58.88 2.67
ASSEMBLAGE PC HBL BIOT EP KSP CHL CC AP

72113 CS IFM P TS
ASSEMBLAGE OPX GRUN BIOT QTZ

72119 265 OBZ

72120 265 EDY

72121 208 OBZ

72122 215 LQQ

72123 215 LQQ P TS
ASSEMBLAGE PC CORD QTZ SILL KSP SP

72124 217 QMC P TS
ASSEMBLAGE QTZ CPX BIOT AMPH PC

72125 208 OBZ

72126 222 UQP P TS
ASSEMBLAGE QTZ +PC HBL OPX +CPX BIOT AP
MODE 41.62 18.13 37.30 0.005 2.24

72127 223 UQQ P TS
ASSEMBLAGE QTZ KSP MUSC BIOT CORD PC SILL AND

72128 231 QMM P TS
ASSEMBLAGE CC PHLOG CPX?
ASSEMBLAGE CC? CPX EP AMPH

72128 231 QMM SECOND THIN SECTION P TS

ASSEMBLAGE OL CC CHL SP PHLOG
ASSEMBLAGE PHLOG CPX

72129 232 LQQ

72130 232 LQA P TS
ASSEMBLAGE QTZ KSP AND FIB MUSC BIOT

72131 232 LQA P TS
ASSEMBLAGE QTZ KSP AND FIB? MUSC BIOT CORD

72132 232 SBX P TS
ASSEMBLAGE BIOT HBL EP CPX PC QTZ KSP CC TIT AP

72133 232 LQQ P TS
ASSEMBLAGE QTZ KSP BIOT MUSC FIB AND

72134 233 LQP P TS
ASSEMBLAGE QTZ BIOT GAR PC CORD?

72135 234 LQA P TS
ASSEMBLAGE AND MUSC CHL QTZ BIOT FIB KSP EP

72136 234 LQP

72137 235 LQA

72138 235 LQA

72139 240 LQQ

72140 240 LQQ

72141 246 EDY

72142 250 LQA P TS
ASSEMBLAGE KSP QTZ CORD SILL FIB

72143 254 LQQ

72144 256 LQQ

72145 264 EDY

72146 266 HGA

72147 274 LQQ P TS
ASSEMBLAGE KSP SILL BIOT PC CORD SP

72148 279 QMC TS

72149 280 IFM P TS
ASSEMBLAGE QTZ GAR CPX GRUN HBL BIOT GRAPHITE
ASSEMBLAGE QTZ GAR CPX GRUN CAMPH? BIOT

72150 CS LQQ P TS
ASSEMBLAGE QTZ BIOT EP KSP MUSC PC

72151 CS LQA P TS
ASSEMBLAGE QTZ KSP MUSC BIOT AND FIB CORD PC
MODE 29.21 57.80 1.15 0.003 0.003 0.002 10.57 TR 0.005

72152 CS LQQ

72153 282 IFM

72154 284 EDY

72155 285 MDY P TS

72156 288 LQQ P TS
ASSEMBLAGE QTZ CAMPH EP PC KSP? BIOT

72157 289 UQQ P TS
ASSEMBLAGE QTZ PC KSP CORD MUSC BIOT FIB? SP

72158 290 EDY

72159 291 UQQ

72160 291 UQQ P TS
ASSEMBLAGE SILL BIOT MUSC PC QTZ KSP CORD

72161 291 UQP
PC AN 90.50 AB OR

72162 292 UQQ P TS
ASSEMBLAGE QTZ KSP BIOT CORD CPX PC

72163 292 SHF

72164 293 LQQ P TS
ASSEMBLAGE AND FIB CORD PC BIOT MUSC QTZ KSP

72165 294 LQQ

72166 294 LQA TS
ASSEMBLAGE QTZ KSP CORD SILL AND FIB BIOT MUSC
MODE 20.92 55.19 3.95 3.51 4.65 5.71 3.07 0.96 0.97

72167 294 SBX P TS
ASSEMBLAGE BIOT QTZ KSP MUSC? PC CC

72168 295 SBX

72169 296 LQQ

72170 297 LQQ TS
ASSEMBLAGE QTZ KSP AND FIB MUSC BIOT CORD

72171 292 UQQ P

72172 CS SBX P TS
ASSEMBLAGE PC HBL BIOT QTZ KSP EP CHL TIT AP
MODE 65.54 14.12 17.79 0.005 0.007 0.012

72173 CS LQQ P TS
ASSEMBLAGE QTZ BIOT EP GAR CAMPH PC MUSC CHL

72174 CS SBX

72175 298 UQQ P TS
ASSEMBLAGE PC QTZ CORD GAR CPX BIOT AP

72176 377 LQC P TS
ASSEMBLAGE QTZ BIOT MUSC GAR KSP PC

72177 385 SBX

72178 386 LQA

72179 388 LQA P TS
ASSEMBLAGE QTZ KSP BIOT MUSC CHL AND FIB CORD

72180 389 MDY

72181 389 MDY

72182 394 LQA

72183 395 MDY

72184 ??? MDY ON SNYDER ISLAND NEAR 395?

72185 399 SBX

72186 401 LQA

72187 241 LQC

72188 405 LQQ OR IFM
ASSEMBLAGE QTZ PC BICT OPX

72189 405 LQA P TS
ASSEMBLAGE KSP QTZ SILL FIB PC CORD

72190 407 OBZ

72191 408 LQQ P TS
ASSEMBLAGE QTZ PC KSP OPX BIOT CORD

72192 410 LQA

72193 412 LQQ P TS
ASSEMBLAGE QTZ KSP AND FIB MUSC BIOT CORD

72194 414 LQQ P TS
ASSEMBLAGE QTZ KSP MUSC BIOT AND FIB CORD

72195 413 LQA P TS
ASSEMBLAGE QTZ KSP AND FIB SILL MUSC BIOT CORD

72196 424 LQA 72196A P RS

72196 425 SBX TS
ASSEMBLAGE CUMM HBL EP BIOT QTZ PC KSP AP

72197 426 LQP

72198 426 LQA P TS
ASSEMBLAGE CORD AND SILL KSP QTZ FIB MUSC
MODE 12.68 1.86 13.76 69.22 0.69 0.09 1.18 0.39

72199 428 LQA

72200 429 LQA P TS
ASSEMBLAGE QTZ KSP AND FIB CHL BIOT MUSC

72201 CS LQQ

72202 390 LQA

72203 285 QMC

72204 285 IFM P TS
ASSEMBLAGE QTZ GRUN CAMPH BICT GAR PC? KSP PX

72205 285 QMC P TS
ASSEMBLAGE QTZ GRUN HBL GAR BIOT CC OPX CPX PC AP

72206 285 QMC P

72207 285 IFM TS
ASSEMBLAGE GAR HBL GRUN BIOT EP QTZ CC PC OPX CPX TOUR

72208 285 MDY

72209 231 QMC P TS
ASSEMBLAGE QTZ GAR BIOT AMPH CPX CC EP
ASSEMBLAGE QTZ GAR BIOT CC EP KSP MUSC

72210 4CO LQA P TS
ASSEMBLAGE QTZ KSP MUSC BICT AND FIB

72211 439 LQQ P TS
ASSEMBLAGE PC BIOT GAR CORD CPX KSP QTZ
ACCESSORY ZIR EP CHL MUSC IL MG W/ IL+USP

72212 440 LQQ P TS
ASSEMBLAGE CORD QTZ AND SILL FIB KSP BIOT
MODE 28.47 21.67 1.27 2.05 5.66 40.01 0.14 0.70

72213 243 LQC P

72214 441 LQA

72215 442 LQQ P TS
ASSEMBLAGE QTZ KSP CORD MUSC BIOT CHL AND FIB

72216 113 MDY

72217 235 LQA

72218 235 LQA P TS
ASSEMBLAGE QTZ KSP AND FIB BIOT MUSC CORD

72219 390 LQA P TS
ASSEMBLAGE QTZ KSP MUSC BIOT AND FIB SILL? CORD

72220 280 LQQ

72221 280 LQQ

72222 280 IFM P TS
ASSEMBLAGE QTZ CPX PC GRUN KSP TIT CC HBL

72223 280 MDY P TS
ASSEMBLAGE BIOT GAR QTZ OPX PC AMPH? KSP MUSC TIT CC CHL

72224 443 QMM P TS
ASSEMBLAGE CC PHLOG CL CHL

72225 443 QMM P TS
ASSEMBLAGE CC OL PHLOG

72226 443 SHF

72227 443 IFM

72228 443 QMC

72229 NC KCM

72230 NC KCM

74231 444 HAM TS
ASSEMBLAGE HBL CUMM? CPX PC BIOT AP

74232 445 HAM

74233 446 LQA

74234 446 HAM

74235 447 LQQ

74236 448 HAM TS
ASSEMBLAGE BIOT CPX HBL TIT AP

74237 449 HAM

74238 450 HAM

74239 451 HAM

74240 451 HAM

74241 452 HAM

74242 453 LQA

74243 454 LQA

74244 454 EDY TS
ASSEMBLAGE PC HBL CPX OPX AP

74245 455 LQA P TS
ASSEMBLAGE SILL AND CORD KSP BIOT MUSC ZIR

74246 456 MDY

74247 456 LQA

74248 457 HAM

74249 457 LQA

74250 458 HAM

74251 459 LQC TS
ASSEMBLAGE QTZ BIOT OPX CORD GAR ZIR CHL MUSC AMPH

74252 459 LQA

74253 460 SBX TS
ASSEMBLAGE BIOT HBL PC CPX? TIT CC

74254 460 SBX

74255 330 LQQ TS

ASSEMBLAGE QTZ AMPH BIOT EP CHL MUSC PC TIT ZIR

74256 398 IFM

74257 461 EDY

74258 461 LQA

74259 462 LQA

74260 462 LQA

74261 463 EDY

74262 464 LQA

74263 465 LQQ TS
ASSEMBLAGE GAR CORD KSP PC BIOT ZIR OP AP SP

74264 465 LQQ

74265 466 UQQ TS
ASSEMBLAGE PC KSP CORD BIOT SILL?

74266 467 LQQ

74267 467 LQQ

74268 467 LQQ

74269 468 IFM

74270 469 LQC

74271 471 LQA

74272 472 LQA LOCATION A

74273 471 LQA

74274 471 LQA

74275 100 UQQ TS
ASSEMBLAGE KSP PC CORD SP BIOT QTZ ZIR

74276 472 UQQ LOCATION B TS
ASSEMBLAGE KSP PC CORD BIOT QTZ ZIR

74277 472 UQP LOCATION B TS
ASSEMBLAGE OPX CPX HBL PC AP

74278 473 UQQ

74279 474 UQQ

74280 475 LQQ TS
ASSEMBLAGE QTZ GAR BIOT CORD KSP

74281 476 LQA

74282 476 MDY

74283 477 LQA TS
ASSEMBLAGE AND SILL FIB KSP QTZ BIOT MUSC MG

MODE 6.19 12.72 4.04 51.59 20.63 0.34 1.11 4.98

74284 478 MDY
ASSEMBLAGE OPX MT QTZ AMPH

74285 478 MDY
ASSEMBLAGE OPX PC MT

74286 479 LQA

74287 480 LQQ TS
ASSEMBLAGE QTZ KSP GAR CORD BIOT ZIR

74288 481 LQQ TS
ASSEMBLAGE GAR CORD KSP PC BIOT QTZ MG SP AP ZIR

74289 482 OBZ

74290 483 LQQ

74291 484 LQQ

74292 484 LQA

74293 485 MDY

74294 485 LQA

74295 485 MDY TS
ASSEMBLAGE BIOT OPX CPX HBL PC QTZ AP

74296 486 QMC TS

ASSEMBLAGE QTZ CPX TREM

74297 486 IFM TS
ASSEMBLAGE GRUN OPX QTZ BIOT GAR PC CC

74298 487 MDY

74299 488 SHF TS
ASSEMBLAGE SILL BIOT MUSC CORD ZIR

74300 488 UQQ TS
ASSEMBLAGE KSP BIOT CORD SILL PC +QTZ MUSC AND ZIR +MG
MODE 35.66 7.13 22.96 3.56 20.43 4.00 0.78 1.74

74301 489 LDY TS
ASSEMBLAGE OPX HBL BIOT AP ZIT

74302 490 LQA TS
ASSEMBLAGE AND SILL FIB MUSC BIOT KSP CORD QTZ MG
MODE 6.12 3.63 8.30 11.52 8.09 28.14 15.99 15.68 2.49

74303 490 LQA

74304 491 LQQ

74305 491 LQQ TS
ASSEMBLAGE QTZ PC CPX BIOT CORD

74306 491 LQC TS
ASSEMBLAGE QTZ OPX BIOT CORD MG SP ZIR AP

74307 491 MDY

74308 492 MDY

74309 492 LQQ TS
ASSEMBLAGE QTZ OPX BIOT CORD GAR ZIR

74310 493 UQQ

74311 494 LQQ

74312 495 LQQ

74313 496 LQA

74314 496 MDY

74315 497 LDY TS
ASSEMBLAGE OL OPX AMPH PC BIOT

74316 497 LDY TS
ASSEMBLAGE BIOT CPX CUMM HBL PC AP

74317 497 LDY TS
ASSEMBLAGE BIOT OPX CUMM HBL

74318 497 LDY TS
ASSEMBLAGE BIOT QTZ PX AMPH

74319 497 LDY TS
ASSEMBLAGE BIOT OPX CUMM QTZ AP

74320 497 QMM TS

ASSEMBLAGE CC PHLOG CHL CL

74321 498 IFM TS
ASSEMBLAGE GAR BIOT GRUN OPX HBL QTZ KSP

74322 499 SBX

74323 500 SHF TS
ASSEMBLAGE CORD BIOT MUSC KSP PC QTZ SILL

74324 500 UQP

74325 501 BBX

74326 ??? SBX

74327 502 LQA TS
ASSEMBLAGE MUSC CHL AND KSP BIOT QTZ PC ZIR SP

74328 MBS LQA TS
ASSEMBLAGE SILL FIB BIOT CORD QTZ ZIR MG

74329 MBS LQQ TS
ASSEMBLAGE BIOT CORD OPX PC EP

74330 MBS LQQ TS
ASSEMBLAGE QTZ CPX HBL

74331 503 QMC

74332 503 IFM TS
ASSEMBLAGE QTZ GAR CPX CPX AP

74333 5C3 QMM TS

74334 5C4 LQQ

74335 5C5 LQA

74336 5C6 HGA TS
ASSEMBLAGE AMPH CPX CPX PC AP

74337 5C7 UQQ

74338 5C8 UQQ TS
ASSEMBLAGE SILL CORD BIOT MUSC KSP QTZ PC TIT SP ZIR SPHAL

74339 5C8 UCP TS
ASSEMBLAGE PC QTZ BICT OPX AP

74340 5C9 UQQ

74341 51C BBX TS
ASSEMBLAGE BIOT QTZ CORD PC KSP SP

74342 511 UQQ TS
ASSEMBLAGE SILL FIB KSP CORD BIOT PC QTZ MG

74343 511 SHF

74344 512 SHF

74345 512 BBX

74346 513 QMM TS
ASSEMBLAGE CC PHLOG CL CHL GRAPH

74347 514 SHF TS
ASSEMBLAGE AND CORD MUSC PC SPHAL

74348 497 SHF TS
ASSEMBLAGE PC SILL FIB AND CORD MUSC? PHLOG

74349 515 OBZ TS
ASSEMBLAGE PC OPX CPX AMPH BIOT AP

74350 516 SBX TS
ASSEMBLAGE HBL EP BICT MUSC PC QTZ AP CC TIT

74351 517 SBX TS
ASSEMBLAGE PC BIOT HBL CHL EP AP TIT

74352 518 ULM

74353 518 ULM TS
ASSEMBLAGE CHL ANTH CC

74354 518 ULM

74355 518 ULM TS
ASSEMBLAGE CHL ANTH CC TALC

74356 390 LQA

74357 283 EDY TS
ASSEMBLAGE AMPH CPX BIOT PC QTZ

74358 283 EDY

74359 283 EDY

74360 283 EDY

74361 283 IFM

74362 283 IFM

74363 231 QMM TS
ASSEMBLAGE CPX CHL
ASSEMBLAGE OL CC PHLOG CPX CHL SP TIT

74364 286 LQQ

74365 153 LQA

74366 418 SBX

74367 519 SBX

74368 385 SBX

74369 235 LQQ

74370 234 SBX

74371 520 LQQ TS
ASSEMBLAGE QTZ BIOT GAR CHL? CORD TOUR ZIR AP

74372 521 QMC

74373 521 SHF TS
ASSEMBLAGE SILL CORD PC KSP QTZ

74374 522 LQQ TS
ASSEMBLAGE GAR BIOT CORD KSP QTZ PC ZIR

74375 524 UQP

74376 525 QMM

74377 526 MDY

74378 527 UQQ TS
ASSEMBLAGE KSP PC QTZ CORD MUSC BIOT

74379 528 UQP

74380 529 BBX

74381 530 UQP

74382 531 BBX

74383 532 IFM TS
ASSEMBLAGE CPX OPX QTZ PC HBL GAR AP

74384 532 QMC

74385 532 LQQ

74386 533 BBX TS
ASSEMBLAGE PC KSP QTZ CORD BIOT ZIR

74387 533 UQP TS
ASSEMBLAGE PC QTZ BICT OPX CPX HBL

74388 534 SHF

74389 534 SHF TS
ASSEMBLAGE BIOT CUMM PC QTZ

74390 534 IFM TS
ASSEMBLAGE QTZ PC CPX OPX BIOT GRUN GAR TIT

74391 534 QMC TS
ASSEMBLAGE QTZ CPX TREM TIT CC AP

74392 535 UQQ TS
ASSEMBLAGE CORD BIOT SILL KSP PC QTZ ZIR

74393 535 UQP TS
ASSEMBLAGE PC QTZ CPX OPX HBL BIOT

74394 537 BBX TS
ASSEMBLAGE PC QTZ BICT OPX CPX CUMM ZIR

74395 538 UQQ

74396 538 UQQ

74397 539 BBX

74398 539 BBX

74399 67 IFM TS
ASSEMBLAGE QTZ PC GAR OPX CPX HBL BIOT CC

74400 541 SHF

74401 542 UQQ

THE FOLLOWING SPECIMENS ARE FROM THE NORTH COAST OF THE KIGLAPAIT MOUNTAINS AND CONSIST OF BASEMENT, SNYDER GROUP, AND ANATECTIC ROCKS THAT HAVE BEEN METAMORPHOSED BY THE KIGLAPAIT INTRUSION IN ZONE III.

7401 CALC-SILICATE
ASSEMBLAGE TREM OPX CPX CHL

7402

7403

7404

7405 SNYDER GROUP MARBLE
ASSEMBLAGE CC OL ?? CPX SP

7406

7407 SNYDER GROUP MARBLE
ASSEMBLAGE CC OL CPX

7408 SNYDER GROUP IFM
ASSEMBLAGE QTZ OPX AMPH

```
7409  SNYDER GROUP SHF
      ASSEMBLAGE  PC  QTZ  CPX  OPX  BIOT  GRAPH  SPHAL

7410  SNYDER GROUP CALC-SILICATE
      ASSEMBLAGE  QTZ  CPX

7411  SNYDER GROUP CALC-SILICATE
      ASSEMBLAGE  PC  CPX  CPX  BIOT  AP  OP

7412  SNYDER GROUP CALC-SILICATE
      ASSEMBLAGE  OPX  CPX  PHLOG  KSP  QTZ  AMPH  OP

7413  OLIVINE WEBSTERITE
      ASSEMBLAGE  PC  AMPH  CPX  CPX  CL  AP  OP

7414

7415

7416  GRANULITE
      ASSEMBLAGE  BIOT  CPX  CPX  PC  KSP  AMPH  OP  AP

7417

7418

7419

7420

7421
```

7422

7423

7424 KIGLAPAIT COAST MIGMATITES
ASSEMBLAGE OPX QTZ PC KSP AP OP

7425 CALC-SILICATE
ASSEMBLAGE AMPH BIOT PC OPX CPX

7426

7427

7428

7429

7430

7431

7432

7433

7434

7435

7436

7437

7438

7439

7440
7441

7442

7443 CALC-SILICATE
ASSEMBLAGE OL CPX AMPH CC OP

7444

7445

7446

7447 ULTRMAFIC
ASSEMBLAGE BIOT AMPH CPX OPX OL? OP

7448 KIGLAPAIT COAST MIGMATITE
ASSEMBLAGE CORD OPX BIOT PC OP

7449
ASSEMBLAGE QTZ GAR CORD CPX BIOT
7450 SNYDER GROUP
ASSEMBLAGE QTZ PC BICT

7451

7452 SNYDER GROUP MARBLE
ASSEMBLAGE CC SP OL PER(BRU)

7452A SNYDER GROUP MARBLE
ASSEMBLAGE OL PHLOG CC CPX

7453 SNYDER GROUP QTZITE
ASSEMBLAGE QTZ OPX PC BIOT CP ZIR AP

TABLE 1 ALUMINOSILICATE ANALYSES FOR THE SNYDER GROUP

	1		2		3		4		5		6		7		8	
SIO2	38.90		36.85		37.82		38.08		36.97		37.59		38.90		37.37	
FE2O3	0.29		3.16		2.67		1.82		3.49		2.22		3.51		3.63	
AL2O3	61.38		59.58		61.14		61.87		59.37		60.46		60.76		59.89	
SUM	100.57		99.59		101.63		101.37		99.83		100.27		103.17		100.89	
SI	1.042	1.042	1.009	1.009	1.013	1.013	1.014	1.014	1.011	1.011	1.014	1.014	1.033	1.033	1.011	1.011
AL	1.937	*	1.922	*	1.929	*	1.942	*	1.913	*	1.935	*	1.885	*	1.910	*
FE3+	0.006	1.943	0.065	1.987	0.054	1.983	0.038	1.980	0.072	1.985	0.045	1.980	0.070	1.956	0.074	1.984
O	5.000	*	5.000	*	5.000	*	5.000	*	5.000	*	5.000	*	5.000	*	5.000	*

1 CHIASTOLITE
2 SN 7215, ANDALUSITE
3 SN 7225, ANDALUSITE
4 SN 7225, SILLIMANITE
5 SN 7237, ANDALUSITE
6 SN 7237, SILLIMANITE
7 SN 7256, LOWER QUARTZITE
8 SN 7273, ANDALUSITE

	9		10		11		12		13		14		15		16	
SIO2	37.20		37.03		37.07		36.82		37.22		36.13		36.00		36.92	
FE2O3	2.27		3.21		1.60		4.51		1.79		3.65		1.35		6.00	
AL2O3	62.54		60.38		61.64		58.22		62.58		60.34		61.32		58.95	
SUM	102.01		100.62		100.31		99.55		101.59		100.12		98.67		101.67	
SI	0.992	0.992	1.004	1.004	1.002	1.002	1.013	1.013	0.995	0.995	0.987	0.987	0.988	0.988	0.998	0.998
AL	1.965	*	1.929	*	1.964	*	1.887	*	1.971	*	1.942	*	1.986	*	1.880	*
FE3+	0.046	2.010	0.065	1.994	0.033	1.996	0.095	1.982	0.036	2.007	0.075	2.017	0.028	2.014	0.122	2.002
O	5.000	*	5.000	*	5.000	*	5.000	*	5.000	*	5.000	*	5.000	*	5.000	*

9 SN 7273, SILLIMANITE
10 SN 7274, ANDALUSITE
11 SN 7274, SILLIMANITE
12 SN 7275, ANDALUSITE
13 SN 7275, SILLIMANITE
14 SN 7278, ANDALUSITE
15 SN 7278, SILLIMANITE
16 SN 7281, ANDALUSITE

	17		18		19		20		21		22		23		24	
SIO2	37.88		37.56		36.96		37.16		37.23		36.94		37.30		36.50	
FE2O3	2.51		0.81		1.00		3.36		2.32		0.41		2.02		2.06	
AL2O3	59.85		62.80		61.75		58.75		60.54		63.46		61.42		60.56	
SUM	100.24		101.17		99.71		99.27		100.09		100.81		100.74		101.21	
SI	1.027	1.027	1.004	1.004	1.003	1.003	1.021	1.021	1.011	1.011	0.990	0.990	1.005	1.005	1.034	1.034
AL	1.912	*	1.978	*	1.975	*	1.902	*	1.937	*	2.004	*	1.951	*	1.912	*
FE3+	0.051	1.963	0.016	1.994	0.020	1.995	0.069	1.971	0.047	1.985	0.008	2.013	0.041	1.992	0.042	1.954
O	5.000	*	5.000	*	5.000	*	5.000	*	5.000	*	5.000	*	5.000	*	5.000	*

17 SN 7281, SILLIMANITE
18 SN 7282, ANDALUSITE
19 SN 7282, SILLIMANITE
20 SN 7288, ANDALUSITE
21 SN 7288, SILLIMANITE
22 SN 72111, SILLIMANITE
23 SN 72123, SILLIMANITE
24 SN 72131, ANDALUSITE

TABLE 1 ALUMINOSILICATE ANALYSES FOR THE SNYDER GROUP

	25		26		27		28		29		30		31		32	
SIO2	38.55		38.43		38.20		37.60		35.07		36.94		37.23		37.11	
FE2O3	2.11		0.22		3.40		4.18		3.12		1.84		2.75		1.52	
AL2O3	61.87		61.08		62.24		61.07		61.51		62.08		61.32		61.79	
SUM	102.53		99.73		103.84		102.85		100.69		99.76		101.30		100.42	
SI	1.020	1.020	1.038	1.038	1.004	1.004	1.001	1.001	0.976	0.976	1.005	1.005	1.001	1.001	1.002	1.002
AL	1.930	*	1.944	*	1.927	*	1.915	*	1.967	*	1.935	*	1.943	*	1.966	*
FE3+	0.042	1.972	0.006	1.949	0.067	1.994	0.084	1.999	0.064	2.031	0.039	1.993	0.056	1.998	0.031	1.997
O	5.000	*	5.000	*	5.000	*	5.000	*	5.000	*	5.000	*	5.000	*	5.000	*

25 SN 72135, ANDALUSITE
26 SN 72160, SILLIMANITE
27 SN 72179, ANDALUSITE
28 SN 72193, ANDALUSITE
29 SN 72195, ANDALUSITE
30 SN 72195, SILLIMANITE
31 SN 72199, ANDALUSITE
32 SN 72199, SILLIMANITE

	33		34		35		36		37		38		39		40	
SIO2	37.43		37.19		37.87		37.44		37.44		37.14		36.53		37.26	
FE2O3	2.80		1.47		4.47		3.22		1.79		1.22		6.28		3.81	
AL2O3	61.96		62.48		62.43		60.27		61.25		62.73		62.27		63.06	
SUM	102.19		101.14		104.77		100.93		100.48		101.09		105.08		104.13	
SI	0.998	0.998	0.997	0.997	0.990	0.990	1.011	1.011	1.011	1.011	0.995	0.995	0.960	0.960	0.979	0.979
AL	1.946	*	1.974	*	1.924	*	1.919	*	1.949	*	1.981	*	1.928	*	1.952	*
FE3+	0.056	2.002	0.030	2.003	0.088	2.012	0.065	1.984	0.036	1.985	0.025	2.006	0.124	2.053	0.075	2.027
O	5.000	*	5.000	*	5.000	*	5.000	*	5.000	*	5.000	*	5.000	*	5.000	*

33 SN 72198, ANDALUSITE
34 SN 72198, SILLIMANITE
35 SN 72219, ANDALUSITE
36 SN 72219, ANDALUSITE
37 SN 72219, SILLIMANITE
38 SN 72245, SILLIMANITE
39 SN 74283, ANDALUSITE
40 SN 74283, SILLIMANITE

	41		42		43		44		45		46		47		48	
SIO2	37.49		37.65		37.84		37.52		37.50		37.38		37.36		38.11	
FE2O3	0.21		0.52		0.35		4.97		2.90		3.80		0.20		0.20	
AL2O3	62.06		62.35		60.83		58.70		62.30		60.68		61.53		62.31	
SUM	99.76		100.52		99.02		101.19		102.70		101.95		99.29		100.71	
SI	1.014	1.014	1.011	1.011	1.030	1.030	1.017	1.017	0.995	0.995	1.002	1.002	1.015	1.015	1.020	1.020
AL	1.977	*	1.974	*	1.952	*	1.875	*	1.948	*	1.918	*	1.973	*	1.966	*
FE3+	0.004	1.991	0.011	1.994	0.007	1.959	0.101	1.977	0.058	2.006	0.079	1.996	0.006	1.979	0.006	1.972
O	5.000	*	5.000	*	5.000	*	5.000	*	5.000	*	5.000	*	5.000	*	5.000	*

41 SN 74299, SILLIMANITE
42 SN 74300, ANDALUSITE
43 SN 74300, SILLIMANITE
44 SN 74302, ANDALUSITE
45 SN 74302, SILLIMANITE
46 SN 74327, ANDALUSITE
47 SN 74339, SILLIMANITE
48 SN 74342, SILLIMANITE

TABLE 1 ALUMINOSILICATE ANALYSES FOR THE SNYDER GROUP (CONTINUED)

	49		50		51	
SIO2	37.93		37.40		37.36	
FE2O3	0.13		0.13		0.31	
AL2O3	62.52		62.83		61.69	
SUM	100.58		100.36		99.36	
SI	1.017	1.017	1.005	1.005	1.014	1.014
AL	1.975	*	1.990	*	1.974	*
FE3+	0.003	1.977	0.003	1.992	0.006	1.980
O	5.000	*	5.000	*	5.000	*

49 SN 74348, ANDALUSITE

50 SN 74348, SILLIMANITE

51 SN 74373, SILLIMANITE

TABLE 2 AMPHIBOLE ANALYSES FOR THE SNYDER GROUP

	1		2		3		4		5		6		7		8	
SIO2	44.81		47.93		49.93		50.43		50.27		49.43		49.52		57.65	
AL2O3	9.33		6.73		1.29		0.96		0.49		7.44		0.75		0.23	
FEO	19.90		17.19		31.30		32.86		34.42		18.19		33.36		0.94	
TIO2	0.92		1.14		0.19		0.18		0.12		0.37		0.0		0.0	
MNO	0.62		0.59		5.65		5.74		5.79		1.17		0.51		0.11	
CAO	11.99		12.09		1.32		0.99		1.44		12.43		0.58		13.88	
MGO	8.80		12.29		5.86		5.16		6.91		8.88		14.20		24.39	
NA2O	0.93		0.93		0.09		0.07		0.0		0.61		0.0		0.0	
K2O	0.91		0.0		0.02		0.01		0.0		0.27		0.0		0.0	
H2O	1.98		2.04		1.87		1.88		1.92		2.03		1.06		2.10	
SUM	100.09		100.93		97.52		98.28		101.35		100.82		100.88		99.39	
SI	5.782	*	7.043	*	7.995	*	8.055	*	7.860	*	7.283	*	7.560	*	7.901	*
AL	1.218	8.000	0.957	8.000	0.305	8.000	0.0	8.055	0.098	7.958	0.717	8.000	0.135	7.704	0.037	7.939
AL	0.446	*	0.228	*	0.239	*	0.181	*	0.0	*	0.575	*	0.0	*	0.0	*
TI	0.093	*	0.126	*	0.023	*	0.022	*	0.014	*	0.041	*	0.0	*	0.0	*
FE	2.519	*	2.112	*	4.191	*	4.389	*	4.501	*	2.241	*	4.264	*	0.108	*
MG	1.985	*	2.692	*	1.399	*	1.228	*	1.610	*	1.957	*	3.235	*	4.982	*
MN	0.079	5.123	0.073	5.212	0.766	6.618	0.777	6.597	0.767	6.892	0.146	4.954	0.066	7.565	0.013	5.103
NA	0.273	*	0.265	*	0.028	*	0.022	*	0.0	*	0.174	*	0.0	*	0.0	*
CA	1.944	*	1.903	*	0.226	*	0.169	*	0.241	*	1.062	*	0.085	*	2.038	*
K	0.176	2.393	0.0	2.158	0.004	0.258	0.002	0.193	0.0	0.241	0.051	2.187	0.0	0.065	0.0	2.038
H	2.000	2.000	2.000	2.000	2.000	2.000	2.000	2.000	2.000	2.000	2.000	2.000	2.000	2.000	2.000	2.000
O	24.000	*	24.000	*	24.000	*	24.000	*	24.000	*	24.000	*	24.000	*	24.000	*
MG		30.41		39.70		21.25		18.72		22.62		30.96		42.23		69.77
FE		38.59		31.15		63.67		66.87		63.22		35.58		55.67		1.51
CA		29.78		28.07		3.44		2.58		3.39		31.15		1.24		28.54
MN		1.22		1.08		11.64		11.83		10.77		2.32		0.86		0.18
MG		30.79		40.13		24.05		21.23		25.35		31.60		42.60		69.90
FE		39.06		31.49		72.06		75.85		70.85		36.42		56.15		1.51
CA		30.15		28.38		3.89		2.93		3.80		31.80		1.25		28.59
MG		43.31		55.19		22.00		19.21		23.41		44.96		42.76		97.64
FE		54.95		43.31		65.94		68.64		65.44		51.67		56.37		2.11
MN		1.73		1.51		12.06		12.14		11.15		3.37		0.87		0.25
F/M		1.309		0.812		3.545		4.205		3.271		1.224		1.330		0.024
F/FM		0.567		0.448		0.780		0.808		0.766		0.550		0.572		0.024

1 SN 7211, SNYDER BRECCIA
2 SN 7258, SNYDER BRECCIA
3 SN 7256, IRON-FORMATION
4 SN 7267, IRON-FORMATION
5 SN 7267, IRON-FORMATION
6 SN 7268, SNYDER BRECCIA
7 SN 7268, SNYDER BRECCIA
8 SN 7284, QUARTZITE MARBLE

TABLE 2 AMPHIBOLE ANALYSES FOR THE SNYDER GROUP (CONTINUED)

	9	10	11	12	13	14	15	16
SIO2	47.40	46.12	48.55	46.75	48.59	45.37	50.59	47.72
A2O3	1.17	8.77	1.80	6.30	6.71	7.63	3.92	6.20
FEO	33.29	17.51	35.15	20.67	19.03	19.41	16.51	17.51
TIO2	0.27	0.45	0.0	0.77	0.38	0.54	0.04	0.04
MNO	8.57	0.72	2.62	0.23	0.33	0.54	2.22	0.51
CAO	3.27	12.24	1.73	11.12	11.33	12.56	12.20	12.61
MGO	4.42	10.62	8.71	10.37	10.60	10.37	12.65	12.15
NA2O	0.02	0.98	0.0	0.91	0.93	0.76	0.42	0.06
K2O	0.01	0.59	0.0	0.0	0.43	0.0	0.0	0.0
H2O	1.86	2.00	1.91	1.97	2.02	1.97	2.03	2.00
SUM	100.27	99.90	100.47	99.30	100.25	99.15	100.57	99.80

SI	7.651	*	6.895	*	7.610	*	7.100	*	7.218	*	6.893	*	7.453	*	7.163	*
AL	0.223	7.874	1.105	8.000	0.332	7.943	0.900	8.000	0.782	8.000	1.137	8.000	0.547	8.000	0.837	8.000
AL	0.0	*	0.440	*	0.0	*	0.228	*	0.393	*	0.259	*	0.117	*	0.260	*
TI	0.033	*	0.051	*	0.0	*	0.088	*	0.042	*	0.062	*	0.006	*	0.005	*
FE	4.493	*	2.189	*	4.608	*	2.625	*	2.364	*	2.465	*	2.034	*	2.158	*
MG	1.063	*	2.366	*	2.035	*	2.348	*	2.347	*	2.348	*	2.778	*	2.719	*
MN	1.172	6.761	0.091	5.137	0.348	6.990	0.030	5.318	0.042	5.189	0.069	5.205	0.277	5.219	0.065	5.246
NA	0.006	*	0.255	*	0.0	*	0.239	*	0.239	*	0.224	*	0.120	*	0.017	*
CA	0.566	*	1.961	*	0.291	*	1.810	*	1.803	*	2.045	*	1.940	*	2.028	*
K	0.002	0.574	0.113	2.328	0.0	0.291	0.0	2.049	0.081	2.124	0.0	2.268	0.0	2.060	0.0	2.046
H	2.000	2.000	2.000	2.000	2.000	2.000	2.000	2.000	2.000	2.000	2.000	2.000	2.000	2.000	2.000	2.000
O	24.000	*	24.000	*	24.000	*	24.000	*	24.000	*	24.000	*	24.000	*	24.000	*
	MG	14.58		35.82		27.95		34.46		35.90		33.90		39.52		38.78
	FE	61.60		33.13		63.28		38.54		36.06		35.50		28.04		31.36
	CA	7.75		29.67		3.99		26.56		27.51		29.51		27.60		28.93
	MN	16.07		1.38		4.78		0.43		0.63		1.00		3.84		0.93
	MG	17.37		36.32		29.35		34.61		36.03		34.24		41.14		39.14
	FE	73.39		33.60		66.46		38.71		36.20		35.06		30.13		31.65
	CA	9.24		30.09		4.19		26.58		27.68		29.81		28.73		29.20
	MG	15.81		50.93		29.11		46.93		49.38		48.08		54.58		54.57
	FE	66.78		47.11		65.91		52.48		49.74		50.50		40.97		44.13
	MN	17.42		1.96		4.98		0.59		0.87		1.42		5.44		1.30
	F/M	5.326		0.964		2.435		1.131		1.025		1.080		0.832		0.832
	F/FM	0.842		0.491		0.709		0.531		0.506		0.519		0.454		0.454

9 SN 72107, IRON-FORMATION
10 SN 72117, SNYDER BRECCIA
11 SN 72118, IRON-FORMATION
12 SN 72126, SNYDER BRECCIA
13 SN 72126, SNYDER BRECCIA
14 SN 72132, SNYDER BRECCIA
15 SN 72156, LOWER QUARTZITE
16 SN 72172, SNYDER BRECCIA

TABLE 2 AMPHIBOLE ANALYSES FOR THE SNYDER GROUP (CONTINUED)

	17	18	19	20	21	22	23	24
SIO2	53.38	47.64	46.42	49.88	45.17	48.28	48.72	44.35
A203	0.55	7.48	9.79	1.31	8.44	3.22	7.67	8.44
FEO	24.75	16.61	24.37	32.26	27.92	26.11	32.76	26.24
TIO2	0.11	0.36	0.19	0.18	0.0	0.0	0.33	1.84
MNO	1.40	0.66	1.98	4.36	1.98	2.41	3.89	10.35
CAO	0.94	11.47	8.98	1.50	10.41	11.03	1.61	6.44
MGO	17.16	12.01	4.78	5.04	5.42	6.40	5.10	0.0
NA20	0.05	0.78	0.76	0.07	0.0	0.0	0.00	0.0
K20	0.0	0.58	0.47	0.03	0.0	0.0	0.03	0.0
H20	2.04	2.02	1.96	1.87	1.85	1.92	1.85	1.89
SUM	100.48	99.61	99.60	97.50	101.29	99.46	96.50	99.54

SI	7.840	*	7.078	*	7.109	*	7.085	*	6.948	*	7.522	*	7.827	*	7.094	*
AL	0.113	7.953	0.922	8.000	0.891	8.000	0.015	8.000	1.052	8.000	0.478	8.000	0.173	8.000	0.906	8.000
AL	0.0	*	0.387	*	0.875	*	0.232	*	0.478	*	0.113	*	0.328	*	0.672	*
TI	0.012	*	0.040	*	0.022	*	0.022	*	0.0	*	0.0	*	0.040	*	0.221	*
FE	3.040	*	2.064	*	3.121	*	4.319	*	3.592	*	3.402	*	4.447	*	3.505	*
MG	3.757	*	2.659	*	1.091	*	1.417	*	1.243	*	1.537	*	1.234	*	0.0	*
MN	0.174	6.983	0.383	5.234	0.244	5.353	0.591	6.581	0.258	5.570	0.318	5.341	0.535	6.584	1.400	5.798
NA	0.014	*	0.225	*	0.226	*	0.022	*	0.0	*	0.0	*	0.028	*	0.0	*
CA	0.148	*	1.926	*	1.473	*	0.274	*	1.716	*	1.841	*	0.290	*	1.102	*
K	0.0	0.162	0.110	2.160	0.092	1.791	0.006	0.302	0.0	1.716	0.0	1.841	0.006	0.315	0.0	1.102
H	2.000	2.000	2.000	2.000	2.000	2.000	2.000	2.000	2.000	2.000	2.000	2.000	2.000	2.000	2.000	2.000
O	24.000	*	24.000	*	24.000	*	24.000	*	24.000	*	24.000	*	24.000	*	24.000	*
	MG	52.77		40.10		18.40		21.47		18.25		21.32		10.00		0.0
	FE	42.70		31.12		52.64		65.42		52.76		48.13		68.46		58.35
	CA	2.08		27.53		24.85		4.16		25.20		26.05		4.31		18.35
	MN	2.45		1.25		4.11		8.95		3.79		4.50		8.23		23.31
	MG	54.09		40.61		19.19		23.58		18.97		22.33		20.70		0.0
	FE	43.78		31.51		54.89		71.85		54.83		50.40		74.60		76.08
	CA	2.13		27.88		25.92		4.57		26.19		27.28		4.70		23.92
	MG	53.89		55.33		24.40		22.40		24.40		28.83		10.85		0.0
	FE	43.61		42.94		70.04		68.26		70.53		65.08		71.54		71.45
	MN	2.50		1.73		5.47		9.34		5.07		6.09		9.60		28.55
	F/M	0.856		0.807		3.084		3.464		3.098		2.468		4.038		0.832
	F/FM	0.461		0.447		0.755		0.776		0.756		0.712		0.801		0.454

17 SN 72196, SNYDER BRECCIA
18 SN 72196, SNYDER BRECCIA
19 SN 72204, IRON-FORMATION
20 SN 72204, IRON-FORMATION
21 SN 72205, IRON-FORMATION
22 SN 72205, IRON-FORMATION
23 SN 72207, IRON-FORMATION
24 SN 72207, IRON-FORMATION

TABLE 2 AMPHIBOLE ANALYSES FOR THE SNYDER GROUP (CONTINUED)

	25	26	27	28	29	30	31	32
SIO2	51.65	42.19	46.82	48.76	49.98	50.88	52.55	49.69
A2O3	3.00	9.42	8.03	5.29	5.29	4.39	1.87	0.83
FEO	20.75	21.22	18.55	14.35	12.40	14.68	21.67	32.83
TIO2	0.31	2.57	1.72	0.09	0.0	0.09	0.06	0.19
MNO	1.28	0.46	0.38	0.44	0.20	0.19	0.33	6.21
CAO	12.47	11.41	12.00	12.79	11.88	11.47	1.97	1.18
MGO	10.62	8.11	9.30	13.14	15.15	13.88	17.39	4.88
NA2O	0.25	1.97	1.22	0.48	0.0	0.70	0.20	0.07
K2O	0.0	1.06	0.68	0.49	0.0	0.40	0.01	0.01
H2O	2.04	1.95	2.01	2.00	2.02	2.03	2.02	1.86
SUM	102.37	100.46	100.71	97.83	96.92	98.71	97.87	97.75

SI	7.569	*	6.465	*	6.966	*	7.308	*	7.409	*	7.501	*	7.797	*	8.022	*
AL	0.431	8.000	1.535	8.000	1.034	8.000	0.692	8.000	0.591	8.000	0.499	8.000	0.203	8.000	0.0	8.022
AL	0.088	*	0.166	*	0.373	*	0.243	*	0.333	*	0.264	*	0.124	*	0.158	*
TI	0.034	*	0.308	*	0.192	*	0.010	*	0.0	*	0.010	*	0.007	*	0.023	*
FE	2.543	*	2.719	*	2.308	*	1.799	*	1.537	*	1.810	*	2.689	*	4.433	*
MG	2.320	*	1.852	*	2.062	*	2.936	*	3.347	*	3.050	*	3.846	*	1.174	*
MN	0.159	5.144	0.060	5.106	0.068	4.984	0.036	5.043	0.025	5.242	0.024	5.158	0.041	6.706	0.849	6.637
NA	0.071	*	0.585	*	0.352	*	0.139	*	0.0	*	0.230	*	0.059	*	0.122	*
CA	1.958	*	1.873	*	1.913	*	2.054	*	1.887	*	1.812	*	0.297	*	0.204	*
K	0.0	2.029	0.207	2.666	0.129	2.394	0.094	2.287	0.0	1.887	0.375	2.087	0.102	0.757	0.902	0.228
H	2.000	2.000	2.000	2.000	2.000	2.000	2.000	2.000	2.000	2.000	2.000	2.000	2.000	2.000	2.000	2.000
O	24.000	*	24.000	*	24.000	*	24.000	*	24.000	*	24.000	*	24.000	*	24.000	*
	MG	33.24		28.49		32.57		42.89		49.25		45.55		55.05		17.63
	FE	36.44		41.81		36.46		26.28		22.62		27.03		39.12		66.55
	CA	28.05		28.80		30.21		30.01		27.76		27.06		4.32		3.06
	MN	2.28		0.92		0.76		0.82		0.37		0.35		0.60		12.75
	MG	34.01		28.74		32.82		43.24		49.43		45.72		56.79		20.21
	FE	37.28		42.19		36.73		26.50		22.70		27.13		39.36		76.28
	CA	28.71		29.07		30.44		30.26		27.86		27.16		4.35		3.51
	MG	46.19		40.00		46.68		61.28		68.18		62.45		58.48		18.19
	FE	50.64		58.72		52.24		37.55		31.31		37.06		40.80		68.66
	MN	3.16		1.29		1.08		1.17		0.51		0.49		0.63		13.15
	F/M	1.165		1.500		1.142		0.632		0.467		0.601		0.710		4.498
	F/FM	0.538		0.600		0.533		0.387		0.318		0.375		0.415		0.818

25 SN 72222, IRON-FORMATION
26 SN 74231, HILL 1300 AMPHIBOLITE
27 SN 74236, HILL 1300 AMPHIBOLITE
28 SN 74255, LOWER QUARTZITE
29 SN 74301, LAYERED DIKE
30 SN 74317, LAYERED DIKE
31 SN 74319, LAYERED DIKE
32 SN 74321, IRON-FORMATION

TABLE 2 AMPHIBOLE ANALYSES FOR THE SNYDER GROUP (CONTINUED)

	33	34	35	36	37	38	39	40
SIO2	45.66	49.69	45.66	43.50	56.28	46.49	50.38	47.20
AL2O3	8.86	5.57	7.15	11.48	0.49	0.84	6.62	10.76
FEO	19.33	15.03	26.44	25.35	19.35	34.99	4.68	4.46
TIO2	0.09	1.15	0.0	0.24	0.23	0.23	0.0	0.0
MNO	0.65	0.19	1.76	2.24	1.03	7.22	0.12	0.23
CAO	12.15	11.52	10.43	10.42	0.76	1.38	12.81	13.19
MGO	9.16	13.42	6.59	3.70	19.10	5.35	19.02	19.05
NA2O	0.95	0.30	0.0	0.05	0.12	0.0	0.0	0.0
K2O	0.45	0.51	0.0	0.02	0.02	0.01	0.0	0.0
H2O	1.98	2.05	1.93	1.92	2.09	1.82	2.07	2.06
SUM	99.29	99.93	99.96	99.02	99.47	98.33	95.70	96.05

SI	6.922	*	7.273	*	7.069	*	6.790	*	8.078	*	7.657	*	7.308	*	6.851	*
AL	1.078	8.000	0.727	8.000	0.931	8.000	1.210	8.000	0.0	8.078	0.153	7.820	0.692	8.000	1.149	8.000
AL	0.505	*	0.234	*	0.373	*	0.896	*	0.083	*	0.0	*	0.440	*	0.571	*
TI	0.010	*	0.127	*	0.0	*	0.028	*	0.025	*	0.028	*	0.0	*	0.0	*
FE	2.451	*	1.840	*	3.423	*	3.301	*	2.323	*	4.819	*	0.568	*	0.541	*
MG	2.070	*	2.928	*	1.521	*	0.859	*	4.086	*	1.313	*	4.112	*	4.121	*
MN	0.083	5.119	0.024	5.152	0.231	5.548	0.295	5.380	0.125	6.642	1.207	7.168	0.015	5.135	0.004	5.237
NA	0.279	*	0.227	*	0.0	*	0.015	*	0.033	*	0.0	*	0.0	*	0.0	*
CA	1.973	*	1.807	*	1.730	*	1.739	*	0.117	*	0.244	*	1.991	*	2.051	*
K	0.087	2.340	0.095	2.129	0.0	1.730	0.004	1.758	0.004	0.154	0.002	0.246	0.0	1.991	0.0	2.051
H	2.000	2.000	2.000	2.000	2.000	2.000	2.000	2.000	2.000	2.000	2.000	2.000	2.000	2.000	2.000	2.000
O	24.000	*	24.000	*	24.000	*	24.000	*	24.000	*	24.000	*	24.000	*	24.000	*
	MG	31.47		44.39		22.02		13.86		61.44		17.70		61.51		61.35
	FE	37.26		27.89		49.58		53.30		34.92		65.27		8.49		8.06
	CA	30.00		27.38		25.06		28.07		1.76		3.30		29.78		30.53
	MN	1.27		0.36		3.34		4.77		1.88		13.64		0.22		0.05
	MG	31.97		44.53		22.79		14.56		62.62		20.60		61.65		61.38
	FE	37.74		27.99		51.29		55.97		35.59		75.58		8.51		8.06
	CA	30.39		27.48		25.92		29.47		1.79		3.82		29.84		30.55
	MG	44.96		61.11		29.39		19.27		62.54		18.39		87.53		88.32
	FE	53.23		38.40		66.15		74.09		35.55		67.50		12.09		11.60
	MN	1.81		0.49		4.46		6.63		1.92		14.11		0.31		0.08
	F/M	1.224		0.636		2.403		4.188		0.599		4.436		0.142		0.132
	F/FM	0.550		0.389		0.706		0.807		0.375		0.816		0.124		0.117

33 SN 74351, SNYDER BRECCIA
34 SN 74351, SNYDER BRECCIA
35 SN 74383, IRON-FORMATION
36 SN 74383, IRON-FORMATION
37 SN 74399, GRAPHITE-SULFIDE HORNFELS
38 SN 74399, IRON-FORMATION
39 NC 7405, CALCSILICATE
40 NC 7443, CALCSILICATE

TABLE 3 BIOTITE ANALYSES FOR THE SNYDER GROUP

	1		2		3		4		5		6		7		8	
SIO2	36.24		34.71		33.82		35.31		32.40		36.08		35.81		36.57	
A2O3	16.81		18.59		19.00		18.64		18.82		19.32		14.92		14.30	
FEO	23.77		22.96		25.75		21.49		26.87		20.67		20.85		23.75	
TIO2	2.58		3.23		1.92		3.37		1.80		4.14		3.56		4.72	
MNO	0.35		0.25		0.60		0.10		0.58		0.27		0.25		0.47	
CAO	0.0		0.02		0.05		0.02		0.03		0.03		0.07		0.16	
MGO	9.56		5.91		4.25		8.17		4.71		6.59		8.85		7.19	
NA2O	0.05		0.0		0.0		0.04		0.0		0.0		0.0		0.0	
K2O	9.93		9.41		9.29		10.31		8.71		9.48		8.95		8.95	
H2O	4.00		3.85		3.77		3.95		3.71		3.98		3.81		3.88	
SUM	103.29		98.93		98.45		101.10		97.63		100.56		97.07		100.08	
SI	5.428	*	5.401	*	5.373	*	5.355	*	5.227	*	5.438	*	5.628	*	5.644	*
AL	2.572	8.000	2.599	8.000	2.627	8.000	2.645	8.000	2.773	8.000	2.562	8.000	2.372	8.000	2.356	8.000
AL	0.394	*	0.809	*	0.930	*	0.686	*	0.805	*	0.869	*	0.391	*	0.261	*
TI	0.291	*	0.378	*	0.229	*	0.350	*	0.218	*	0.469	*	0.421	*	0.548	*
FE	2.977	*	2.988	*	3.421	*	2.725	*	3.625	*	2.605	*	2.740	*	3.065	*
MN	0.044	*	0.033	*	0.081	*	0.013	*	0.079	*	0.034	*	0.033	*	0.061	*
MG	2.134	5.941	1.371	5.578	1.006	5.667	1.847	5.621	1.133	5.861	1.480	5.459	2.073	5.659	1.654	5.590
CA	0.0	*	0.003	*	0.009	*	0.003	*	0.005	*	0.005	*	0.012	*	0.026	*
NA	0.015	*	0.0	*	0.0	*	0.012	*	0.0	*	0.0	*	0.0	*	0.0	*
K	1.997	1.911	1.967	1.871	1.882	1.891	1.994	2.009	1.792	1.798	1.922	1.827	1.794	1.806	1.762	1.788
H	4.000	4.000	4.000	4.000	4.000	4.000	4.000	4.000	4.000	4.000	4.000	4.000	4.000	4.000	4.000	4.000
O	24.000	*	24.000	*	24.000	*	24.000	*	24.000	*	24.000	*	24.000	*	24.000	*
F/M		1.416		2.204		3.480		1.483		3.271		1.783		1.338		1.890
F/FM		0.586		0.698		0.777		0.597		0.766		0.641		0.572		0.654

1 SN 7211, SNYDER BRECCIA
2 SN 7215, LOWER QUARTZITE
3 SN 7225, LOWER QUARTZITE
4 SN 7237, LOWER QUARTZITE
5 SN 7241, LOWER QUARTZITE
6 SN 7256, LOWER QUARTZITE
7 SN 7259, SNYDER BRECCIA
8 SN 7269, SNYDER BRECCIA

TABLE 3 BIOTITE ANALYSES FOR THE SNYDER GROUP (CONTINUED)

	9		10		11		12		13		14		15		16	
SIO2	33.01		35.61		36.59		37.42		34.45		33.87		39.00		37.13	
AL2O3	16.15		19.59		18.29		18.76		19.10		18.46		17.00		16.58	
FEO	28.87		20.34		20.56		16.64		25.13		25.92		10.57		14.79	
TIO2	6.85		2.53		2.69		2.00		2.96		1.37		2.37		4.52	
MNO	0.15		0.06		0.07		0.08		0.35		0.23		0.15		0.09	
CAO	0.02		0.06		0.07		0.0		0.05		0.01		0.01		0.0	
MGO	3.57		9.62		9.73		12.70		4.38		4.42		12.96		13.85	
NA2O	0.02		0.16		0.09		0.12		0.12		0.07		0.07		0.11	
K2O	9.20		9.78		9.87		10.21		9.38		9.90		10.12		9.84	
H2O	3.83		4.01		4.02		4.10		3.84		3.72		3.58		4.08	
SUM	101.77		101.67		101.98		102.12		99.76		97.06		96.13		100.99	
SI	5.168	*	5.316	*	5.447	*	5.463	*	5.371	*	5.459	*	5.965	*	5.451	*
AL	2.832	8.000	2.584	8.000	2.553	8.000	2.537	8.000	2.629	8.000	2.550	8.000	2.135	8.000	2.549	8.000
AL	0.147	*	0.747	*	0.655	*	0.690	*	0.979	*	0.951	*	0.977	*	0.320	*
TI	0.806	*	0.284	*	0.301	*	0.229	*	0.347	*	0.166	*	0.268	*	0.499	*
FE	3.780	*	2.539	*	2.560	*	2.032	*	3.276	*	3.498	*	1.329	*	1.916	*
MN	0.020	*	0.008	*	0.009	*	0.010	*	0.046	*	0.031	*	0.019	*	0.011	*
MG	0.856	5.609	2.141	5.718	2.159	5.684	2.763	5.724	1.919	5.567	1.060	5.696	2.882	5.376	3.031	5.676
CA	0.003	*	0.010	*	0.011	*	0.0	*	0.008	*	0.002	*	0.002	*	0.0	*
NA	0.006	*	0.046	*	0.026	*	0.034	*	0.036	*	0.022	*	0.020	*	0.031	*
K	1.837	1.846	1.862	1.918	1.874	1.911	1.901	1.935	1.965	1.913	1.955	1.969	1.941	1.963	1.843	1.874
H	4.000	4.000	4.000	4.000	4.000	4.000	4.000	4.000	4.000	4.000	4.000	4.000	4.000	4.000	4.000	4.000
O	24.000	*	24.000	*	24.000	*	24.000	*	24.000	*	24.000	*	24.000	*	24.000	*
F/M		4.437		1.190		1.190		0.739		3.265		3.320		0.469		0.603
F/FM		0.816		0.543		0.543		0.425		0.766		0.765		0.319		0.376

9 SN 7272, LOWER QUARTZITE
10 SN 7274, LOWER QUARTZITE
11 SN 7278, LOWER QUARTZITE
12 SN 7281, LOWER QUARTZITE
13 SN 7283, LOWER QUARTZITE
14 SN 7299, LOWER QUARTZITE
15 SN 7296, GRAPHITE-SULFIDE HORNFELS
16 SN 72111, UPPER QUARTZITE

TABLE 3 BIOTITE ANALYSES FOR THE SNYDER GROUP (CONTINUED)

	17		18		19		20		21		22		23		24	
SIO2	36.18		36.97		35.22		34.40		37.06		33.43		34.17		34.33	
A2O3	16.29		17.32		19.01		19.89		15.63		18.11		17.85		19.07	
FEO	21.55		16.44		24.31		20.57		22.49		28.47		26.27		26.36	
TIO2	2.29		3.23		2.70		3.77		5.27		4.13		1.65		3.05	
MNO	0.19		0.11		0.26		0.15		0.42		0.29		0.20		0.27	
CAO	0.04		0.04		0.08		0.02		0.04		0.02		0.19		0.04	
MGO	11.14		8.24		5.11		6.32		7.33		3.39		6.90		5.21	
NA2O	0.08		0.0		0.0		0.08		0.0		0.0		0.13		0.12	
K2O	8.69		9.25		9.25		9.64		9.59		9.43		9.51		9.49	
H2O	3.95		3.85		3.87		3.84		3.97		3.92		3.85		3.85	
SUM	100.39		95.45		99.81		97.67		101.80		101.09		100.82		100.79	
SI	5.487	*	5.748	*	5.446	*	5.373	*	5.587	*	5.244	*	5.321	*	5.339	*
AL	2.513	8.000	2.252	8.000	2.554	8.000	2.627	8.000	2.413	8.000	2.756	8.000	2.679	8.000	2.661	8.000
AL	0.399	*	0.922	*	0.910	*	0.848	*	0.363	*	0.592	*	0.596	*	0.651	*
TI	0.261	*	0.378	*	0.314	*	0.443	*	0.597	*	0.487	*	0.193	*	0.357	*
FE	2.733	*	2.138	*	3.144	*	2.687	*	2.835	*	3.735	*	3.421	*	3.429	*
MN	0.023	*	0.014	*	0.034	*	0.020	*	0.054	*	0.039	*	0.040	*	0.036	*
MG	2.519	5.935	1.910	5.361	1.178	5.580	1.471	5.469	1.647	5.497	0.793	5.645	1.601	5.851	1.208	5.680
CA	0.007	*	0.007	*	0.013	*	0.003	*	0.006	*	0.033	*	0.032	*	0.007	*
NA	0.024	*	0.0	*	0.0	*	0.024	*	0.0	*	0.0	*	0.039	*	0.036	*
K	1.681	1.711	1.834	1.841	1.924	1.838	1.920	1.948	1.944	1.850	1.887	1.890	1.989	1.960	1.883	1.925
H	4.000	4.000	4.000	4.000	4.000	4.000	4.000	4.000	4.000	4.000	4.000	4.000	4.000	4.000	4.000	4.000
O	24.000	*	24.000	*	24.000	*	24.000	*	24.000	*	24.000	*	24.000	*	24.000	*
F/M		1.005		1.127		2.698		1.840		1.754		4.761		2.161		2.868
F/FM		0.523		0.530		0.730		0.648		0.637		0.826		0.684		0.741

17 SN 72117, SNYDER BRECCIA
18 SN 72127, UPPER QUARTZITE
19 SN 72130, LOWER QUARTZITE
20 SN 72131, LOWER QUAPTZITE
21 SN 72132, SNYDER BRECCIA
22 SN 72133, LOWER QUARTZITE
23 SN 72134, LOWER QUARTZITE
24 SN 72135, LOWER QUARTZITE

TABLE 3 BIOTITE ANALYSES FOR THE SNYDER GROUP (CONTINUED)

	25	26	27	28	29	30	31	32
SIO2	36.10	35.18	35.49	36.23	36.99	36.36	36.78	36.05
A2O3	15.97	19.23	16.60	16.92	16.65	15.21	15.02	15.88
FEO	25.18	21.95	21.45	21.86	18.93	20.88	21.80	20.09
TIO2	4.25	3.04	1.36	1.39	2.48	6.07	4.07	0.11
MNO	0.13	0.07	0.0	0.0	0.28	0.06	0.38	0.70
CAO	0.04	0.02	0.05	0.05	0.03	0.02	0.16	0.10
MGO	8.15	8.09	10.75	10.95	12.31	8.97	7.54	10.74
NA2O	0.10	0.07	0.19	0.19	0.07	0.06	0.0	0.23
K2O	9.72	10.09	9.52	9.72	9.75	10.01	8.95	8.51
H2O	3.99	3.97	3.88	3.96	4.03	3.98	3.86	3.90
SUM	103.63	101.71	99.29	101.27	101.52	101.62	98.56	96.21

SI	5.422	*	5.303	*	5.473	*	5.478	*	5.503	*	5.475	*	5.707	*	5.685	*
AL	2.578	8.000	2.697	8.000	2.527	8.000	2.522	8.000	2.497	8.000	2.525	8.000	2.298	8.000	2.315	8.000
AL	0.248	*	0.719	*	0.490	*	0.492	*	0.421	*	0.174	*	0.444	*	0.636	*
TI	0.480	*	0.345	*	0.158	*	0.158	*	0.277	*	0.587	*	0.474	*	0.013	*
FE	3.163	*	2.767	*	2.766	*	2.764	*	2.355	*	2.630	*	2.826	*	2.649	*
MN	0.017	*	0.009	*	0.0	*	0.0	*	0.035	*	0.008	*	0.050	*	0.093	*
MG	1.824	5.731	1.818	5.658	2.471	5.985	2.468	5.882	2.729	5.819	2.013	5.512	1.742	5.538	2.524	5.916
CA	0.006	*	0.003	*	0.008	*	0.008	*	0.005	*	0.003	*	0.027	*	0.017	*
NA	0.029	*	0.020	*	0.057	*	0.056	*	0.020	*	0.018	*	0.0	*	0.070	*
K	1.862	1.897	1.940	1.964	1.873	1.938	1.874	1.938	1.850	1.875	1.923	1.943	1.770	1.796	1.712	1.799
H	4.000	4.000	4.000	4.000	4.000	4.000	4.000	4.000	4.000	4.000	4.000	4.000	4.000	4.000	4.000	4.000
O	24.000	*	24.000	*	24.000	*	24.000	*	24.000	*	24.000	*	24.000	*	24.000	*
F/M		1.743		1.527		1.120		1.120		0.876		1.310		1.651		1.087
F/FM		0.635		0.604		0.528		0.528		0.467		0.567		0.623		0.521

25 SN 72147, LOWER QUARTZITE
26 SN 72151, LOWER QUARTZITE
27 SN 72157, UPPER QUARTZITE
28 SN 72157, UPPER QUARTZITE
29 SN 72160, UPPER QUARTZITE
30 SN 72162, UPPER QUARTZITE
31 SN 72172, SNYDER BRECCIA
32 SN 72173, LOWER QUARTZITE

TABLE 3 BIOTITE ANALYSES FOR THE SNYDER GROUP (CONTINUED)

	33		34		35		36		37		38		39		40	
SIO2	37.59		35.67		34.11		34.48		33.50		35.66		34.38		35.37	
A2O3	15.83		17.05		17.05		16.55		20.56		13.00		13.00		18.21	
FEO	20.31		20.20		27.14		25.86		25.01		23.94		25.00		23.17	
TIO2	0.22		4.62		6.93		5.40		3.60		5.07		5.24		2.43	
MNO	0.58		0.04		0.29		0.25		0.12		0.66		0.24		0.18	
CAO	0.08		0.0		0.01		0.02		0.02		0.33		0.04		0.04	
MGO	9.64		9.93		3.95		5.62		3.71		9.13		5.63		6.47	
NA2O	0.06		0.05		0.0		0.14		0.04		0.04		0.24		0.07	
K2O	8.40		9.59		9.27		9.77		9.20		8.46		8.81		8.51	
H2O	3.84		3.99		3.91		3.89		3.85		3.82		3.72		3.85	
SUM	96.65		101.24		102.66		101.98		99.61		99.11		98.20		99.00	
SI	5.879	*	5.360	*	5.228	*	5.306	*	5.218	*	5.597	*	5.541	*	5.459	*
AL	2.121	8.000	2.640	8.000	2.772	8.000	2.694	8.000	2.782	8.000	2.403	7.987	2.459	8.000	2.541	8.000
AL	0.788	*	0.380	*	0.307	*	0.308	*	0.991	*	0.0	*	0.010	*	0.798	*
TI	0.026	*	0.522	*	0.799	*	0.625	*	0.422	*	0.597	*	0.635	*	0.284	*
FE	2.649	*	2.539	*	3.479	*	3.328	*	3.258	*	3.137	*	3.503	*	3.016	*
MN	0.077	*	0.005	*	0.038	*	0.033	*	0.016	*	0.088	*	0.033	*	0.024	*
MG	2.241	5.781	2.224	5.670	0.902	5.524	1.289	5.583	0.861	5.548	1.899	5.720	1.353	5.534	1.501	5.624
CA	0.013	*	0.0	*	0.002	*	0.003	*	0.003	*	0.055	*	0.007	*	0.007	*
NA	0.018	*	0.015	*	0.0	*	0.042	*	0.012	*	0.012	*	0.075	*	0.021	*
K	1.671	1.703	1.857	1.872	1.812	1.814	1.918	1.963	1.829	1.843	1.691	1.758	2.017	2.090	1.888	1.916
H	4.000	4.000	4.000	4.000	4.000	4.000	4.000	4.000	4.000	4.000	4.000	4.000	4.000	4.000	4.000	4.000
O	24.000	*	24.000	*	24.000	*	24.000	*	24.000	*	24.000	*	24.000	*	24.000	*
F/M		1.216		1.144		3.807		2.607		3.801		1.698		2.614		2.025
F/F+M		0.549		0.534		0.796		0.723		0.792		0.629		0.723		0.669

33 SN 72173, LOWER QUARTZITE
34 SN 72175,
35 SN 72176, LOWER QUAPTZITE
36 SN 72176, LOWER QUARTZITE
37 SN 72179, LOWER QUARTZITE
38 SN 72188, IRON-FORMATION
39 SN 72191, LOWER QUAPTZITE
40 SN 72193, LOWER QUARTZITE

TABLE 3 BIOTITE ANALYSES FOR THE SNYDER GROUP (CONTINUED)

	41	42	43	44	45	46	47	48
SIO2	35.64	35.33	36.76	36.64	35.06	33.43	33.88	34.00
A2O3	21.85	19.93	16.51	14.51	17.17	20.40	14.42	18.30
FEO	19.32	22.73	18.16	20.21	21.00	24.94	26.62	23.52
TIO2	2.96	2.72	2.84	4.38	3.35	2.56	4.18	3.50
MNO	0.06	0.05	0.18	0.26	0.13	0.17	0.10	0.07
CAO	0.02	0.0	0.58	0.10	0.03	0.01	0.30	0.07
MGO	7.03	7.67	13.07	8.63	9.56	7.58	5.29	6.52
NA2O	0.05	0.09	0.22	0.0	0.27	0.15	0.10	0.08
K2O	9.35	9.73	8.78	8.89	10.07	8.54	8.09	8.00
H2O	4.01	4.00	4.04	3.85	3.99	3.94	3.60	3.91
SUM	100.29	102.25	101.14	97.47	99.53	101.67	96.74	100.95

SI	5.331	*	5.296	*	5.455	*	5.705	*	5.406	*	5.085	*	5.504	*	5.361	*
AL	2.669	8.000	2.704	8.000	2.545	8.000	2.295	8.000	2.594	8.000	2.915	8.000	2.496	8.000	2.639	8.000
AL	1.182	*	0.816	*	0.343	*	0.368	*	0.526	*	0.741	*	0.264	*	0.666	*
TI	0.333	*	0.307	*	0.317	*	0.513	*	0.388	*	0.293	*	0.511	*	0.403	*
FE	2.417	*	2.849	*	2.254	*	2.632	*	2.708	*	3.172	*	3.616	*	3.314	*
MN	0.008	*	0.006	*	0.023	*	0.034	*	0.017	*	0.015	*	0.014	*	0.000	*
MG	1.567	5.505	1.714	5.692	2.891	5.827	2.003	5.549	1.967	5.807	1.718	5.940	1.278	5.683	1.499	5.581
CA	0.003	*	0.0	*	0.092	*	0.017	*	0.005	*	0.002	*	0.068	*	0.011	*
NA	0.014	*	0.026	*	0.063	*	0.0	*	0.081	*	0.044	*	0.031	*	0.024	*
K	1.784	1.801	1.860	1.886	1.662	1.817	1.766	1.782	1.981	2.066	1.657	1.703	1.674	1.773	1.952	1.988
H	4.000	4.000	4.000	4.000	4.000	4.000	4.000	4.000	4.000	4.000	4.000	4.000	4.000	4.000	4.000	4.000
O	24.000	*	24.000	*	24.000	*	24.000	*	24.000	*	24.000	*	24.000	*	24.000	*
F/M		1.547		1.666		0.787		1.331		1.385		1.855		2.840		2.030
F/FM		0.607		0.625		0.441		0.571		0.581		0.650		0.740		0.670

41 SN 72194, LOWER QUARTZITE
42 SN 72195, LOWER QUARTZITE
43 SN 72196, SNYDER BRECCIA
44 SN 72196A, LOWER QUARTZITE
45 SN 72200, LOWER QUARTZITE
46 SN 72111, UPPER QUARTZITE
47 SN 72211, LOWER QUARTZITE
48 SN 72215, LOWER QUARTZITE

TABLE 3 BIOTITE ANALYSES FOR THE SNYDER GROUP (CONTINUED)

	49		50		51		52		53		54		55		56	
SIO2	36.80		36.53		34.46		34.21		38.41		39.21		33.84		37.40	
A2O3	19.13		15.04		15.69		16.34		15.23		15.53		16.31		18.98	
FEO	17.90		22.77		25.56		28.27		12.60		12.85		28.37		16.34	
TIO2	3.51		3.47		3.74		4.51		2.69		2.74		4.93		2.52	
MNO	0.06		0.12		0.17		0.18		0.07		0.07		0.08		0.03	
CAO	0.0		0.12		0.32		0.17		0.02		0.02		0.03		0.0	
MGO	10.17		10.50		7.46		4.94		16.85		17.15		4.39		11.79	
NA2O	0.12		0.12		0.14		0.0		0.22		0.22		0.00		0.10	
K2O	9.50		9.08		8.75		8.63		9.27		8.44		9.75		10.01	
H2O	4.06		3.97		3.84		3.84		4.06		4.14		3.83		4.08	
SUM	101.25		101.72		100.13		101.19		98.42		100.37		101.62		101.25	
SI	5.431	*	5.516	*	5.377	*	5.334	*	5.671	*	5.676	*	5.295	*	5.489	*
AL	2.569	8.000	2.484	8.000	2.623	8.000	2.666	8.000	2.329	8.000	2.324	8.000	2.705	8.000	2.511	8.000
AL	0.758	*	0.192	*	0.262	*	0.337	*	0.320	*	0.324	*	0.302	*	0.772	*
TI	0.390	*	0.394	*	0.439	*	0.541	*	0.299	*	0.298	*	0.580	*	0.278	*
FE	2.209	*	2.875	*	3.335	*	3.686	*	1.556	*	1.555	*	3.712	*	2.006	*
MN	0.008	*	0.015	*	0.022	*	0.024	*	0.009	*	0.009	*	0.011	*	0.004	*
MG	2.237	5.602	2.363	5.839	1.735	5.794	1.148	5.735	3.708	5.991	3.700	5.887	1.324	5.628	2.579	5.638
CA	0.0	*	0.019	*	0.053	*	0.028	*	0.003	*	0.003	*	0.005	*	0.0	*
NA	0.034	*	0.035	*	0.042	*	0.0	*	0.063	*	0.057	*	0.027	*	0.028	*
K	1.788	1.823	1.749	1.803	1.741	1.837	1.716	1.745	1.557	1.623	1.558	1.623	1.946	1.978	1.874	1.902
H	4.000	4.000	4.000	4.000	4.000	4.000	4.000	4.000	4.000	4.000	4.000	4.000	4.000	4.000	4.000	4.000
O	24.000	*	24.000	*	24.000	*	24.000	*	24.000	*	24.000	*	24.000	*	24.000	*
F/M		0.991		1.223		1.935		3.232		0.422		0.423		3.636		0.779
F/FM		0.498		0.550		0.659		0.764		0.297		0.297		0.784		0.438

49 SN 72223, META DIKE
50 SN 74236, HILL 1300 AMPHIBOLITE
51 SN 74251, LOWER QUARTZITE
52 SN 74251, LOWER QUARTZITE
53 SN 74255, LOWER QUARTZITE
54 SN 74255, LOWER QUARTZITE
55 SN 74263, LOWER QUARTZITE
56 SN 74275, UPPER QUARTZITE

TABLE 3 BIOTITE ANALYSES FOR THE SNYDER GROUP (CONTINUED)

	57		58		59		60		61		62		63		64	
SIO2	35.98		34.97		36.09		34.85		35.03		41.95		34.70		37.18	
A2O3	15.78		16.72		18.06		15.18		15.97		16.64		19.27		16.96	
FEO	19.58		27.52		18.55		26.41		25.77		9.98		23.03		14.36	
TIO2	5.06		4.52		2.97		7.62		5.29		1.63		3.16		3.93	
MNO	0.06		0.10		0.07		0.08		0.07		0.02		0.13		0.02	
CAO	0.02		0.04		0.03		0.04		0.03		0.05		0.01		0.0	
MGO	9.12		5.74		8.90		5.85		7.08		15.63		7.86		13.69	
NA2O	0.13		0.12		0.06		0.10		0.07		0.09		0.12		0.00	
K2O	10.21		10.03		9.43		9.82		9.86		9.69		9.65		10.70	
H2O	3.93		3.93		3.91		3.96		3.94		4.18		3.97		4.06	
SUM	99.87		103.59		98.07		103.91		103.11		99.66		101.99		100.19	
ST	5.491	*	5.316	*	5.532	*	5.277	*	5.322	*	5.999	*	5.243	*	5.489	*
AL	2.509	8.000	2.684	8.000	2.468	8.000	2.709	7.986	2.678	8.000	2.001	8.000	2.757	8.000	2.511	8.000
AL	0.329	*	0.319	*	0.794	*	0.0	*	0.181	*	0.810	*	0.674	*	0.440	*
TI	0.581	*	0.518	*	0.342	*	0.868	*	0.604	*	0.176	*	0.359	*	0.425	*
FE	2.499	*	3.508	*	2.378	*	3.345	*	3.274	*	1.194	*	2.919	*	1.773	*
MN	0.008	*	0.013	*	0.009	*	0.010	*	0.009	*	0.002	*	0.017	*	0.003	*
MG	2.075	5.491	1.304	5.663	2.033	5.557	1.320	5.543	1.603	5.572	3.339	5.517	1.770	5.721	3.013	5.653
CA	0.003	*	0.007	*	0.005	*	0.006	*	0.005	*	0.008	*	0.002	*	0.0	*
NA	0.038	*	0.035	*	0.018	*	0.029	*	0.021	*	0.025	*	0.035	*	0.026	*
K	1.987	2.029	1.950	1.992	1.844	1.866	1.897	1.933	1.911	1.936	1.772	1.804	1.960	1.997	1.983	1.990
H	4.000	4.000	4.000	4.000	4.000	4.000	4.000	4.000	4.000	4.000	4.000	4.000	4.000	4.000	4.000	4.000
O	24.000	*	24.000	*	24.000	*	24.000	*	24.000	*	24.000	*	24.000	*	24.000	*
F/M		1.209		2.700		1.174		2.541		2.048		0.355		1.653		0.589
F/FM		0.547		0.730		0.540		0.718		0.672		0.262		0.623		0.371

57 SN 74276, UPPER QUARTZITE
58 SN 74280, LOWER QUARTZITE
59 SN 74283, LOWER QUARTZITE
60 SN 74287, LOWER QUARTZITE
61 SN 74288, LOWER QUARTZITE
62 SN 74299, GRAPHITE-SULFIDE HORNFELS
63 SN 74302, LOWER QUARTZITE
64 SN 74302, LOWER QUARTZITE

TABLE 3 BIOTITE ANALYSES FOR THE SNYDER GROUP (CONTINUED)

	65		66		67		68		69		70		71		72	
SIO2	35.60		34.68		34.76		34.32		35.42		34.78		35.22		35.03	
A2O3	14.55		14.12		14.33		15.48		13.08		17.60		17.62		14.20	
FEO	24.30		23.22		25.73		26.95		27.79		18.07		18.68		21.56	
TIO2	4.35		5.74		5.68		5.28		4.54		2.31		2.98		6.39	
MNO	0.12		0.19		0.25		0.08		0.93		0.06		0.14		0.14	
CAO	0.12		0.02		0.04		0.02		0.22		0.12		0.01		0.07	
MGO	9.24		8.52		6.26		5.75		5.59		13.98		9.55		9.70	
NA2O	0.23		0.07		0.0		0.07		0.10		0.14		0.11		0.04	
K2O	9.15		10.07		9.20		9.78		7.50		9.74		10.46		9.98	
H2O	3.92		3.96		3.80		3.85		3.77		4.02		3.89		3.92	
SUM	101.59		100.59		99.55		101.58		98.93		96.52		98.66		101.12	
SI	5.444	*	5.377	*	5.408	*	5.338	*	5.636	*	5.784	*	5.424	*	5.352	*
AL	2.556	8.000	2.580	7.956	2.592	8.000	2.662	8.000	2.364	8.000	2.216	8.000	2.576	8.000	2.556	7.908
AL	0.066	*	0.0	*	0.073	*	0.174	*	0.089	*	0.878	*	0.622	*	0.0	*
TI	0.501	*	0.669	*	0.674	*	0.619	*	0.543	*	0.225	*	0.345	*	0.734	*
FE	3.108	*	3.011	*	3.397	*	3.505	*	3.698	*	1.256	*	2.406	*	2.755	*
MN	0.016	*	0.025	*	0.033	*	0.011	*	0.112	*	0.008	*	0.018	*	0.018	*
MG	2.106	5.796	1.992	5.697	1.473	5.650	1.333	5.640	1.326	5.768	3.108	5.475	2.132	5.584	2.220	5.736
CA	0.020	*	0.003	*	0.007	*	0.003	*	0.038	*	0.018	*	0.002	*	0.011	*
NA	0.068	*	0.021	*	0.0	*	0.021	*	0.031	*	0.040	*	0.033	*	0.012	*
K	1.785	1.872	1.991	2.016	1.852	1.859	1.940	1.954	1.543	1.611	1.853	1.913	2.055	2.089	1.945	1.968
H	4.000	4.000	4.000	4.000	4.000	4.000	4.000	4.000	4.000	4.000	4.000	4.000	4.000	4.000	4.000	4.000
O	24.000	*	24.000	*	24.000	*	24.000	*	24.000	*	24.000	*	24.000	*	24.000	*
F/M		1.483		1.524		2.329		2.638		2.974		0.407		1.106		1.244
F/FM		0.597		0.604		0.700		0.725		0.742		0.289		0.525		0.554

65 SN 74305, LOWER QUARTZITE
66 SN 74306, LOWER QUARTZITE
67 SN 74306, LOWER QUARTZITE
68 SN 74309, LOWER QUARTZITE
69 SN 74321, IRON-FORMATION
70 SN 74323, GRAPHITE-SULFIDE HORNFELS
71 SN 74327, LOWER QUARTZITE
72 SN 74329, LOWER QUARTZITE

TABLE 3 BIOTITE ANALYSES FOR THE SNYDER GROUP (CONTINUED)

	73		74		75		76		77		78		79		80	
SIO2	37.70		36.86		38.69		41.64		35.89		35.46		34.55		33.70	
A203	18.53		20.47		16.45		15.47		17.14		14.80		16.29		15.74	
FEO	15.01		17.13		12.73		0.90		21.59		29.26		31.00		28.92	
TIO2	2.40		2.56		2.43		0.86		2.23		0.18		0.16		7.12	
MNO	0.08		0.08		0.04		0.01		0.39		0.21		0.26		0.16	
CAO	0.07		0.0		0.01		0.0		0.0		0.25		0.20		0.02	
MGO	10.59		11.07		13.47		23.09		10.85		7.75		5.14		3.73	
NA2O	0.08		0.12		0.10		0.14		0.04		0.15		0.0		0.0	
K2O	9.43		9.95		10.03		11.04		9.69		8.97		7.76		9.23	
H2O	3.99		4.12		4.01		4.20		3.98		3.80		3.73		3.86	
SUM	97.98		102.36		97.96		97.35		101.90		100.83		99.09		102.38	
SI	5.660	*	5.366	*	5.775	*	5.938	*	5.400	*	5.594	*	5.543	*	5.234	*
AL	2.340	8.000	2.634	8.000	2.225	8.000	2.062	8.000	2.600	8.000	2.416	8.000	2.457	8.000	2.766	8.000
AL	0.957	*	0.877	*	0.669	*	0.537	*	0.439	*	0.331	*	0.623	*	0.115	*
TI	0.271	*	0.280	*	0.273	*	0.092	*	0.252	*	0.021	*	0.019	*	0.832	*
FE	1.885	*	2.085	*	1.589	*	0.107	*	2.717	*	3.856	*	4.160	*	3.743	*
MN	0.010	*	0.010	*	0.005	*	0.001	*	0.050	*	0.028	*	0.035	*	0.021	*
MG	2.370	5.492	2.402	5.655	2.997	5.532	4.907	5.645	2.433	5.891	1.819	6.053	1.229	6.067	0.863	5.574
CA	0.011	*	0.0	*	0.002	*	0.0	*	0.0	*	0.042	*	0.034	*	0.003	*
NA	0.023	*	0.034	*	0.029	*	0.039	*	0.012	*	0.046	*	0.0	*	0.0	*
K	1.806	1.840	1.848	1.881	1.910	1.940	2.008	2.047	1.860	1.871	1.802	1.800	1.588	1.622	1.828	1.832
H	4.000	4.000	4.000	4.000	4.000	4.000	4.000	4.000	4.000	4.000	4.000	4.000	4.000	4.000	4.000	4.000
O	24.000	*	24.000	*	24.000	*	24.000	*	24.000	*	24.000	*	24.000	*	24.000	*
F/M	0.800		0.872		0.532		0.022		1.137		2.134		3.413		4.360	
F/FM	0.444		0.466		0.347		0.022		0.532		0.681		0.773		0.813	

73 SN 74338, UPPER QUARTZITE
74 SN 74341, BORDER BRECCIA
75 SN 74342, UPPER QUARTZITE
76 SN 74348, GRAPHITE-SULFIDE HORNFELS
77 SN 74351, SNYDER BRECCIA
78 SN 74371, LOWER QUARTZITE
79 SN 74371, LOWER QUARTZITE
80 SN 74374, LOWER QUARTZITE

TABLE 3 BIOTITE ANALYSES FOR THE SNYDER GROUP (CONTINUED)

	81		82		83		84		85		86		87		88	
SIO2	35.07		35.48		35.34		36.70		35.80		42.93		42.07		37.84	
A203	15.53		18.24		15.71		20.30		18.93		13.54		13.28		13.70	
FEO	25.93		17.79		19.99		17.28		20.12		2.50		2.45		14.32	
TI02	4.89		3.63		5.26		2.02		3.59		1.36		1.33		3.01	
MNO	0.10		0.10		0.06		0.03		0.09		0.0		0.0		0.07	
CAO	0.08		0.05		0.01		0.0		0.0		0.0		0.0		0.09	
MGO	7.36		8.47		8.94		10.78		10.47		26.41		25.98		16.53	
NA20	0.07		0.13		0.11		0.14		0.14		0.31		0.30		0.09	
K20	9.96		9.52		10.02		9.83		9.01		10.39		10.08		9.55	
H20	3.93		3.88		3.89		4.07		4.05		4.36		4.28		4.01	
SUM	102.92		97.29		99.33		101.15		102.20		131.80		99.77		99.21	
SI	5.350	*	5.477	*	5.438	*	5.408	*	5.291	*	5.894	*	5.891	*	5.648	*
AL	2.650	8.000	2.523	8.000	2.562	8.000	2.592	8.000	2.709	8.000	2.105	8.000	2.109	8.000	2.352	8.000
AL	0.142	*	0.795	*	0.286	*	0.934	*	0.587	*	0.085	*	0.092	*	0.058	*
TI	0.561	*	0.421	*	0.609	*	0.224	*	0.399	*	0.140	*	0.140	*	0.338	*
FE	3.308	*	2.297	*	2.572	*	2.130	*	2.487	*	0.297	*	0.297	*	1.788	*
MN	0.013	*	0.013	*	0.008	*	0.004	*	0.011	*	0.0	*	0.0	*	0.009	*
MG	1.674	5.698	1.949	5.475	2.050	5.526	2.368	5.659	2.306	5.790	5.435	5.917	5.477	5.931	3.679	5.870
CA	0.013	*	0.008	*	0.002	*	0.0	*	0.0	*	0.0	*	0.0	*	0.014	*
NA	0.021	*	0.039	*	0.033	*	0.040	*	0.040	*	0.033	*	0.081	*	0.026	*
K	1.938	1.972	1.874	1.922	1.967	2.001	1.848	1.888	1.698	1.738	1.823	1.902	1.800	1.882	1.818	1.859
H	4.000	4.000	4.000	4.000	4.000	4.000	4.000	4.000	4.000	4.000	4.000	4.000	4.000	4.000	4.000	4.000
O	24.000	*	24.000	*	24.000	*	24.000	*	24.000	*	24.000	*	24.000	*	24.000	*
	F/M	1.984		1.185		1.258		0.901		1.093		0.053		0.052		0.488
	F/FM	0.665		0.542		0.557		0.474		0.520		0.050		0.050		0.328

81 SN 74374, LOWER QUARTZITE
82 SN 74378, UPPER QUARTZITE
83 SN 74386, BORDER BRECCIA
84 SN 74389, GRAPHITE-SULFIDE HORNFELS
85 SN 74392, UPPER QUARTZITE
86 NC 7412,
87 NC 7412,
88 NC 7448,

TABLE 4 CHLORITE ANALYSES FOR THE SNYDER GROUP (CONTINUED)

	1		2		3	
SIO2	23.79		27.25		26.18	
A2O3	21.49		21.10		21.03	
FEO	37.53		28.14		26.27	
TIO2	0.29		0.21		0.12	
MNO	0.29		0.20		0.29	
CAO	0.01		0.01		0.0	
MGO	7.05		13.95		15.41	
NA2O	0.0		0.0		0.0	
K2O	0.03		0.09		0.01	
H2O	10.97		11.70		11.55	
SUM	101.45		102.65		100.86	
SI	2.598	*	2.791	*	2.717	*
AL	1.402	4.000	1.209	4.000	1.283	4.000
AL	1.364	*	1.338	*	1.288	*
TI	0.024	*	0.016	*	0.009	*
FE	3.428	*	2.410	*	2.280	*
MN	0.027	*	0.017	*	0.025	*
MG	1.148	*	2.130	*	2.383	*
CA	0.0	5.996	0.0	5.924	0.0	5.988
NA	0.0	*	0.0	*	0.0	*
K	0.004	5.996	0.012	5.924	0.001	5.988
H	8.000	8.000	8.000	8.000	8.000	8.000
O	18.000	*	18.000	*	18.000	*
F/M	3.010		1.140		0.967	
F/FM	0.751		0.533		0.492	

1 SN 72135, LOWER QUAPTZITE
2 SN 72200, LOWER QUARTZITE
3 SN 74327, LOWER QUARTZITE

TABLE 5 CORDIERITE ANALYSES FOR THE SNYDER GROUP

	1	2	3	4	5	6	7	8
SIO2	49.37	49.47	48.33	47.54	48.13	49.04	48.96	48.17
A203	32.25	33.02	31.59	31.05	32.05	32.15	33.34	33.**
FEO	9.91	9.98	11.89	14.77	9.98	9.59	10.10	11.46
MNO	0.20	0.38	0.27	0.27	0.45	0.34	0.04	0.06
CAO	0.01	0.01	0.01	0.01	0.01	0.03	0.0	0.0
MGO	7.98	7.17	6.92	4.86	7.63	7.75	7.02	6.37
SUM	99.72	100.03	99.01	98.50	98.25	98.90	99.46	100.04

SI	5.046	*	5.040	*	5.028	*	5.039	*	5.007	*	5.049	*	5.013	*	4.939	*
AL	0.954	6.000	0.960	6.000	0.972	6.000	0.961	6.000	0.993	6.000	0.951	6.000	0.987	6.000	1.061	6.000
AL	2.929	2.929	3.003	3.003	2.901	2.901	2.917	2.917	2.935	2.935	2.950	2.950	3.035	3.035	3.045	3.045
FE	0.847	*	0.850	*	1.036	*	1.309	*	0.868	*	0.826	*	0.865	*	0.983	*
MG	1.216	*	1.089	*	1.073	*	0.768	*	1.193	*	1.189	*	1.071	*	0.974	*
MN	0.017	2.080	0.033	1.972	0.024	2.131	0.024	2.101	0.040	2.091	0.030	2.045	0.003	1.939	0.005	1.961
CA	0.001	0.001	0.001	0.001	0.001	0.001	0.001	0.001	0.001	0.001	0.003	0.003	0.0	0.0	0.0	0.0
O	18.000	*	18.000	*	18.000	*	18.000	*	18.000	*	18.000	*	18.000	*	18.000	*
	FE	40.72		43.12		48.54		62.31		41.52		40.38		44.50		50.19
	MG	58.44		55.22		50.35		36.54		56.58		58.17		55.23		49.63
	MN	0.83		1.66		1.12		1.15		1.90		1.45		0.18		0.27
	FE	41.06		43.85		49.08		63.03		42.33		40.98		44.67		50.23
	MG	58.94		56.15		50.92		36.97		57.67		59.02		55.33		49.77
	F/M	0.711		0.811		0.986		1.737		0.767		0.710		0.810		1.015
	F/FM	0.416		0.448		0.497		0.635		0.434		0.418		0.448		0.504

1 SN 7215, LOWER QUARTZITE
2 SN 7218, LOWER QUARTZITE
3 SN 7225, LOWER QUARTZITE
4 SN 7229, GRAPHITE-SULFIDE HORNFELS
5 SN 7237, LOWER QUARTZITE
6 SN 7256, LOWER QUARTZITE
7 SN 7274, LOWER QUARTZITE
8 SN 7275, LOWER QUARTZITE

TABLE 5 CORDIERITE ANALYSES FOR THE SNYDER GROUP (CONTINUED)

	9	10	11	12	13	14	15	16
SIO2	49.07	47.54	48.20	49.18	48.93	50.09	48.46	48.33
A2O3	33.58	33.36	32.68	34.47	33.74	33.30	32.03	32.82
FEO	10.42	12.49	14.21	7.16	7.09	7.50	14.19	14.65
MNO	0.09	1.02	0.22	0.12	0.09	0.14	0.0	0.07
CAO	0.0	0.0	0.0	0.0	0.0	0.0	0.0	0.02
MGO	7.33	5.21	4.50	9.80	8.99	9.21	5.72	5.67
SUM	100.49	99.62	99.81	100.73	98.84	100.24	100.40	101.26

SI	4.984	*	4.942	*	5.016	*	4.918	*	4.978	*	5.032	*	5.015	*	4.944	*
AL	1.016	6.000	1.058	6.000	0.984	6.000	1.082	6.000	1.022	6.000	0.968	6.000	0.985	6.000	1.056	6.000
AL	3.002	3.002	3.029	3.029	3.024	3.024	2.980	2.980	3.023	3.023	2.974	2.974	2.920	2.920	2.925	2.925
FE	0.885	*	1.086	*	1.237	*	0.599	*	0.603	*	0.630	*	1.228	*	1.261	*
MG	1.110	*	0.807	*	0.698	*	1.461	*	1.363	*	1.379	*	0.882	*	0.870	*
MN	0.008	2.002	0.090	1.993	0.019	1.954	0.010	2.070	0.008	1.974	0.013	2.021	0.0	2.110	0.006	2.137
CA	0.0	0.0	0.0	0.0	0.0	0.0	0.0	0.0	0.0	0.0	0.0	0.0	0.0	0.0	0.002	0.002
O	18.000	*	18.000	*	18.000	*	18.000	*	18.000	*	18.000	*	18.000	*	18.000	*
	FE	44.20		54.76		63.29		28.93		30.56		31.18		58.19		59.01
	MG	55.41		40.71		35.72		70.58		69.05		68.23		41.81		40.70
	MN	0.39		4.53		0.99		0.49		0.39		0.59		0.0		0.29
	FE	44.37		57.36		63.92		29.07		30.68		31.36		58.19		59.18
	MG	55.63		42.64		36.08		70.93		69.32		68.64		41.81		40.82
	F/M	0.805		1.456		1.800		0.417		0.448		0.466		1.392		1.457
	F/FM	0.446		0.593		0.643		0.294		0.309		0.318		0.582		0.593

9 SN 7278, LOWER QUARTZITE
10 SN 7282, LOWER QUARTZITE
11 SN 7289, LOWER QUARTZITE
12 SN 72111, UPPER QUARTZITE
13 SN 72111, UPPER QUARTZITE
14 SN 72111, UPPER QUARTZITE
15 SN 72123, LOWER QUARTZITE
16 SN 72123, LOWER QUARTZITE

TABLE 5 CORDIERITE ANALYSES FOR THE SNYDER GROUP (CONTINUED)

	17	18	19	20	21	22	23	24
SIO2	49.28	48.84	48.00	50.22	49.48	49.83	48.64	50.43
AL2O3	32.51	32.57	32.20	32.99	32.66	33.70	32.69	33.21
FEO	8.38	10.99	16.65	9.91	14.11	8.38	9.44	10.18
MNO	0.08	0.25	0.37	0.34	0.30	0.17	0.07	0.03
CAO	0.0	0.01	0.01	0.01	0.01	0.0	0.0	0.0
MGO	8.68	6.15	3.70	7.32	5.19	8.21	7.81	7.93
SUM	98.93	98.81	100.93	100.79	101.75	100.29	98.74	101.78
SI	5.038 *	5.057 *	5.003 *	5.071 *	5.046 *	5.021 *	5.008 *	5.045 *
AL	0.962 6.000	0.943 6.000	0.997 6.000	0.929 6.000	0.954 6.000	0.979 6.000	0.992 6.000	0.955 6.000
AL	2.955 2.955	3.031 3.031	2.958 2.958	2.996 2.996	2.971 2.971	3.022 3.022	2.974 2.974	2.959 2.959
FE	0.717 *	0.952 *	1.451 *	0.837 *	1.203 *	0.706 *	0.813 *	0.852 *
MG	1.323 *	0.949 *	0.575 *	1.102 *	0.789 *	1.233 *	1.214 *	1.182 *
MN	0.007 2.045	0.022 1.923	0.033 2.059	0.029 1.968	0.026 2.018	0.015 1.954	0.006 2.033	0.003 2.037
CA	0.0 0.0	0.001 0.001	0.001 0.001	0.001 0.001	0.001 0.001	0.0 0.0	0.0 0.0	0.0 0.0
O	18.000 *	18.000 *	18.000 *	18.000 *	18.000 *	18.000 *	18.000 *	18.000 *
FE	35.02	49.49	70.49	42.53	59.63	36.14	39.99	41.87
MG	64.64	49.36	27.92	55.99	39.09	63.11	59.71	58.06
MN	0.34	1.14	1.59	1.48	1.28	0.74	0.30	0.12
FE	35.14	50.07	71.63	43.17	60.40	36.41	40.11	41.87
MG	64.86	49.93	28.37	56.83	39.60	63.59	59.89	58.13
F/M	0.547	1.026	2.582	0.786	1.558	0.584	0.675	0.722
F/FM	0.354	0.506	0.721	0.440	0.609	0.369	0.403	0.419

17 SN 72127, UPPER QUARTZITE
18 SN 72131, LOWER QUARTZITE
19 SN 72142, LOWER QUARTZITE
20 SN 72147, LOWER QUARTZITE
21 SN 72151, LOWER QUARTZITE
22 SN 72157, UPPER QUARTZITE
23 SN 72160, UPPER QUARTZITE
24 SN 72162, UPPER QUARTZITE

TABLE 5 CORDIERITE ANALYSES FOR THE SNYDER GROUP (CONTINUED)

	25	26	27	28	29	30	31	32
SIO2	48.01	48.60	47.18	48.69	48.44	47.78	48.77	50.96
A203	32.54	32.36	32.14	32.73	32.52	31.17	31.96	33.60
FEO	11.39	10.75	14.80	12.37	10.37	13.48	11.11	9.77
MNO	0.03	0.14	0.21	0.21	0.39	0.22	0.30	0.34
CAO	0.0	0.01	0.01	0.01	0.0	0.01	0.01	0.01
MGO	7.11	7.53	4.16	6.64	7.84	4.80	7.00	7.80
SUM	99.08	99.39	98.50	100.65	99.56	97.55	99.24	102.48

SI	4.975	*	5.006	*	4.997	*	4.989	*	4.980	*	5.076	*	5.040	*	5.056	*
AL	1.025	6.000	0.994	6.000	1.003	6.000	1.011	6.000	1.020	6.000	0.924	6.000	0.960	6.000	0.944	6.000
AL	2.948	2.948	2.933	2.933	3.008	3.008	2.940	2.940	2.920	2.920	2.978	2.978	2.932	2.932	2.894	2.894
FE	0.987	*	0.926	*	1.311	*	1.060	*	0.892	*	1.198	*	0.960	*	0.911	*
MG	1.098	*	1.156	*	0.657	*	1.014	*	1.201	*	0.774	*	1.092	*	1.153	*
MN	0.003	2.088	0.012	2.094	0.019	1.986	0.018	2.092	0.034	2.127	0.020	1.992	0.026	2.079	0.029	1.993
CA	0.0	0.0	0.001	0.001	0.001	0.001	0.001	0.001	0.0	0.0	0.001	0.001	0.001	0.001	0.001	0.001
T	18.000	*	18.000	*	18.000	*	18.000	*	18.000	*	18.000	*	18.000	*	18.000	*
	FE	47.28		44.22		65.99		50.66		41.92		60.13		46.19		40.68
	MG	52.60		55.20		33.06		48.47		56.48		38.88		52.54		57.89
	MN	0.13		0.58		0.95		0.87		1.60		0.99		1.26		1.43
	FE	47.34		44.48		66.62		51.11		42.60		60.72		46.79		41.27
	MG	52.66		55.52		33.38		48.89		57.40		39.27		53.21		58.73
	F/M	0.901		0.812		2.025		1.063		0.770		1.572		0.903		0.729
	F/FM	0.474		0.449		0.669		0.515		0.435		0.611		0.475		0.421

25 SN 72162, UPPER QUARTZITE
26 SN 72175
27 SN 72179, LOWER QUARTZITE
28 SN 72189, LOWER QUARTZITE
29 SN 72191, LOWER QUARTZITE
30 SN 72193, LOWER QUARTZITE
31 SN 72195, LOWER QUARTZITE
32 SN 72198, LOWER QUARTZITE

TABLE 5 CORDIERITE ANALYSES FOR THE SNYDER GROUP (CONTINUED)

	33	34	35	36	37	38	39	40
SIO2	48.20	48.64	47.13	48.33	48.54	49.55	48.26	47.99
A2O3	32.69	33.36	31.65	33.00	32.95	31.50	32.62	32.38
FEO	12.59	10.17	12.26	15.04	11.96	12.18	14.01	15.28
MNO	0.07	0.21	0.19	0.13	0.19	0.16	0.15	0.06
CAO	0.01	0.0	0.01	0.0	0.01	0.02	0.0	0.01
MGO	6.94	7.65	6.09	4.90	6.43	6.89	5.52	5.16
SUM	100.50	100.03	97.33	101.40	100.08	100.30	100.56	100.78

SI	4.954	*	4.965	*	4.998	*	4.971	*	4.990	*	5.085	*	4.985	*	4.967	*
AL	1.046	6.000	1.035	6.000	1.002	6.000	1.029	6.000	1.010	6.000	0.915	6.000	1.015	6.000	1.033	6.000
AL	2.912	2.912	2.977	2.977	2.954	2.954	2.971	2.971	2.981	2.981	2.894	2.894	2.955	2.955	2.924	2.924
FE	1.082	*	0.868	*	1.087	*	1.294	*	1.028	*	1.045	*	1.210	*	1.325	*
MG	1.063	*	1.164	*	0.963	*	0.751	*	0.985	*	1.054	*	0.850	*	0.798	*
MN	0.006	2.151	0.018	2.050	0.017	2.067	0.011	2.056	0.017	2.030	0.014	2.113	0.013	2.073	0.005	2.128
CA	0.001	0.001	0.0	0.0	0.001	0.001	0.0	0.0	0.001	0.001	0.002	0.002	0.0	0.0	0.001	0.001
O	18.000	*	18.000	*	18.000	*	18.000	*	18.000	*	18.000	*	18.000	*	18.000	*
	FE	50.30		42.34		52.60		52.92		50.65		49.47		58.37		62.27
	MG	49.42		56.77		46.57		36.53		48.53		49.87		40.99		37.48
	MN	0.29		0.99		0.83		0.55		0.81		0.66		0.63		0.25
	FE	50.44		42.72		53.04		63.26		51.07		49.80		58.75		62.43
	MG	49.56		57.28		46.96		36.74		48.93		50.20		41.25		37.57
	F/M	1.024		0.761		1.147		1.737		1.060		1.005		1.439		1.669
	F/FM	0.506		0.432		0.534		0.635		0.515		0.501		0.590		0.625

33 SN 72211, LOWER QUARTZITE
34 SN 72212, LOWER QUARTZITE
35 SN 72215, LOWER QUARTZITE
36 SN 74242, LOWER QUARTZITE
37 SN 74243, LOWER QUARTZITE
38 SN 74251, LOWER QUARTZITE
39 SN 74260, LOWER QUARTZITE
40 SN 74263, LOWER QUARTZITE

TABLE 5 CORDIERITE ANALYSES FOR THE SNYDER GROUP (CONTINUED)

	41		42		43		44		45		46		47		48	
SIO2	48.12		49.15		48.15		48.86		48.38		47.78		48.47		49.88	
A2O3	32.20		31.74		32.39		32.82		31.52		32.04		32.00		32.37	
FEO	12.06		10.70		10.71		12.45		13.77		13.54		13.00		5.43	
MNO	0.14		0.14		0.0		0.12		0.03		0.02		0.14		0.10	
CAO	0.01		0.0		0.0		0.0		0.02		0.01		0.01		0.0	
MGO	6.19		7.11		6.71		5.71		5.76		6.33		5.58		9.28	
SUM	98.72		98.84		97.96		99.96		99.48		99.72		99.20		97.06	
SI	5.018	*	5.082	*	5.023	*	5.032	*	5.044	*	4.971	*	5.048	*	5.117	*
AL	0.982	6.000	0.918	6.000	0.977	6.000	0.968	6.000	0.956	6.000	1.029	6.000	0.952	6.000	0.883	6.000
AL	2.974	2.974	2.949	2.949	3.006	3.006	3.015	3.015	2.917	2.917	2.900	2.900	2.975	2.975	3.030	3.030
FE	1.052	*	0.925	*	0.934	*	1.072	*	1.201	*	1.178	*	1.132	*	0.466	*
MG	0.962	*	1.096	*	1.043	*	0.877	*	0.895	*	0.982	*	0.866	*	1.419	*
MN	0.012	2.026	0.012	2.033	0.0	1.978	0.010	1.950	0.003	2.098	0.002	2.162	0.012	2.011	0.009	1.894
CA	0.001	0.001	0.0	0.0	0.0	0.0	0.0	0.0	0.002	0.002	0.001	0.001	0.001	0.001	0.0	0.0
O	18.000	*	18.000	*	18.000	*	18.000	*	18.000	*	18.000	*	18.000	*	18.000	*
FF	51.91		45.50		47.24		54.73		57.22		54.50		56.31		24.60	
MG	47.48		53.89		52.76		44.74		42.66		45.41		43.08		74.94	
MN	0.61		0.60		0.0		0.53		0.13		0.08		0.61		0.46	
FE	52.22		45.78		47.24		55.02		57.29		54.55		56.66		24.72	
MG	47.78		54.22		52.76		44.98		42.71		45.45		43.34		75.28	
F/M	1.106		0.856		0.896		1.235		1.344		1.202		1.321		0.334	
F/FM	0.525		0.461		0.472		0.553		0.573		0.546		0.569		0.251	

41 SN 74271, LOWER QUARTZITE
42 SN 74272, LOWER QUARTZITE
43 SN 74275, UPPER QUARTZITE
44 SN 74280, LOWER QUARTZITE
45 SN 74287, LOWER QUARTZITE
46 SN 74288, LOWER QUARTZITE
47 SN 74290, LOWER QUARTZITE
48 SN 74299, GRAPHITE-SULFIDE HORNFELS

TABLE 5 CORDIERITE ANALYSES FOR THE SNYDER GROUP (CONTINUED)

	49	50	51	52	53	54	55	56
SIO2	48.86	46.35	48.81	49.13	49.99	49.99	48.81	49.55
A203	31.96	31.05	32.73	31.59	34.09	33.91	33.48	33.51
FEO	12.20	15.61	10.31	13.20	5.94	7.42	9.11	9.17
MNO	0.07	0.16	0.25	0.0	0.10	0.20	0.06	0.0
CAO	0.01	0.0	0.02	0.01	0.0	0.0	0.0	0.17
MGO	7.25	3.71	8.41	6.39	8.67	8.47	7.37	8.67
SUM	100.35	96.88	100.53	100.32	98.78	99.89	98.83	101.07

SI	5.017	*	5.016	*	4.967	*	5.062	*	5.049	*	5.034	*	5.007	*	4.979	*
AL	0.983	6.000	0.984	6.000	1.033	6.000	0.938	6.000	0.951	6.000	0.966	6.000	0.993	6.000	1.021	6.000
AL	2.884	2.884	2.976	2.976	2.892	2.892	2.898	2.898	3.105	3.105	3.045	3.045	3.054	3.054	2.947	2.947
FE	1.048	*	1.413	*	0.877	*	1.137	*	0.502	*	0.625	*	0.782	*	0.771	*
MG	1.110	*	0.598	*	1.276	*	0.981	*	1.305	*	1.271	*	1.127	*	1.290	*
MN	0.006	2.163	0.015	2.026	0.022	2.175	0.0	2.119	0.009	1.816	0.017	1.913	0.005	1.914	0.0	2.069
CA	0.001	0.001	0.0	0.0	0.002	0.002	0.001	0.001	0.0	0.0	0.0	0.0	0.0	0.0	0.018	0.018
O	18.000	*	18.000	*	18.000	*	18.000	*	18.000	*	18.000	*	18.000	*	18.000	*
	FE	48.43		59.74		40.35		53.68		27.64		32.66		40.84		37.24
	MG	51.29		29.54		58.66		46.32		71.89		66.45		58.90		62.76
	MN	0.28		0.72		0.99		0.0		0.47		0.90		0.27		0.0
	FE	48.56		70.24		40.75		53.68		27.77		32.95		40.95		37.24
	MG	51.44		29.76		59.25		46.32		72.23		67.05		59.05		62.76
	F/M	0.950		2.385		0.705		1.159		0.391		0.505		0.698		0.593
	F/FM	0.487		0.705		0.413		0.537		0.281		0.336		0.411		0.372

49 SN 74302, LOWER QUARTZITE
50 SN 74303, LOWER QUARTZITE
51 SN 74306, LOWER QUARTZITE
52 SN 74309, LOWER QUARTZITE
53 SN 74323, GRAPHITE-SULFIDE HORNFELS
54 SN 74329, LOWER QUARTZITE
55 SN 74338, UPPER QUARTZITE
56 SN 74341, BORDER BRECCIA

TABLE 5 CORDIERITE ANALYSES FOR THE SNYDER GROUP (CONTINUED)

	57	58	59	60	61	62	63	64
SIO2	48.13	51.23	50.37	48.56	48.93	50.22	49.06	50.95
A203	33.04	34.94	33.51	33.32	33.87	31.31	33.46	34.36
FEO	7.52	0.40	5.96	13.52	9.19	11.19	10.20	4.99
MNO	0.04	0.02	0.10	0.39	0.07	0.04	0.07	0.08
CAO	0.0	0.0	0.0	0.01	0.0	0.01	0.0	0.04
MGO	7.92	13.25	10.65	5.82	7.26	7.81	6.63	10.93
SUM	96.65	99.84	100.59	101.32	99.31	100.58	99.51	101.25

SI	5.013	*	5.002	*	5.011	*	4.963	*	4.996	*	5.112	*	5.022	*	5.007	*
AL	0.987	6.000	0.998	6.000	0.989	6.000	1.037	6.000	1.004	6.000	0.888	6.000	0.978	6.000	0.993	6.000
AL	3.069	3.069	3.023	3.023	2.939	2.939	2.977	2.977	3.070	3.070	2.867	2.867	3.059	3.059	2.987	2.987
FE	0.655	*	0.033	*	0.496	*	1.156	*	0.784	*	0.953	*	0.881	*	0.402	*
MG	1.230	*	1.928	*	1.579	*	0.887	*	1.105	*	1.185	*	1.012	*	1.601	*
MN	0.004	1.888	0.002	1.963	0.008	2.083	0.008	2.050	0.006	1.895	0.003	2.141	0.006	1.899	0.007	2.010
CA	0.0	0.0	0.0	0.0	0.0	0.0	0.001	0.001	0.0	0.0	0.001	0.001	0.0	0.0	0.004	0.004
O	18.000	*	18.000	*	18.000	*	18.000	*	18.000	*	18.000	*	18.000	*	18.000	*
	FE	34.69		1.66		23.80		56.37		41.37		44.49		46.49		20.00
	MG	65.12		98.25		75.80		43.25		58.31		55.35		53.28		79.67
	MN	0.19		0.08		0.40		0.38		0.32		0.16		0.32		0.33
	FE	34.76		1.67		23.90		56.59		41.59		44.56		46.55		20.07
	MG	65.24		98.33		76.10		43.41		58.50		55.44		53.45		79.93
	F/M	0.536		0.018		0.319		1.312		0.715		0.807		0.877		0.255
	F/FM	0.349		0.017		0.242		0.568		0.417		0.447		0.467		0.203

57 SN 74342, UPPER QUARTZITE
58 SN 74348, GRAPHITE-SULFIDE HORNFELS
59 SN 74373, GRAPHITE-SULFIDE HORNFELS
60 SN 74374, LOWER QUARTZITE
61 SN 74378, UPPER QUARTZITE
62 SN 74386, BORDER BRECCIA
63 SN 74392, UPPER QUARTZITE
64 NC 7430

	65	66	67
SIO2	49.97	50.98	49.11
A203	32.85	34.73	33.19
FEO	4.52	4.91	11.33
MNO	0.11	0.11	0.17
CAO	0.01	0.0	0.0
MGO	11.36	10.53	7.09
SUM	98.82	101.26	100.89

SI	5.029	*	5.007	*	4.992	*
AL	0.971	6.000	0.993	6.000	1.008	6.000
AL	2.925	2.925	3.027	3.027	2.967	2.967
FE	0.380	*	0.403	*	0.963	*
MG	1.704	*	1.542	*	1.074	*
MN	0.009	2.094	0.009	1.954	0.015	2.052
CA	0.001	0.001	0.0	0.0	0.0	0.0
O	18.000	*	18.000	*	18.000	*
	FE	18.17		20.64		46.94
	MG	81.38		78.89		52.35
	MN	0.45		0.47		0.71
	FE	18.25		20.74		47.27
	MG	81.75		79.26		52.73
	F/M	0.229		0.268		0.910
	F/FM	0.186		0.211		0.477

65 NC 7438
66 NC 7448
67 NC 7449

TABLE 6 GARNET ANALYSES FOR THE SNYDER GROUP

	1		2		3		4		5		6		7		8	
SIO2	37.43		35.64		37.59		36.35		37.05		36.95		37.03		36.98	
A203	21.31		21.51		21.27		21.43		21.28		21.63		20.24		20.14	
FEO	36.99		24.44		23.18		36.62		35.41		21.92		33.82		34.50	
MNO	0.46		16.02		12.51		1.48		3.00		14.59		4.07		3.66	
CAO	2.00		1.03		6.37		1.53		1.83		3.97		1.46		1.28	
MGO	3.75		1.08		1.23		2.48		2.95		2.49		1.96		2.09	
SUM	101.94		99.72		102.15		99.89		101.52		101.55		98.58		98.65	
SI	2.963	*	2.929	*	2.979	*	2.951	*	2.959	*	2.943	*	3.042	*	3.039	*
AL	0.037	3.000	0.071	3.000	0.021	3.000	0.049	3.000	0.041	3.000	0.060	3.000	0.0	3.042	0.0	3.039
AL	1.951	1.951	2.011	2.011	1.965	1.965	2.001	2.001	1.962	1.962	1.969	1.969	1.959	1.959	1.950	1.950
FE	2.449	*	1.680	*	1.536	*	2.486	*	2.365	*	1.459	*	2.324	*	2.371	*
MG	0.442	*	0.132	*	0.145	*	0.300	*	0.351	*	0.295	*	0.240	*	0.256	*
MN	0.031	*	1.115	*	0.840	*	0.102	*	0.203	*	0.983	*	0.283	*	0.255	*
CA	0.0	2.922	0.0	2.927	0.0	2.521	0.0	2.988	0.0	2.919	0.0	2.737	0.0	2.847	0.0	2.882
O	12.000	*	12.000	*	12.000	*	12.000	*	12.000	*	12.000	*	12.000	*	12.000	*
AL		79.20		55.66		50.17		82.29		76.99		47.42		78.10		79.18
PY		14.31		4.38		4.74		9.93		11.42		9.60		8.07		8.55
SP		1.00		36.95		27.42		3.37		6.60		31.97		9.52		8.51
GR		5.49		3.01		17.66		4.40		5.00		11.00		4.32		3.76
F/M		5.604		21.126		16.353		8.624		7.313		8.269		10.861		10.257
F/FM		0.849		0.955		0.942		0.896		0.880		0.892		0.916		0.911

1 SN 7236, LOWER QUARTZITE
2 SN 7241, LOWER QUARTZITE
3 SN 7266, IRON-FORMATION
4 SN 7272, LOWER QUARTZITE
5 SN 7282, LOWER QUARTZITE
6 SN 72100, DIKE
7 SN 72134, LOWER QUARTZITE
8 SN 72134, LOWER QUARTZITE

	9		10		11		12		13		14		15		16	
SIO2	36.84		36.86		37.05		37.04		37.06		36.99		36.98		36.62	
A203	20.54		20.46		21.46		21.78		20.99		21.37		21.04		21.11	
FEO	27.87		27.77		30.45		23.45		34.05		35.54		35.44		23.95	
MNO	10.51		10.40		7.28		12.56		1.93		3.78		3.40		11.74	
CAO	2.87		2.74		2.39		3.23		0.56		1.21		1.26		6.82	
MGO	2.59		2.68		3.08		3.78		5.20		2.88		2.79		1.08	
SUM	101.22		100.91		101.71		101.94		99.79		101.77		100.91		101.32	
SI	2.964	*	2.971	*	2.948	*	2.924	*	2.971	*	2.954	*	2.974	*	2.940	*
AL	0.036	3.000	0.029	3.000	0.052	3.000	0.076	3.000	0.029	3.000	0.045	3.000	0.026	3.000	0.060	3.000
AL	1.912	1.912	1.915	1.915	1.960	1.960	1.950	1.950	1.954	1.954	1.965	1.965	1.969	1.969	1.938	1.938
FE	1.875	*	1.872	*	2.026	*	1.548	*	2.283	*	2.373	*	2.384	*	1.608	*
MG	0.311	*	0.322	*	0.365	*	0.445	*	0.621	*	0.343	*	0.334	*	0.129	*
MN	0.716	*	0.710	*	0.491	*	0.846	*	0.131	*	0.256	*	0.232	*	0.798	*
CA	0.0	2.902	0.0	2.934	0.0	2.882	0.0	2.839	0.0	3.035	0.0	2.972	0.0	2.950	0.0	2.536
O	12.000	*	12.000	*	12.000	*	12.000	*	12.000	*	12.000	*	12.000	*	12.000	*
AL		59.54		59.60		65.66		49.74		74.04		77.17		77.94		51.50
PY		9.86		10.25		11.84		14.29		20.15		11.15		10.94		4.14
SP		22.74		22.61		15.90		27.20		4.25		8.31		7.57		25.57
GR		7.86		7.53		6.60		8.78		1.56		3.37		3.55		18.79
F/M		8.343		8.019		6.890		5.384		3.885		7.670		7.820		18.620
F/FM		0.893		0.889		0.873		0.843		0.795		0.885		0.887		0.949

9 SN 72149, IRON-FORMATION
10 SN 72149, IRON-FORMATION
11 SN 72155, DIKE
12 SN 72173, LOWER QUARTZITE
13 SN 72175
14 SN 72176, LOWER QUARTZITE
15 SN 72176, LOWER QUARTZITE
16 SN 72205, IRON-FORMATION

TABLE 6 GARNET ANALYSES FOR THE SNYDER GROUP (CONTINUED)

	17		18		19		20		21		22		23		24	
SIO2	37.15		36.85		38.36		38.62		37.15		37.23		37.42		37.27	
A2O3	20.17		21.86		21.60		22.74		21.89		21.86		21.16		22.86	
FEO	25.19		35.51		31.10		35.65		38.50		37.35		37.07		37.39	
MNO	10.15		0.86		4.60		1.14		0.73		0.29		1.04		0.53	
CAO	6.90		1.55		1.89		1.77		0.85		1.68		1.44		1.61	
MGO	1.25		3.67		4.57		4.22		3.05		3.42		3.49		3.43	
SUM	100.81		100.30		102.12		104.14		102.26		101.83		101.62		103.09	
SI	2.994	*	2.950	*	2.996	*	2.963	*	2.945	*	2.949	*	2.976	*	2.913	*
AL	0.006	3.000	0.050	3.000	0.004	3.000	0.037	3.000	0.055	3.000	0.051	3.000	0.024	3.000	0.087	3.000
AL	1.910	1.910	2.012	2.012	1.984	1.984	2.019	2.019	1.991	1.991	1.993	1.990	1.959	1.959	2.019	2.019
FE	1.698	*	2.377	*	2.031	*	2.287	*	2.559	*	2.474	*	2.466	*	2.444	*
MG	0.150	*	0.438	*	0.532	*	0.483	*	0.360	*	0.404	*	0.414	*	0.400	*
MN	0.693	*	0.058	*	0.304	*	0.074	*	0.049	*	0.019	*	0.070	*	0.035	*
CA	0.0	2.541	0.0	2.873	0.0	2.867	0.0	2.844	0.0	2.968	0.0	2.897	0.0	2.940	0.0	2.879
O	12.000	*	12.000	*	12.000	*	12.000	*	12.000	*	12.000	*	12.000	*	12.000	*
AL		54.13		79.07		67.13		76.51		84.16		81.39		80.26		81.10
PY		4.79		14.57		17.58		16.14		11.85		13.28		13.47		13.26
SP		22.09		1.94		10.06		2.48		1.61		0.64		2.29		1.16
GR		19.00		4.42		5.23		4.87		2.37		4.69		3.98		4.47
F/M	15.921		5.562		4.390		4.893		7.235		6.176		6.129		6.204	
F/FM	0.941		0.849		0.814		0.830		0.879		0.861		0.860		0.861	

17 SN 72207, IRON-FORMATION
18 SN 72211, LOWER QUARTZITE
19 SN 72223, DIKE
20 SN 74251, LOWER QUARTZITE
21 SN 74263, LOWER QUARTZITE
22 SN 74270, LOWER QUARTZITE
23 SN 74280, LOWER QUARTZITE
24 SN 74287, LOWER QUARTZITE

	25		26		27		28		29		30		31		32	
SIO2	37.28		37.56		37.93		37.50		37.55		37.15		36.88		36.86	
A2O3	22.23		22.19		20.01		19.90		20.07		20.82		20.26		20.06	
FEO	37.04		36.98		22.01		22.78		23.69		35.57		28.93		36.46	
MNO	0.57		0.38		13.24		14.08		14.57		2.74		8.77		3.51	
CAO	0.91		1.84		7.49		5.93		5.72		0.76		3.58		2.93	
MGO	3.98		3.84		0.45		0.90		0.0		3.96		2.31		1.61	
SUM	102.71		102.79		101.13		101.19		101.60		101.00		100.63		101.43	
SI	2.939	*	2.940	*	3.043	*	3.027	*	3.027	*	2.974	*	2.982	*	2.985	*
AL	0.061	3.000	0.060	3.000	0.0	3.043	0.0	3.027	0.0	3.027	0.026	3.000	0.018	3.000	0.015	3.000
AL	2.004	2.004	1.987	1.987	1.892	1.892	1.888	1.888	1.936	1.936	1.938	1.938	1.913	1.913	1.899	1.899
FE	2.442	*	2.421	*	1.477	*	1.534	*	1.597	*	2.381	*	1.950	*	2.469	*
MG	0.468	*	0.448	*	0.054	*	0.108	*	0.0	*	0.473	*	0.278	*	0.194	*
MN	0.038	*	0.025	*	0.900	*	0.960	*	0.995	*	0.186	*	0.601	*	0.241	*
CA	0.0	2.947	0.0	2.994	0.0	2.431	0.0	2.602	0.0	2.592	0.0	3.040	0.0	2.829	0.0	2.904
O	12.000	*	12.000	*	12.000	*	12.000	*	12.000	*	12.000	*	12.000	*	12.000	*
AL		80.74		79.41		48.04		49.26		51.75		76.70		62.11		78.19
PY		15.45		14.70		1.75		3.47		0.0		15.22		8.87		6.15
SP		1.26		0.83		29.27		30.84		32.24		5.98		19.14		7.62
GR		2.54		5.06		20.94		16.43		16.01		2.10		9.89		8.05
F/M	5.303		5.459		44.162		23.092		7.235		5.433		9.160		13.945	
F/FM	0.841		0.845		0.978		0.958		0.879		0.845		0.902		0.933	

25 SN 74288, LOWER QUARTZITE
26 SN 74309, LOWER QUARTZITE
27 SN 74321, IRON-FORMATION
28 SN 74332, IRON-FORMATION
29 SN 74332, IRON-FORMATION
30 SN 74358, DIKE
31 SN 74364, LOWER QUARTZITE
32 SN 74371, LOWER QUARTZITE

TABLE 6 GARNET ANALYSES FOR THE SNYDER GROUP (CONTINUED)

	33		34		35		36		37	
SIO2	37.83		37.83		37.34		37.47		38.14	
A203	22.74		21.19		20.15		20.21		22.44	
FEO	36.43		22.12		16.08		22.55		35.46	
MNO	0.71		11.50		15.36		12.36		1.74	
CAO	1.55		9.45		10.55		7.10		1.40	
MGO	3.87		0.37		0.32		1.00		4.39	
SUM	103.13		102.46		99.80		100.69		103.57	
SI	2.941	*	2.986	*	3.016	*	3.016	*	2.950	*
AL	0.059	3.000	0.014	3.000	0.0	3.016	0.0	3.016	0.050	3.000
AL	2.024	2.024	1.956	1.956	1.918	1.918	1.917	1.917	1.996	1.996
FE	2.368	*	1.460	*	1.086	*	1.518	*	2.294	*
MG	0.448	*	0.044	*	0.039	*	0.120	*	0.506	*
MN	0.047	*	0.769	*	1.051	*	0.843	*	0.114	*
CA	0.0	2.864	0.0	2.272	0.0	2.176	0.0	2.480	0.0	2.914
O	12.000	*	12.000	*	12.000	*	12.000	*	12.000	*
AL		79.14		47.54		35.17		49.08		75.70
PY		14.98		1.42		1.25		3.89		16.70
SP		1.56		25.03		34.02		27.25		3.76
GR		4.31		26.02		29.56		19.80		3.83
F/M		5.386		51.205		55.471		19.676		4.757
F/FM		0.843		0.981		0.982		0.952		0.826

33 SN 74374, LOWER QUARTZITE
34 SN 74383, IRON-FORMATION
35 SN 74390, IRON-FORMATION
36 SN 74399, IRON-FORMATION
37 MC 7449, LOWER QUARTZITE

TABLE 7 MUSCOVITE ANALYSES FOR THE SNYDER GROUP

	1		2		3		4		5		6		7		8	
SIO2	46.02		45.15		45.09		46.25		46.05		44.90		45.69		45.55	
A203	35.53		34.74		32.44		35.19		35.45		35.53		34.61		34.95	
FEO	2.97		3.11		3.55		2.65		1.77		2.82		2.69		2.76	
TIO2	0.74		0.14		1.46		0.0		0.97		0.39		0.70		0.49	
MNO	0.0		0.03		0.01		0.0		0.0		0.0		0.0		0.0	
CAO	0.05		0.0		0.01		0.0		0.0		0.02		0.0		0.0	
MGO	0.30		0.32		0.23		0.57		0.49		0.38		0.39		0.44	
NA20	0.13		0.51		0.31		0.46		0.37		0.24		0.44		0.43	
K20	10.57		10.42		10.51		10.53		10.58		10.74		10.93		11.22	
H2O	4.52		4.42		4.36		4.49		4.51		4.45		4.46		4.47	
SUM	100.83		98.84		97.97		100.14		100.19		99.47		99.01		100.31	
SI	6.105	*	6.125	*	6.197	*	6.168	*	6.119	*	6.051	*	6.134	*	6.104	*
AL	1.895	8.000	1.875	8.000	1.803	8.000	1.832	8.000	1.881	8.000	1.949	8.000	1.866	8.000	1.896	8.000
AL	3.660	*	3.677	*	3.451	*	3.699	*	3.670	*	3.694	*	3.610	*	3.623	*
TI	0.074	*	0.014	*	0.151	*	0.0	*	0.097	*	0.040	*	0.071	*	0.049	*
FE	0.330	*	0.353	*	0.408	*	0.296	*	0.197	*	0.318	*	0.302	*	0.309	*
MN	0.0	*	0.003	*	0.001	*	0.0	*	0.0	*	0.0	*	0.0	*	0.0	*
MG	0.059	4.122	0.065	4.113	0.047	4.058	0.113	4.108	0.097	4.061	0.076	4.127	0.078	4.061	0.088	4.069
CA	0.007	*	0.0	*	0.001	*	0.0	*	0.0	*	0.003	*	0.0	*	0.0	*
NA	0.033	*	0.134	*	0.083	*	0.119	*	0.095	*	0.063	*	0.115	*	0.112	*
K	1.789	1.829	1.803	1.937	1.842	1.926	1.791	1.910	1.793	1.888	1.846	1.912	1.872	1.986	1.918	2.029
H	4.000	4.000	4.000	4.000	4.000	4.000	4.000	4.000	4.000	4.000	4.000	4.000	4.000	4.000	4.000	4.000
O	24.000	*	24.000	*	24.000	*	24.000	*	24.000	*	24.000	*	24.000	*	24.000	*
F/M		5.555		5.506		8.685		2.609		2.027		4.164		3.870		3.519
F/FM		0.847		0.846		0.897		0.723		0.670		0.806		0.795		0.779

1 SN 7237, LOWER QUARTZITE, II
2 SN 7241, LOWER QUARTZITE
3 SN 7256, LOWER QUARTZITE
4 SN 7278, LOWER QUARTZITE, II
5 SN 72131, LOWER QUARTZITE, I
6 SN 72135, LOWER QUARTZITE, I
7 SN 72160, UPPER QUARTZITE, III
8 SN 72164, LOWER QUARTZITE, I

TABLE 7 MUSCOVITE ANALYSES FOR THE SNYDER GROUP (CONTINUED)

	9		10		11		12		13		14		15		16	
SIO2	47.39		45.58		46.21		45.63		47.34		45.59		44.76		46.89	
A203	36.87		34.06		34.87		34.84		34.04		35.42		34.73		35.00	
FEO	2.02		3.41		3.49		3.04		3.14		3.40		3.32		0.73	
TIO2	0.07		0.0		0.13		0.51		0.0		0.05		0.05		0.02	
MNO	0.0		0.06		0.0		0.01		0.0		0.0		0.0		0.0	
CAO	0.01		0.03		0.01		0.0		0.0		0.0		0.0		0.0	
MGO	0.32		0.53		0.51		0.28		0.36		0.54		0.48		0.44	
NA2O	0.37		0.28		0.32		0.22		0.39		0.33		0.59		0.35	
K2O	10.16		10.11		11.13		10.23		10.79		10.64		10.10		10.66	
H2O	4.61		4.41		4.50		4.45		4.50		4.48		4.44		4.47	
SUM	101.81		98.57		101.17		99.21		100.56		100.45		99.37		98.56	
SI	6.166	*	6.202	*	6.147	*	6.146	*	6.301	*	6.092	*	6.046	*	6.286	*
AL	1.834	8.000	1.798	8.000	1.853	8.000	1.854	8.000	1.699	8.000	1.908	8.000	1.954	8.000	1.714	8.000
AL	3.818	*	3.652	*	3.614	*	3.675	*	3.639	*	3.669	*	3.574	*	3.815	*
TI	0.007	*	0.0	*	0.013	*	0.052	*	0.0	*	0.005	*	0.007	*	0.002	*
FE	0.220	*	0.387	*	0.388	*	0.342	*	0.350	*	0.380	*	0.375	*	0.082	*
MN	0.0	*	0.007	*	0.0	*	0.001	*	0.0	*	0.0	*	0.0	*	0.0	*
MG	0.062	4.107	0.107	4.153	0.101	4.116	0.056	4.127	0.071	4.060	0.108	4.162	0.097	4.142	0.088	3.987
CA	0.001	*	0.004	*	0.001	*	0.0	*	0.0	*	0.0	*	0.0	*	0.0	*
NA	0.093	*	0.074	*	0.083	*	0.057	*	0.101	*	0.085	*	0.155	*	0.091	*
K	1.686	1.781	1.751	1.829	1.889	1.972	1.757	1.815	1.832	1.932	1.813	1.899	1.740	1.895	1.823	1.914
H	4.000	4.000	4.000	4.000	4.000	4.000	4.000	4.000	4.000	4.000	4.000	4.000	4.000	4.000	4.000	4.000
O	24.000	*	24.000	*	24.000	*	24.000	*	24.000	*	24.000	*	24.000	*	24.000	*
F/M		3.542		3.674		3.840		6.112		4.894		3.533		3.891		0.931
F/FM		0.780		0.786		0.793		0.859		0.830		0.779		0.795		0.482

9 SN 72179, LOWER QUARTZITE, I
10 SN 72193, LOWER QUARTZITE, I
11 SN 72195, LOWER QUARTZITE, II
12 SN 72200, LOWER QUAPTZITE
13 SN 72215, LOWER QUARTZITE, I
14 SN 74302, LOWER QUARTZITE, II
15 SN 74327, LOWER QUARTZITE, I
16 SN 74378, UPPER QUARTZITE,

TABLE 8 OLIVINE ANALYSES FOR THE SNYDER GROUP

	1		2		3		4		5	
SIO2	41.46		37.19		36.56		43.87		41.93	
A203	0.0		0.15		0.0		0.0		0.0	
FEO	5.28		24.47		31.78		5.03		4.67	
MNO	0.53		4.51		0.36		0.22		0.33	
CAO	0.0		0.32		0.02		0.11		0.12	
MGO	53.15		33.75		34.01		52.47		52.76	
SUM	100.42		100.39		102.73		101.70		99.81	
SI	0.993	*	0.995	*	0.970	*	1.029	*	1.005	*
AL	0.0	0.993	0.005	0.999	0.0	0.970	0.0	1.029	0.0	1.005
MG	0.0	2.014	0.0	2.004	0.0	2.059	0.0	1.941	0.0	1.989
FE	0.106	*	0.547	*	0.705	*	0.099	*	0.094	*
MN	0.011	*	0.102	*	0.008	*	0.004	*	0.007	*
CA	0.0	2.014	0.009	2.004	0.001	2.059	0.003	1.941	0.003	1.989
O	4.000	*	4.000	*	4.000	*	4.000	*	4.000	*
FO	94.21		57.13		65.33		94.55		94.80	
FA	5.25		27.31		34.25		5.09		4.71	
TP	0.53		5.10		0.39		0.23		0.34	
MT	0.0		0.46		0.03		0.14		0.15	
F/M	0.061		0.483		0.530		0.056		0.053	
F/FM	0.058		0.326		0.347		0.053		0.051	

1 SN 7284, MARBLE
2 SN 72128, MARBLE
3 NC 7413, OLIVINE WEBSTERITE
4 NC 7452A, MARBLE
5 NC 7452A, MARBLE

TABLE 9 PLAGIOCLASE ANALYSES FOR THE SNYDER GROUP

	1	2	3	4	5	6	7	8
SIO2	58.32	45.78	55.01	57.23	58.92	44.40	47.08	48.31
A2O3	28.35	34.77	25.21	27.84	28.00	36.06	33.74	35.79
CAO	9.55	18.45	9.83	9.06	9.78	19.39	17.42	17.94
NA2O	6.08	0.23	7.36	5.86	5.91	0.42	1.03	1.78
K2O	0.10	0.0	0.0	0.0	0.08	0.10	0.0	0.03
SUM	102.40	99.23	97.41	99.99	102.59	100.37	99.27	103.85

SI	2.550	*		2.117	*		2.555	*		2.557	*		2.566	*		2.044	*		2.171	*		2.127	*	
AL	1.461	4.011		1.894	4.011		1.380	3.934		1.466	4.022		1.439	4.005		1.956	3.999		1.933	4.005		1.965	4.092	
CA	0.447	*		0.914	*		0.489	*		0.434	*		0.457	*		0.956	*		0.861	*		0.850	*	
NA	0.515	*		0.021	*		0.663	*		0.508	*		0.500	*		0.037	*		0.092	*		0.153	*	
K	0.006	0.969		0.0	0.935		0.0	1.152		0.0	0.941		0.004	0.961		0.006	1.000		0.0	0.953		0.002	1.005	
O	8.000	*		8.000	*		8.000	*		8.000	*		8.000	*		8.000	*		8.000	*		8.000	*	
AN		46.20			97.79			42.46			46.07			47.55			95.66			90.33			94.64		
AB		53.22			2.21			57.54			53.93			51.99			3.75			9.67			15.20		
OR		0.58			0.0			0.0			0.0			0.46			0.59			0.0			0.17		

1 SN 7211, SNYDER BRECCIA
2 SN 7222, SNYDER BRECCIA, III
3 SN 7289, LOWER QUARTZITE, II
4 SN 7289, LOWER QUARTZITE, II
5 SN 72117, SNYDER BRECCIA
6 SN 72123, LOWER QUARTZITE, III
7 SN 72126, SNYDER BRECCIA
8 SN 72126, SNYDER BRECCIA

	9	10	11	12	13	14	15	16
SIO2	61.44	44.38	60.69	61.86	50.57	47.95	48.05	50.23
A2O3	25.33	36.17	23.86	23.41	33.11	32.08	32.56	26.34
CAO	6.56	19.49	5.53	5.63	15.52	16.65	18.26	7.91
NA2O	8.11	0.42	8.17	8.59	2.94	2.17	1.13	7.07
K2O	0.07	0.05	0.35	0.0	0.05	0.0	0.0	0.30
SUM	101.51	100.51	98.60	99.49	102.19	98.85	100.00	100.85

SI	2.692	*		2.040	*		2.733	*		2.757	*		2.258	*		2.223	*		2.205	*		2.624	*	
AL	1.308	3.999		1.959	3.999		1.266	3.999		1.230	3.987		1.742	3.999		1.752	3.975		1.761	3.966		1.375	4.000	
CA	0.308	*		0.960	*		0.267	*		0.269	*		0.742	*		0.827	*		0.898	*		0.376	*	
NA	0.689	*		0.037	*		0.713	*		0.742	*		0.254	*		0.195	*		0.101	*		0.607	*	
K	0.004	1.001		0.003	1.000		0.020	1.000		0.0	1.011		0.003	1.000		0.0	1.022		0.0	0.998		0.017	1.000	
O	8.000	*		8.000	*		8.000	*		8.000	*		8.000	*		8.000	*		8.000	*		8.000	*	
AN		30.77			95.96			26.69			26.59			74.26			90.92			89.93			37.56		
AB		68.84			3.74			71.32			73.41			25.46			19.08			10.07			60.75		
OR		0.39			0.29			2.01			0.0			0.28			0.0			0.0			1.70		

9 SN 72127, UPPER QUARTZITE, II
10 SN 72173, LOWER QUARTZITE, I
11 SN 72188, IRON-FORMATION, III
12 SN 72188, IRON-FORMATION
13 SN 72191, LOWER QUARTZITE, III
14 SN 72211, LOWER QUARTZITE, III
15 SN 72223, METAMORPHOSED DIKE
16 SN 74231, HILL 1390 AMPHIBOLITE

TABLE 9 PLAGIOCLASE ANALYSES FOR THE SNYDER GROUP (CONTINUED)

	17	18	19	20	21	22	23	24
SIO2	61.05	61.97	62.14	58.75	59.68	59.86	49.37	59.75
A2O3	25.01	24.71	25.03	25.76	25.38	26.45	32.64	24.62
CAO	6.39	5.92	6.15	7.55	7.01	7.86	15.41	6.37
NA2O	8.10	8.37	8.27	7.24	7.61	7.30	2.78	7.85
K2O	0.07	0.17	0.24	0.13	0.11	0.15	0.04	0.13
SUM	100.62	101.14	101.83	99.43	99.79	101.62	100.24	98.72

SI	2.697	*		2.721	*		2.712	*		2.637	*		2.664	*		2.630	*		2.248	*		2.692	*	
AL	1.302	3.999		1.279	4.000		1.287	3.999		1.362	3.999		1.335	4.000		1.369	3.999		1.751	4.000		1.307	3.999	
CA	0.302	*		0.279	*		0.288	*		0.363	*		0.335	*		0.370	*		0.752	*		0.308	*	
NA	0.694	*		0.713	*		0.700	*		0.630	*		0.659	*		0.622	*		0.245	*		0.686	*	
K	0.004	1.000		0.010	1.001		0.013	1.001		0.007	1.001		0.006	1.000		0.008	1.000		0.002	1.000		0.007	1.001	
O	8.000	*		8.000	*		8.000	*		8.000	*		8.000	*		8.000	*		8.000	*		8.000	*	
AN		30.24			27.83			28.74			36.29			33.52			36.99			75.21			30.73		
AB		69.37			71.21			69.93			62.97			65.85			62.17			24.55			68.53		
OR		0.39			0.95			1.34			0.74			0.63			0.84			0.23			0.75		

17 SN 74236, HILL 1330 AMPHIBOLITE
18 SN 74263, LOWER QUARTZITE, III
19 SN 74263, LOWER QUARTZITE, III
20 SN 74275, UPPER QUARTZITE, III
21 SN 74276, UPPER QUARTZITE, III
22 SN 74288, LOWER QUARTZITE, III
23 SN 74305, LOWER QUARTZITE, III
24 SN 74323, GRAPHITE-SULFIDE HORNFELS

	25	26	27	28	29	30
SIO2	43.69	44.09	65.89	65.82	55.23	59.86
A2O3	36.33	36.01	19.69	20.73	28.68	24.97
CAO	19.78	20.00	0.87	1.74	10.77	6.64
NA2O	0.20	0.0	10.93	10.60	5.44	7.38
K2O	0.04	0.0	0.10	0.10	0.11	0.72
SUM	100.04	100.10	97.48	98.09	100.23	99.57

SI	2.020	*		2.036	*		2.958	*		2.917	*		2.481	*		2.681	*	
AL	1.979	3.999		1.959	3.995		1.042	4.000		1.083	4.000		1.518	4.000		1.318	3.999	
CA	0.980	*		0.989	*		0.042	*		0.083	*		0.518	*		0.319	*	
NA	0.018	*		0.0	*		0.951	*		0.911	*		0.474	*		0.641	*	
K	0.002	1.000		0.0	0.989		0.006	0.999		0.006	0.999		0.006	0.999		0.041	1.001	
O	8.000	*		8.000	*		8.000	*		8.000	*		8.000	*		8.000	*	
AN		97.97			100.00			4.19			8.27			51.92			31.84		
AB		1.79			0.0			95.24			91.16			47.45			64.05		
OR		0.24			0.0			0.57			0.57			0.63			4.11		

25 SN 74329, LOWER QUARTZITE, III
26 SN 74329, LOWER QUARTZITE, III
27 SN 74347, GRAPHITE-SULFIDE HORNFELS
28 SN 74348, GRAPHITE-SULFIDE HORNFELS
29 SN 74373, GRAPHITE-SULFIDE HORNFELS
30 NC 7448

TABLE 10 POTASSIUM FELDSPAR ANALYSES FOR THE SNYDER GROUP

	1		2		3		4		5		6		7		8	
SIO2	61.91		63.90		63.83		64.70		65.26		64.90		65.55		64.58	
A2O3	17.56		18.10		18.06		18.33		18.52		18.41		18.58		18.27	
CAO	0.05		0.03		0.01		0.03		0.06		0.04		0.03		0.0	
NA2O	1.35		0.50		0.62		0.46		1.29		1.91		1.15		1.51	
K2O	14.10		15.93		15.73		16.19		15.06		14.03		15.36		14.58	
SUM	94.97		98.46		98.25		99.71		100.19		99.29		100.67		98.94	
SI	2.998	*	2.998	*	2.999	*	2.998	*	2.997	*	2.998	*	2.998	*	3.000	*
AL	1.002	3.999	1.001	3.999	1.000	4.000	1.001	3.999	1.002	3.999	1.002	4.000	1.001	4.000	1.000	4.000
CA	0.003	*	0.002	*	0.001	*	0.001	*	0.003	*	0.002	*	0.001	*	0.0	*
NA	0.127	*	0.045	*	0.056	*	0.041	*	0.115	*	0.171	*	0.102	*	0.136	*
K	0.871	1.000	0.953	1.000	0.943	1.000	0.957	1.000	0.882	1.000	0.827	1.000	0.896	1.000	0.864	1.000
O	8.000	*	8.000	*	8.000	*	8.000	*	8.000	*	8.000	*	8.000	*	8.000	*
AN	0.26		0.15		0.05		0.15		0.30		0.20		0.15		0.0	
AB	12.67		4.55		5.65		4.13		11.49		17.11		10.20		13.60	
OR	87.07		95.30		94.30		95.72		88.22		82.69		89.65		86.40	

1 SN 7215, LOWER QUARTZITE,I
2 SN 7225, LOWER QUARTZITE, II
3 SN 7225, LOWER QUARTZITE, II
4 SN 7237, LOWER QUARTZITE, II
5 SN 7256, LOWER QUARTZITE, I
6 SN 7273, LOWER QUARTZITE, II
7 SN 7274, LOWER QUARTZITE, II
8 SN 7278, LOWER QUARTZITE, II

	9		10		11		12		13		14		15		16	
SIO2	64.72		64.35		64.81		65.16		65.24		65.30		65.20		65.56	
A2O3	18.37		17.95		18.41		18.52		18.51		18.51		18.51		18.61	
CAO	0.06		0.06		0.08		0.08		0.05		0.04		0.06		0.06	
NA2O	1.97		1.21		1.13		1.56		0.70		1.36		1.35		1.32	
K2O	3.88		14.68		15.17		14.61		15.95		14.97		14.95		15.10	
SUM	89.00		97.35		99.60		99.93		100.45		100.18		100.07		100.65	
SI	3.112	*	3.038	*	2.996	*	2.996	*	2.997	*	2.998	*	2.997	*	2.997	*
AL	1.041	4.153	0.949	3.987	1.003	3.999	1.003	4.000	1.002	4.000	1.001	4.000	1.003	4.000	1.002	3.999
CA	0.003	*	0.003	*	0.004	*	0.004	*	0.002	*	0.002	*	0.003	*	0.003	*
NA	0.184	*	0.111	*	0.101	*	0.139	*	0.062	*	0.121	*	0.120	*	0.117	*
K	0.238	0.425	0.884	0.998	0.895	1.000	0.857	1.000	0.935	1.000	0.877	1.000	0.876	1.000	0.880	1.000
O	8.000	*	8.000	*	8.000	*	8.000	*	8.000	*	8.000	*	8.000	*	8.000	*
AN	0.73		0.30		0.40		0.39		0.25		0.20		0.30		0.29	
AB	43.24		11.10		10.13		13.91		6.24		12.11		12.03		11.69	
OR	56.03		88.60		89.47		85.70		93.52		87.69		87.67		88.01	

9 SN 7278, LOWER QUARTZITE, II
10 SN 7289, LOWER QUARTZITE, II
11 SN 7289, LOWER QUARTZITE, II
12 SN 72109, LOWER QUARTZITE, II
13 SN 72123, LOWER QUARTZITE, II
14 SN 72127, UPPER QUARTZITE, II
15 SN 72130, LOWER QUARTZITE, I
16 SN 72131, LOWER QUARTZITE, I

TABLE 10 POTASSIUM FELDSPAR ANALYSES FOR THE SNYDER GROUP (CONTINUED)

	17	18	19	20	21	22	23	24
SIO2	65.80	65.29	63.70	61.62	62.43	65.88	63.51	64.93
A2O3	18.66	18.55	18.03	17.50	17.71	19.91	18.06	18.48
CAO	0.05	0.07	0.01	0.06	0.04	0.15	0.03	0.10
NA2O	1.14	1.63	1.12	1.15	0.99	2.46	0.99	2.04
K2O	15.44	14.54	14.94	14.32	14.78	13.40	15.06	13.91
SUM	101.09	100.08	97.80	94.65	95.95	100.70	97.65	99.36

SI	2.998	*	2.996	*	2.999	*	2.997	*	2.999	*	2.993	*	2.997	*	2.995	*
AL	1.002	3.999	1.003	4.000	1.000	4.000	1.003	4.000	1.002	4.000	1.007	3.999	1.004	4.001	1.004	4.000
CA	0.002	*	0.003	*	0.001	*	0.003	*	0.002	*	0.007	*	0.002	*	0.005	*
NA	0.101	*	0.145	*	0.102	*	0.108	*	0.092	*	0.217	*	0.091	*	0.182	*
K	0.897	1.000	0.851	1.000	0.897	1.000	0.888	1.000	0.905	0.999	0.776	1.000	0.896	0.999	0.813	1.000
O	8.000	*	8.000	*	8.000	*	8.000	*	8.000	*	8.000	*	8.000	*	8.000	*
AN		0.24		0.34		0.05		0.31		0.21		0.73		0.15		0.49
AB		10.07		14.51		10.22		10.85		9.22		21.66		9.07		18.25
OR		89.69		85.15		89.72		88.84		90.57		77.61		90.78		81.26

17 SN 72133, LOWER QUARTZITE, I
18 SN 72142, LOWER QUARTZITE, III
19 SN 72147, LOWER QUARTZITE, III
20 SN 72191, LOWER QUARTZITE, III
21 SN 72218, LOWER QUARTZITE, I
22 SN 74275, UPPER QUARTZITE, III
23 SN 74276, UPPER QUARTZITE, III
24 SN 74298, LOWER QUARTZITE, III

	25	26
SIO2	63.76	64.34
A2O3	18.05	18.34
CAO	0.02	0.12
NA2O	1.21	1.56
K2O	14.90	14.38
SUM	97.84	98.74

SI	2.999	*	2.994	*
AL	1.000	4.000	1.006	3.999
CA	0.001	*	0.006	*
NA	0.110	*	0.141	*
K	0.888	0.999	0.853	1.000
O	8.000	*	8.000	*
AN		0.10		0.60
AB		11.04		14.07
OR		88.86		85.33

25 SN 74323, GRAPHITE-SULFIDE HORNFELS, III
26 SN 74373, GRAPHITE-SULFIDE HORNFELS, III

TABLE 11 PYROXENE ANALYSES FOR THE SNYDER GROUP

	1	2	3	4	5	6	7	8
SIO2	53.86	53.92	49.82	53.13	51.25	51.30	50.99	51.92
A2O3	1.69	0.62	0.68	0.23	0.17	0.28	0.28	0.30
FEO	19.11	3.03	36.82	7.95	34.86	15.65	15.49	12.57
TIO2	0.0	0.0	0.0	0.0	0.0	0.02	0.02	0.0
MNO	0.32	0.76	0.65	1.19	6.65	1.40	1.40	1.70
CAO	0.38	24.81	0.53	24.12	0.75	21.47	21.44	22.03
MGO	24.67	16.02	13.46	13.76	6.07	11.46	10.37	10.55
NA2O	0.0	0.0	0.0	0.0	0.0	0.12	0.12	0.12
K2O	0.0	0.0	0.0	0.0	0.0	0.0	0.0	0.0
SUM	100.03	99.16	101.96	100.38	99.75	101.70	100.06	99.14

SI	1.969	*	1.990	*	1.956	*	1.984	*	2.086	*	1.953	*	1.972	*	2.000	*
AL	0.031	2.000	0.010	2.000	0.031	1.988	0.010	1.994	0.0	2.086	0.013	1.966	0.013	1.985	0.0	2.000
AL	0.042	*	0.017	*	0.0	*	0.0	*	0.008	*	0.0	*	0.0	*	0.014	*
CA	0.0	1.995	0.0	1.997	0.0	2.041	0.0	2.017	0.0	1.825	0.0	2.079	0.0	2.040	0.0	1.997
MG	1.344	*	0.881	*	0.788	*	0.766	*	0.368	*	0.553	*	0.595	*	0.606	*
FE	0.584	*	0.094	*	1.209	*	0.248	*	1.186	*	0.498	*	0.501	*	0.403	*
MN	0.010	*	0.024	*	0.022	*	0.038	*	0.229	*	0.045	*	0.046	*	0.055	*
TI	0.0	*	0.0	*	0.0	*	0.0	*	0.0	*	0.001	*	0.001	*	0.0	*
K	0.0	*	0.0	*	0.0	*	0.0	*	0.0	*	0.0	*	0.0	*	0.0	*
NA	0.0	1.995	0.0	1.997	0.0	2.041	0.0	2.017	0.0	1.825	0.009	2.079	0.009	2.040	0.009	1.997
O	6.000	*	6.000	*	6.000	*	6.000	*	6.000	*	6.000	*	6.000	*	6.000	*
WO		0.76		49.56		1.09		47.85		1.80		42.32		43.76		46.07
FS		29.91		4.72		59.25		12.31		65.31		24.08		24.69		20.43
EN		68.82		44.52		38.60		37.87		20.27		31.42		29.30		30.69
MN		0.51		1.20		1.06		1.87		12.62		2.18		2.26		2.81
WO		0.77		50.16		1.10		48.76		2.06		43.26		44.77		47.40
FS		30.06		4.79		59.88		12.54		74.74		24.61		25.25		21.03
EN		69.17		45.06		39.01		38.70		23.20		32.12		29.98		31.58
F/M		0.442		0.133		1.562		0.373		3.845		0.836		0.919		0.757
F/FM		0.307		0.117		0.610		0.272		0.794		0.455		0.479		0.431

1 SN 7219, HILL 800 ULTRAMAFIC
2 SN 7220, QUARTZITE MARBLE
3 SN 7222, SNYDER BRECCIA
4 SN 7227, QUARTZITE MARBLE
5 SN 7267, IRON FORMATION
6 SN 7268, SNYDER BRECCIA
7 SN 7268, SNYDER BRECCIA
8 SN 7268, SNYDER BRECCIA

TABLE 11 PYROXENE ANALYSES FOR THE SNYDER GROUP (CONTINUED)

	9	10	11	12	13	14	15	16
SIO2	54.44	51.70	48.02	47.26	48.08	48.11	48.90	50.93
A203	0.29	0.46	0.36	0.34	1.31	0.68	0.49	0.66
FEO	6.16	7.75	36.33	37.05	23.57	41.40	42.02	14.22
TIO2	0.0	1.87	0.15	0.0	0.0	0.0	0.0	0.0
MNO	1.92	23.12	8.63	9.15	4.80	3.51	2.83	2.51
CAO	24.96	12.63	1.90	1.74	17.35	0.62	0.59	20.97
MGO	14.81	0.0	6.77	5.48	5.22	9.58	7.60	10.19
NA2O	0.0	0.0	0.0	0.0	0.0	0.0	0.0	0.0
K2O	0.0	0.0	0.0	0.0	0.0	0.0	0.0	0.0
SUM	101.68	97.53	101.66	101.02	100.33	102.90	102.43	99.38

SI	1.989	*	2.116	*	1.974	*	1.971	*	1.941	*	1.944	*	1.980	*	1.974	*
AL	0.011	2.000	0.0	2.116	0.017	1.991	0.017	1.987	0.059	2.000	0.032	1.977	0.020	2.000	0.026	2.000
AL	0.001	*	0.022	*	0.0	*	0.0	*	0.003	*	0.0	*	0.004	*	0.004	*
CA	0.0	2.005	0.0	1.700	0.0	2.022	0.0	2.034	0.0	2.028	0.0	2.063	0.0	2.008	0.0	2.011
MG	0.806	*	0.0	*	0.384	*	0.341	*	0.314	*	0.517	*	0.450	*	0.590	*
FE	0.188	*	0.265	*	1.249	*	1.292	*	0.796	*	1.380	*	1.423	*	0.462	*
MN	0.032	*	0.801	*	0.300	*	0.323	*	0.164	*	0.129	*	0.097	*	0.083	*
TI	0.0	*	0.058	*	0.005	*	0.0	*	0.0	*	0.0	*	0.0	*	0.0	*
K	0.0	*	0.0	*	0.0	*	0.0	*	0.0	*	0.0	*	0.0	*	0.0	*
NA	0.0	2.005	0.0	1.700	0.0	2.022	0.0	2.034	0.0	2.028	0.0	2.063	0.0	2.008	0.0	2.011
O	6.000	*	6.000	*	6.000	*	6.000	*	6.000	*	6.000	*	6.000	*	6.000	*
WO		48.77		34.19		4.15		3.82		37.07		1.30		1.28		43.48
FS		9.40		16.37		61.91		63.54		39.31		67.82		70.00		23.01
EN		40.26		0.0		19.04		16.75		15.52		25.05		22.90		29.39
MN		1.58		49.46		14.90		15.89		8.11		5.82		4.84		4.11
WO		49.55		67.62		4.87		4.55		40.34		1.38		1.34		45.35
FS		9.55		32.38		72.75		75.54		42.78		72.02		74.61		24.00
EN		40.90		0.0		22.38		19.91		16.88		26.60		24.05		30.65
F/M		0.273		0.133		4.033		4.742		3.056		2.940		3.314		0.923
F/FM		0.214		0.117		0.801		0.826		0.753		0.746		0.768		0.480

9 SN 7285, QUARTZITE MARBLE
10 SN 72101, QUARTZITE MARBLE
11 SN 72107, IRON FORMATION
12 SN 72107, IRON FORMATION
13 SN 72107, IRON FORMATION
14 SN 72118, IRON FORMATION
15 SN 72118, IRON FORMATION
16 SN 72124, QUARTZITE MARBLE

TABLE 11 PYROXENE ANALYSES FOR THE SNYDER GROUP (CONTINUED)

	17	18	19	20	21	22	23	24
SIO2	50.47	50.96	50.72	53.12	51.68	49.17	48.33	48.19
A2O3	0.49	0.35	1.26	0.96	0.84	0.78	2.14	1.93
FEO	33.92	34.20	15.28	5.31	12.64	37.50	38.15	35.98
TIO2	0.0	0.06	0.0	0.0	0.0	4.57	0.0	0.0
MNO	0.77	0.82	0.36	1.25	0.96	0.54	0.34	0.76
CAO	1.31	1.13	21.49	23.69	22.91	10.33	0.08	0.14
MGO	12.80	13.57	10.43	16.57	11.95	0.0	11.57	13.44
NA2O	0.0	0.0	0.0	0.0	0.0	0.0	0.0	0.0
K2O	0.0	0.01	0.0	0.0	0.0	0.0	0.0	0.0
SUM	99.75	101.10	99.54	100.90	100.98	102.89	100.61	101.44

SI	2.001	*	1.994	*	1.959	*	1.949	*	1.955	*	1.974	*	1.934	*	1.933	*
AL	0.0	2.001	0.006	2.000	0.041	2.000	0.042	1.991	0.037	1.993	0.026	2.000	0.066	2.000	0.067	2.000
AL	0.023	*	0.010	*	0.017	*	0.0	*	0.0	*	0.011	*	0.035	*	0.022	*
CA	0.0	1.997	0.0	1.997	0.0	2.012	0.0	2.039	0.0	2.033	0.0	1.870	0.0	2.016	0.0	2.023
MG	0.762	*	0.791	*	0.601	*	0.906	*	0.674	*	0.0	*	0.600	*	0.787	*
FE	1.121	*	1.119	*	0.494	*	0.163	*	0.400	*	1.259	*	1.276	*	1.192	*
MN	0.026	*	0.027	*	0.012	*	0.039	*	0.031	*	0.019	*	0.012	*	0.025	*
TI	0.0	*	0.002	*	0.0	*	0.0	*	0.0	*	0.138	*	0.0	*	0.0	*
K	0.0	*	0.000	*	0.0	*	0.0	*	0.0	*	0.0	*	0.0	*	0.0	*
NA	0.0	1.997	0.0	1.997	0.0	2.012	0.0	2.039	0.0	2.033	0.0	1.870	0.0	2.016	0.0	2.023
O	6.000	*	6.000	*	6.000	*	6.000	*	6.000	*	6.000	*	6.000	*	6.000	*
	WO	2.83		2.39		44.57		45.67		45.67		25.81		0.17		0.29
	FS	57.08		56.38		24.74		7.99		19.67		73.13		64.42		59.10
	EN	38.77		39.87		30.10		44.44		33.14		0.0		34.82		39.34
	MN	1.32		1.37		0.59		1.90		1.51		1.07		0.59		1.26
	WO	2.87		2.42		44.84		46.55		46.38		26.09		0.17		0.30
	FS	57.84		57.15		24.89		8.15		19.97		73.91		64.80		59.85
	EN	39.29		40.42		30.28		45.30		33.65		0.0		35.03		39.85
	F/M	1.506		1.448		0.842		0.223		0.639		2.940		1.867		1.534
	F/FM	0.601		0.592		0.457		0.182		0.390		0.746		0.651		0.605

17 SN 72126, SNYDER BRECCIA
18 SN 72126, SNYDER BRECCIA
19 SN 72126, SNYDER BRECCIA
20 SN 72128, QUARTZ MARBLE
21 SN 72132, SNYDER BRECCIA
22 SN 72149, IRON FORMATION
23 SN 72162, LOWER QUARTZITE
24 SN 72175

TABLE 11 PYROXENE ANALYSES FOR THE SNYDER GROUP (CONTINUED)

	25	26	27	28	29	30	31	32
SIO2	53.12	50.13	47.72	50.35	50.89	50.70	49.79	49.31
A2O3	0.96	0.98	2.74	0.83	0.99	1.19	0.40	0.50
FEO	5.31	31.69	34.08	35.13	34.76	34.99	29.05	29.81
TIO2	0.0	0.0	0.0	0.12	0.0	0.0	0.0	0.0
MNO	1.25	5.45	0.30	4.98	4.60	4.64	3.38	3.34
CAO	23.69	0.44	0.11	1.73	1.57	3.02	20.91	19.95
MGO	16.57	14.47	14.14	7.21	8.10	6.70	6.60	6.27
NA2O	0.0	0.0	0.0	0.09	0.0	0.0	0.0	0.0
K2O	0.0	0.0	0.0	0.0	0.0	0.0	0.0	0.0
SUM	100.90	103.15	99.09	100.44	101.00	101.24	101.13	100.08

SI	1.949	*	1.939	*	1.906	*	2.033	*	2.030	*	2.029	*	1.963	*	1.968	*
AL	0.042	1.991	0.045	1.993	0.094	2.000	0.0	2.033	0.0	2.030	0.0	2.029	0.019	1.982	0.024	1.991
AL	0.0	*	0.0	*	0.035	*	0.039	*	0.047	*	0.056	*	0.0	*	0.0	*
CA	0.0	2.039	0.0	2.055	0.0	2.030	0.0	1.915	0.0	1.916	0.0	1.914	0.0	2.065	0.0	2.029
MG	0.906	*	0.834	*	0.842	*	0.434	*	0.487	*	0.400	*	0.388	*	0.373	*
FE	0.163	*	1.025	*	1.138	*	1.186	*	1.160	*	1.171	*	0.661	*	0.695	*
MN	0.039	*	0.179	*	0.010	*	0.170	*	0.155	*	0.157	*	0.113	*	0.113	*
TI	0.0	*	0.0	*	0.0	*	0.004	*	0.0	*	0.0	*	0.0	*	0.0	*
K	0.0	*	0.0	*	0.0	*	0.0	*	0.0	*	0.0	*	0.0	*	0.0	*
NA	0.0	2.039	0.0	2.055	0.0	2.030	0.007	1.915	0.0	1.916	0.0	1.914	0.0	2.065	0.0	2.029
O	6.000	*	6.000	*	6.000	*	6.000	*	6.000	*	6.000	*	6.000	*	6.000	*
WO	45.67		0.89		0.24		4.01		3.59		6.97		43.19		41.83	
FS	7.99		49.85		57.06		63.59		62.04		63.05		32.33		34.23	
EN	44.44		40.59		42.20		23.26		26.05		21.52		18.97		18.38	
MN	1.90		8.69		0.51		9.13		8.32		8.47		5.52		5.56	
WO	46.55		0.97		0.24		4.42		3.92		7.62		45.71		44.29	
FS	8.15		54.59		57.35		69.99		67.67		68.89		34.21		36.24	
EN	45.30		44.44		42.41		25.60		28.42		23.51		20.07		19.46	
F/M	0.223		1.442		1.364		3.126		2.900		3.324		1.905		2.165	
F/FM	0.182		0.591		0.577		0.758		0.730		0.769		0.666		0.684	

25 SN 72188, IRON FORMATION
26 SN 72188, IRON FORMATION
27 SN 72191, LOWER QUARTZITE
28 SN 72204, IRON FORMATION
29 SN 72205, IRON FORMATION
30 SN 72205, IRON FORMATION
31 SN 72205, IRON FORMATION
32 SN 72205, IRON FORMATION

TABLE 11 PYROXENE ANALYSES FOR THE SNYDER GROUP (CONTINUED)

	33	34	35	36	37	38	39	40
SIO2	44.17	51.12	46.60	46.86	47.13	51.56	49.25	51.54
A2O3	0.99	0.26	2.97	2.45	2.78	0.96	1.76	0.90
FEO	26.77	12.06	38.25	38.33	37.23	15.67	34.04	15.32
TIO2	0.0	0.0	0.0	0.21	0.0	0.0	0.0	0.0
MNO	1.10	4.34	0.29	0.34	0.25	1.34	2.05	0.59
CAO	22.01	22.72	0.17	0.20	0.12	21.24	0.22	21.13
MGO	6.68	9.77	9.92	10.04	12.58	10.17	13.40	10.78
NA2O	0.0	0.0	0.0	0.02	0.0	0.0	0.0	0.0
K2O	0.0	0.0	0.0	0.02	0.0	0.0	0.0	0.0
SUM	101.72	100.27	98.10	98.47	100.09	101.94	100.72	100.16

SI	1.803	*	1.974	*	1.922	*	1.927	*	1.893	*	1.957	*	1.944	*	1.976	*
AL	0.048	1.851	0.012	1.986	0.078	2.000	0.073	2.000	0.107	2.000	0.043	2.000	0.056	2.000	0.024	2.000
AL	0.0	*	0.0	*	0.066	*	0.045	*	0.024	*	0.003	*	0.026	*	0.012	*
CA	0.0	2.322	0.0	2.034	0.0	2.006	0.0	2.009	0.0	2.041	0.0	2.018	0.0	2.015	0.0	2.006
MG	0.407	*	0.562	*	0.604	*	0.615	*	0.753	*	0.576	*	0.788	*	0.616	*
FE	0.914	*	0.389	*	1.319	*	1.318	*	1.250	*	0.537	*	1.124	*	0.491	*
MN	0.038	*	0.142	*	0.010	*	0.012	*	0.009	*	0.043	*	0.069	*	0.019	*
TI	0.0	*	0.0	*	0.0	*	0.006	*	0.0	*	0.0	*	0.0	*	0.0	*
K	0.0	*	0.0	*	0.0	*	0.001	*	0.0	*	0.0	*	0.0	*	0.0	*
NA	0.0	2.322	0.0	2.034	0.0	2.006	0.002	2.009	0.0	2.041	0.0	2.018	0.0	2.015	0.0	2.006
O	6.000	*	6.000	*	6.000	*	6.000	*	6.000	*	6.000	*	6.000	*	6.000	*
WO		41.49		46.22		0.39		0.45		0.26		42.94		0.47		43.52
FS		39.37		19.15		67.98		67.45		61.99		26.31		56.47		24.63
EN		17.51		27.65		31.11		31.49		37.33		28.61		39.62		30.89
MN		1.64		6.99		0.52		0.61		0.42		2.14		3.44		0.96
WO		42.17		49.69		0.39		0.45		0.26		43.88		0.48		43.94
FS		40.03		20.59		68.34		67.86		62.25		26.88		58.48		24.87
EN		17.80		29.72		31.27		31.68		37.49		29.23		41.03		31.19
F/M		2.342		0.945		2.202		2.161		1.672		0.995		1.517		0.828
F/FM		0.701		0.486		0.688		0.684		0.626		0.490		0.602		0.453

33 SN 72207, IRON FORMATION
34 SN 72209, IRON FORMATION
35 SN 72211, LOWER QUARTZITE
36 SN 72211, LOWER QUARTZITE
37 SN 72211, LOWER QUARTZITE
38 SN 72222, IRON FORMATION
39 SN 72223, DIKE
40 SN 74231, HILL 1300 AMPHIBOLITE

TABLE 11 PYROXENE ANALYSES FOR THE SNYDER GROUP (CONTINUED)

	41	42	43	44	45	46	47	48
SIO2	50.53	48.15	51.25	50.69	50.91	53.56	49.07	49.25
A2O3	0.88	2.78	0.81	0.43	1.18	0.58	2.34	2.74
FEO	14.46	37.36	16.77	34.75	13.26	31.32	34.82	35.40
TIO2	0.0	0.0	0.0	0.0	0.0	0.0	0.0	0.0
MNO	0.45	0.70	0.32	0.64	0.49	0.92	0.44	0.33
CAO	22.16	0.16	19.52	1.22	20.63	1.01	0.35	0.24
MGO	9.74	11.35	10.82	14.39	11.60	15.85	12.61	14.80
NA2O	0.0	0.0	0.0	0.0	0.0	0.0	0.0	0.0
K2O	0.0	0.0	0.0	0.0	0.0	0.0	0.0	0.0
SUM	98.22	100.50	99.49	102.12	98.07	103.24	99.63	102.76

SI	1.977	*	1.924	*	1.980	*	1.969	*	1.973	*	1.972	*	1.951	*	1.900	*
AL	0.023	2.000	0.076	2.000	0.020	2.000	0.020	1.988	0.027	2.000	0.027	1.999	0.049	2.000	0.100	2.000
AL	0.018	*	0.055	*	0.017	*	0.0	*	0.027	*	0.0	*	0.060	*	0.024	*
CA	0.0	2.003	0.0	2.010	0.0	2.001	0.0	2.033	0.0	2.000	0.0	2.016	0.0	1.995	0.0	2.038
MG	0.568	*	0.576	*	0.623	*	0.833	*	0.670	*	0.921	*	0.747	*	0.851	*
FE	0.473	*	1.249	*	0.542	*	1.129	*	0.430	*	1.022	*	1.159	*	1.142	*
MN	0.015	*	0.024	*	0.010	*	0.021	*	0.016	*	0.030	*	0.015	*	0.011	*
TI	0.0	*	0.0	*	0.0	*	0.0	*	0.0	*	0.0	*	0.0	*	0.0	*
K	0.0	*	0.0	*	0.0	*	0.0	*	0.0	*	0.0	*	0.0	*	0.0	*
NA	0.0	2.003	0.0	2.010	0.0	2.001	0.0	2.033	0.0	2.000	0.0	2.016	0.0	1.995	0.0	2.038
O	6.000	*	6.000	*	6.000	*	6.000	*	6.000	*	6.000	*	6.000	*	6.000	*
	WO	46.80		0.35		40.74		2.50		43.43		2.00		0.77		0.49
	FS	23.84		63.86		27.32		55.50		21.79		50.68		59.84		56.71
	EN	28.62		34.58		31.41		40.96		33.97		45.71		38.69		42.26
	MN	0.75		1.21		0.53		1.04		0.82		1.51		0.77		0.54
	WO	47.15		0.35		40.95		2.52		43.78		2.13		0.78		0.50
	FS	24.02		64.64		27.46		56.08		21.97		51.46		60.30		57.02
	EN	28.83		35.00		31.58		41.39		34.25		46.41		38.92		42.49
	F/M	0.859		1.882		0.886		1.380		0.665		1.142		1.569		1.355
	F/FM	0.462		0.653		0.470		0.580		0.400		0.533		0.611		0.575

41 SN 74236, HILL 1300 AMPHIBOLITE
42 SN 74251, LOWER QUARTZITE
43 SN 74277, SNYDER BRECCIA
44 SN 74277, SNYDER BRECCIA
45 SN 74295, SNYDER BRECCIA
46 SN 74295, SNYDER BRECCIA
47 SN 74305, LOWER QUARTZITE
48 SN 74305, LOWER QUARTZITE

TABLE 11 PYROXENE ANALYSES FOR THE SNYDER GROUP (CONTINUED)

	49	50	51	52	53	54	55	56
SIO2	48.96	46.96	49.93	49.98	50.92	52.72	48.04	49.05
A2O3	3.74	3.63	1.35	0.60	0.35	0.91	0.37	4.01
FEO	36.83	41.88	20.68	19.59	29.06	26.90	36.55	32.01
TIO2	0.0	0.0	0.28	0.0	0.0	0.0	0.0	0.0
MNO	1.31	0.09	0.56	0.55	0.60	0.36	7.11	0.92
CAO	0.23	0.22	19.28	20.31	1.01	0.38	1.65	0.23
MGO	12.05	10.05	7.03	8.31	17.06	20.54	6.70	16.72
NA2O	0.0	0.0	0.38	0.0	0.0	0.0	0.06	0.0
K2O	0.0	0.0	0.04	0.0	0.0	0.0	0.0	0.0
SUM	103.12	102.83	99.53	99.34	99.90	101.81	100.57	102.94
SI	1.900 *	1.870 *	1.971 *	1.973 *	1.977 *	1.966 *	1.984 *	1.864 *
AL	0.100 2.000	0.130 2.000	0.029 2.000	0.027 2.000	0.016 1.993	0.034 2.000	0.016 2.000	0.136 2.000
AL	0.070 *	0.041 *	0.034 *	0.001 *	0.0 *	0.006 *	0.002 *	0.043 *
CA	0.0 2.015	0.0 2.044	0.0 2.004	0.0 2.013	0.0 2.022	0.0 2.014	0.0 2.009	0.0 2.046
MG	0.697 *	0.597 *	0.414 *	0.489 *	0.987 *	1.142 *	0.418 *	0.947 *
FE	1.195 *	1.395 *	0.683 *	0.647 *	0.973 *	0.839 *	1.262 *	1.017 *
MN	0.043 *	0.003 *	0.019 *	0.018 *	0.020 *	0.011 *	0.249 *	0.030 *
TI	0.0 *	0.0 *	0.008 *	0.0 *	0.0 *	0.0 *	0.0 *	0.0 *
K	0.0 *	0.0 *	0.002 *	0.0 *	0.0 *	0.0 *	0.0 *	0.0 *
NA	0.0 2.015	0.0 2.044	0.029 2.004	0.0 2.013	0.0 2.022	0.0 2.014	0.005 2.009	0.0 2.046
O	6.000 *	6.000 *	6.000 *	6.000 *	6.000 *	6.000 *	6.000 *	6.000 *
WO	0.49	0.47	42.24	42.67	2.08	0.76	3.65	0.47
FS	61.46	69.61	35.36	32.13	48.11	41.80	63.05	50.78
EN	35.84	29.77	21.43	24.29	48.83	56.88	20.88	47.27
WO	2.21	0.15	0.97	0.91	0.98	0.57	12.42	1.48
WO	0.50	0.47	42.65	43.06	2.10	0.76	4.15	0.47
FS	62.85	59.71	35.71	32.42	48.59	42.03	72.00	51.54
EN	36.65	29.82	21.64	24.51	49.31	57.20	23.84	47.98
F/M	1.777	2.343	1.696	1.360	1.005	0.745	3.615	1.105
F/FM	0.640	0.701	0.629	0.576	0.501	0.427	0.783	0.525

49 SN 74306, LOWER QUARTZITE
50 SN 74309, LOWER QUARTZITE
51 SN 74316, HILL 900 ULTRAMAFIC
52 SN 74316, HILL 800 ULTRAMAFIC
53 SN 74317, HILL 800 ULTRAMAFIC
54 SN 74319, HILL 800 ULTRAMAFIC
55 SN 74321, IRON FORMATION
56 SN 74329, LOWER QUARTZITE

TABLE 11 PYROXENE ANALYSES FOR THE SNYDER GROUP (CONTINUED)

	57	58	59	60	61	62	63	64
SIO2	51.55	51.03	47.30	50.65	47.31	47.98	49.70	47.72
A2O3	1.18	0.93	0.48	0.51	0.43	0.52	4.19	0.42
FEO	13.62	13.40	37.14	32.72	37.27	34.60	33.36	37.58
TIO2	0.0	0.0	0.0	0.0	0.31	0.0	0.99	0.0
MNO	0.90	1.16	8.02	0.58	7.03	6.71	4.10	6.09
CAO	24.80	22.83	1.26	0.96	1.61	4.03	3.97	1.45
MGO	10.47	9.42	6.99	15.72	6.21	6.45	4.04	6.97
NA2O	0.0	0.16	0.0	0.0	0.06	0.0	0.16	0.0
K2O	0.0	0.0	0.0	0.0	0.0	0.0	0.38	0.0
SUM	102.52	98.93	101.19	101.14	100.23	100.29	101.79	100.23

SI	1.939	*	1.981	*	1.956	*	1.967	*	1.971	*	1.990	*	1.966	*	1.979	*
AL	0.052	1.991	0.019	2.000	0.023	1.980	0.023	1.990	0.021	1.992	0.020	2.000	0.034	2.000	0.021	1.999
AL	0.0	*	0.024	*	0.0	*	0.0	*	0.0	*	0.005	*	0.161	*	0.0	*
CA	0.0	2.044	0.0	2.004	0.0	2.052	0.0	2.031	0.0	2.019	0.0	2.008	0.0	1.923	0.0	2.012
MG	0.587	*	0.545	*	0.431	*	0.910	*	0.386	*	0.397	*	0.291	*	0.431	*
FE	0.428	*	0.435	*	1.285	*	1.063	*	1.299	*	1.194	*	1.104	*	1.303	*
MN	0.029	*	0.038	*	0.281	*	0.019	*	0.248	*	0.234	*	0.137	*	0.214	*
TI	0.0	*	0.0	*	0.0	*	0.0	*	0.010	*	0.0	*	0.029	*	0.0	*
K	0.0	*	0.0	*	0.0	*	0.0	*	0.0	*	0.0	*	0.019	*	0.0	*
NA	0.0	2.044	0.012	2.004	0.0	2.052	0.0	2.031	0.005	2.019	0.0	2.008	0.012	1.923	0.0	2.012
O	6.000	*	6.000	*	6.000	*	6.000	*	6.000	*	6.000	*	6.000	*	6.000	*
WO	48.91		48.26		2.72		1.97		3.59		8.89		9.89		3.20	
FS	20.97		22.11		62.59		52.31		64.79		59.60		64.90		64.76	
EN	28.72		27.70		21.00		44.79		19.24		19.80		17.13		21.41	
MN	1.40		1.94		13.69		0.94		12.38		11.71		8.08		10.63	
WO	49.60		49.21		3.15		1.98		4.09		10.07		10.76		3.58	
FS	21.26		22.54		72.52		52.80		73.95		67.50		70.60		72.46	
EN	29.13		28.25		24.33		45.21		21.96		22.43		18.63		23.95	
F/M	0.779		0.869		3.633		1.189		4.011		3.601		4.261		3.522	
F/F+M	0.438		0.465		0.784		0.543		0.800		0.783		0.810		0.779	

57 SN 74330, LOWER QUARTZITE
58 SN 74330, LOWER QUARTZITE
59 SN 74332, IRON FORMATION
60 SN 74339, SNYDER BRECCIA
61 SN 74383, IRON FORMATION
62 SN 74383, IRON FORMATION
63 SN 74383, IRON FORMATION
64 SN 74383, IRON FORMATION

TABLE 11 PYROXENE ANALYSES FOR THE SNYDER GROUP (CONTINUED)

	65	66	67	68	69	70	71	72
SIO2	50.79	50.11	48.62	48.88	49.13	52.47	51.51	51.45
A203	1.11	0.42	0.67	0.54	0.37	0.77	0.46	0.45
FEO	14.20	32.13	19.45	18.95	34.64	13.73	12.87	31.58
TIO2	0.0	0.0	0.33	0.0	0.0	0.0	0.59	0.0
MNO	0.29	0.57	3.62	5.35	6.29	0.30	0.32	0.55
CAO	20.98	1.19	19.84	20.35	1.54	21.16	21.57	1.03
MGO	11.97	16.43	3.94	6.15	10.98	12.44	11.34	16.21
NA2O	0.0	0.0	0.08	0.0	0.0	0.0	0.20	0.0
K2O	0.0	0.0	0.01	0.0	0.0	0.0	0.0	0.0
SUM	99.34	100.95	96.56	100.22	102.95	100.87	98.86	101.27

SI	1.954	*	1.950	*	2.005	*	1.954	*	1.949	*	1.977	*	1.982	*	1.981	*
AL	0.046	2.000	0.019	1.970	0.0	2.005	0.025	1.980	0.017	1.967	0.023	2.000	0.018	2.000	0.019	2.000
AL	0.004	*	0.0	*	0.033	*	0.0	*	0.0	*	0.011	*	0.002	*	0.001	*
CA	0.0	2.021	0.0	2.071	0.0	1.966	0.0	2.053	0.0	2.076	0.0	2.006	0.0	1.998	0.0	2.009
MG	0.686	*	0.953	*	0.242	*	0.367	*	0.649	*	0.699	*	0.650	*	0.930	*
FE	0.457	*	1.046	*	0.671	*	0.634	*	1.149	*	0.433	*	0.414	*	1.017	*
MN	0.009	*	0.022	*	0.126	*	0.181	*	0.211	*	0.010	*	0.010	*	0.018	*
TI	0.0	*	0.0	*	0.010	*	0.0	*	0.0	*	0.0	*	0.017	*	0.0	*
K	0.0	*	0.0	*	0.001	*	0.0	*	0.0	*	0.0	*	0.0	*	0.0	*
NA	0.0	2.021	0.0	2.071	0.006	1.966	0.0	2.053	0.0	2.076	0.0	2.006	0.015	1.998	0.0	2.009
O	6.000	*	6.000	*	6.000	*	6.000	*	6.000	*	6.000	*	6.000	*	6.000	*
WO	42.86		2.40		45.75		42.46		3.15		42.82		45.27		2.12	
FS	22.65		50.51		35.01		30.86		55.38		21.69		21.00		50.65	
EN	34.02		46.03		12.64		17.85		31.28		35.02		33.11		46.34	
MN	0.47		1.07		6.60		8.92		10.19		0.48		0.53		0.89	
WO	43.07		2.42		48.98		46.57		3.51		43.02		45.51		2.14	
FS	22.75		51.05		37.48		33.95		61.66		21.79		21.20		51.11	
EN	34.18		46.53		13.53		19.58		34.83		35.19		33.29		46.76	
F/M	0.679		1.120		3.292		2.223		2.096		0.633		0.653		1.112	
F/FM	0.405		0.528		0.767		0.690		0.677		0.388		0.395		0.527	

65 SN 74387, SNYDER BRECCIA
66 SN 74387, SNYDER BRECCIA
67 SN 74390, IRON FORMATION
68 SN 74390, IRON FORMATION
69 SN 74390, IRON FORMATION
70 SN 74393, SNYDER BRECCIA
71 SN 74393, SNYDER BRECCIA
72 SN 74393, SNYDER BRECCIA

TABLE 11 PYROXENE ANALYSES FOR THE SNYDER GROUP (CONTINUED)

	73	74	75	76	77	78	79	80
SIO2	52.43	51.18	47.87	47.80	49.27	56.92	52.90	52.52
A2O3	0.65	0.35	0.29	0.26	1.06	0.99	1.66	1.97
FEO	15.03	33.49	35.36	36.98	3.29	10.75	1.22	5.22
TIO2	0.0	0.0	0.0	0.0	0.0	0.0	0.0	0.0
MNO	0.38	0.93	7.28	6.93	0.04	0.19	0.31	0.15
CAO	21.46	1.37	1.52	1.24	22.91	0.66	24.81	22.30
MGO	11.62	14.84	7.18	7.79	19.16	32.23	16.48	15.78
NA2O	0.0	0.0	0.0	0.0	0.0	0.0	0.0	0.0
K2O	0.0	0.0	0.0	0.0	0.0	0.0	0.0	0.0
SUM	101.57	101.86	99.50	101.00	95.73	101.74	97.38	97.94

SI	1.976	*	1.981	*	1.990	*	1.967	*	1.891	*	1.969	*	1.969	*	1.964	*
AL	0.024	2.000	0.016	1.997	0.010	2.000	0.013	1.980	0.049	1.939	0.031	2.000	0.031	2.000	0.036	2.000
AL	0.005	*	0.0	*	0.004	*	0.0	*	0.0	*	0.009	*	0.042	*	0.051	*
CA	0.0	2.010	0.0	2.015	0.0	2.003	0.0	2.047	0.0	2.145	0.0	2.011	0.0	1.994	0.0	1.992
MG	0.653	*	0.856	*	0.445	*	0.478	*	1.096	*	1.561	*	0.914	*	0.880	*
FE	0.474	*	1.084	*	1.229	*	1.273	*	0.106	*	0.311	*	0.038	*	0.163	*
MN	0.012	*	0.030	*	0.256	*	0.242	*	0.001	*	0.006	*	0.010	*	0.005	*
TI	0.0	*	0.0	*	0.0	*	0.0	*	0.0	*	0.0	*	0.0	*	0.0	*
K	0.0	*	0.0	*	0.0	*	0.0	*	0.0	*	0.0	*	0.0	*	0.0	*
NA	0.0	2.010	0.0	2.015	0.0	2.003	0.0	2.047	0.0	2.145	0.0	2.011	0.0	1.994	0.0	1.992
O	6.000	*	6.000	*	6.000	*	6.000	*	6.000	*	6.000	*	6.000	*	6.000	*
WO		43.22		2.20		3.39		2.67		43.92		1.22		50.70		46.03
FS		23.63		53.80		61.52		62.18		4.92		15.53		1.95		8.41
EN		32.55		42.49		22.26		23.35		51.10		82.97		46.85		45.31
WO		0.60		1.51		12.83		11.80		0.06		0.28		0.50		0.24
WO		43.48		2.24		3.89		3.03		43.95		1.22		50.96		46.14
FS		23.77		54.62		70.57		70.50		4.93		15.57		1.96		8.43
EN		32.75		43.14		25.54		26.47		51.13		83.20		47.09		45.42
F/M		0.744		1.302		3.339		3.169		0.098		0.190		0.052		0.191
F/FM		0.427		0.566		0.770		0.760		0.089		0.160		0.050		0.160

73 SN 74394, BORDER BRECCIA
74 SN 74394, BORDER BRECCIA
75 SN 74399, IRON FORMATION
76 SN 74399, IRON FORMATION
77 NC 7401, CALCSILICATE
78 NC 7401, CALCSILICATE
79 NC 7405, CALCSILICATE
80 NC 7411, CALCSILICATE

TABLE 11 PYROXENE ANALYSES FOR THE SNYDER GROUP (CONTINUED)

	81	82	83	84	85	86	87	88
SIO2	55.65	54.36	57.50	51.73	54.80	53.62	51.68	53.17
A2O3	1.02	0.38	0.09	2.08	1.31	1.44	2.31	2.24
FEO	12.90	2.19	5.08	7.97	18.85	16.75	7.20	6.10
TIO2	0.0	0.0	0.0	0.0	0.0	0.0	0.0	0.0
MNO	0.26	0.04	0.0	0.16	0.29	0.50	0.24	0.17
CAO	0.82	22.77	0.26	21.58	1.05	0.85	21.86	22.12
MGO	29.53	19.73	38.85	16.81	26.20	27.78	15.81	16.10
NA2O	0.0	0.0	0.0	0.0	0.0	0.0	0.0	0.0
K2O	0.0	0.0	0.0	0.0	0.0	0.0	0.0	0.0
SUM	100.18	99.47	101.78	100.33	102.50	100.94	99.10	99.90

SI	1.976	*	1.976	*	1.943	*	1.914	*	1.956	*	1.932	*	1.939	*	1.953	*
AL	0.024	2.000	0.016	1.992	0.004	1.946	0.086	2.000	0.044	2.000	0.061	1.993	0.071	2.000	0.047	2.000
AL	0.018	*	0.0	*	0.0	*	0.004	*	0.011	*	0.0	*	0.031	*	0.050	*
CA	0.0	2.003	0.0	2.024	0.0	2.109	0.0	2.041	0.0	2.016	0.0	2.045	0.0	2.020	0.0	1.998
MG	1.563	*	1.069	*	1.956	*	0.932	*	1.394	*	1.492	*	0.880	*	0.882	*
FE	0.383	*	0.067	*	0.144	*	0.243	*	0.563	*	0.505	*	0.228	*	0.190	*
MN	0.008	*	0.001	*	0.0	*	0.005	*	0.009	*	0.015	*	0.008	*	0.005	*
TI	0.0	*	0.0	*	0.0	*	0.0	*	0.0	*	0.0	*	0.0	*	0.0	*
K	0.0	*	0.0	*	0.0	*	0.0	*	0.0	*	0.0	*	0.0	*	0.0	*
NA	0.0	2.003	0.0	2.024	0.0	2.109	0.0	2.041	0.0	2.016	0.0	2.045	0.0	2.020	0.0	1.998
O	6.000	*	6.000	*	6.000	*	6.000	*	6.000	*	6.000	*	6.000	*	6.000	*
WO		1.57		43.82		0.45		42.01		2.09		1.60		43.95		44.70
FS		19.30		3.29		6.80		11.96		28.06		24.68		11.44		9.76
EN		79.74		52.83		92.75		45.79		69.50		72.96		44.72		45.26
MN		0.39		0.05		0.0		0.25		0.44		0.75		0.38		0.27
WO		1.58		43.85		0.45		42.11		2.01		1.62		44.12		44.82
FS		19.37		3.29		6.80		11.99		28.18		24.87		11.48		9.79
EN		79.05		52.86		92.75		45.90		69.81		73.51		44.39		45.39
F/M		0.250		0.063		0.073		0.267		0.410		0.349		0.267		0.222
F/FM		0.200		0.060		0.068		0.210		0.291		0.258		0.211		0.181

81 NC 7411, CALCSILICATE
82 SN 7412, CALCSILICATE
83 NC 7412, CALCSILICATE
84 NC 7413, OLIVINE WEBSTERITE
85 NC 7413, OLIVINE WEBSTERITE
86 NC 7416, CALCSILICATE
87 NC 7416, CALCSILICATE
88 NC 7425, CALCSILICATE

TABLE 11 PYROXENE ANALYSES FOR THE SNYDER GROUP (CONTINUED)

	89	90	91	92	93	94
SIO2	55.23	53.04	55.12	51.86	52.10	46.61
A2O3	1.77	0.86	1.46	1.03	1.79	4.15
FEO	13.40	2.08	12.05	4.76	19.97	39.80
TIO2	0.0	0.0	0.0	0.0	0.0	0.0
MNO	0.29	0.06	0.25	0.13	0.18	1.11
CAO	1.64	24.74	0.70	22.86	0.06	0.19
MGO	28.50	17.25	30.49	16.12	25.77	11.58
NA2O	0.0	0.0	0.0	0.0	0.0	0.0
K2O	0.0	0.0	0.0	0.0	0.0	0.0
SUM	100.83	98.03	100.07	97.66	99.87	102.44

SI	1.958	*	1.969	*	1.953	*	1.948	*	1.921	*	1.847	*
AL	0.042	2.000	0.031	2.000	0.047	2.000	0.052	2.000	0.078	1.999	0.153	2.000
AL	0.032	*	0.007	*	0.014	*	0.033	*	0.0	*	0.041	*
CA	0.0	2.005	0.0	2.012	0.0	2.016	0.0	2.009	0.0	2.040	0.0	2.056
MG	1.506	*	0.955	*	1.611	*	0.902	*	1.417	*	0.684	*
FE	0.397	*	0.065	*	0.357	*	0.150	*	0.616	*	1.296	*
MN	0.009	*	0.002	*	0.008	*	0.004	*	0.006	*	0.037	*
TI	0.0	*	0.0	*	0.0	*	0.0	*	0.0	*	0.0	*
K	0.0	*	0.0	*	0.0	*	0.0	*	0.0	*	0.0	*
NA	0.0	2.005	0.0	2.012	0.0	2.016	0.0	2.009	0.0	2.040	0.0	2.056
O	6.000	*	6.000	*	6.000	*	6.000	*	6.000	*	6.000	*
WO	3.16		49.09		1.33		46.55		0.12		0.40	
FS	20.12		3.22		17.84		7.57		30.18		63.81	
EN	76.28		47.61		80.46		45.67		69.42		33.94	
MN	0.44		0.09		0.37		0.21		0.28		1.85	
WO	3.17		49.13		1.33		46.65		0.12		0.41	
FS	20.21		3.22		17.91		7.58		30.27		65.01	
EN	76.62		47.65		80.76		45.77		69.62		34.58	
F/M	0.270		0.070		0.226		0.170		0.439		1.934	
F/FM	0.212		0.065		0.185		0.145		0.305		0.659	

89 NC 7425, CALCSILICATE
90 SN 7443,, CALCSILICATE
91 NC 7447, ULTRAMAFICS
92 NC 7447, ULTRAMAFICS
93 NC 7448, KIGLAPAIT COAST MIGMATITES
94 NC 7449, LOWER QUARTZITE

TABLE 12 SPINEL ANALYSES FOR THE SNYDER GROUP

	1		2		3	
AL2O3	71.94		60.69		69.82	
FEO	6.23		33.63		6.79	
MGO	21.91		5.66		23.37	
SUM	99.98		99.98		99.98	
AL	2.054	2.054	1.988	1.988	2.007	2.007
MG	0.792	*	0.235	*	0.850	*
FE	0.126	0.919	0.782	1.016	0.139	0.988
O	4.000	*	4.000	*	4.000	*
F/M	0.160		3.334		0.163	
F/FM	0.138		0.769		0.140	

1 SN 7284, MARBLE

2 SN 72111, UPPER QUARTZITE

3 NC 74524, MARBLE

Table 13. Temperature estimates for two-pyroxene-bearing metabasites in the Kiglapait contact aureole using the Wood-Banno geothermometer (1973) calculated with a computer program of Hewins (1975) and rounded off to the nearest 10°C.

Specimen	Temperature, °C
SN 72126	810
SN 74394	840
SN 74387	850
SN 74295	850
SN 74393	860
SN 74277	870
NC 7447	950
NC 7416	960
NC 7411	980
NC 7425	1000

The vita has been removed from the scanned document

THE STRATIGRAPHY AND METAMORPHISM OF THE SNYDER GROUP, LABRADOR

by

J. Alexander Speer

(ABSTRACT)

The Snyder Group is a thin Aphebian sedimentary sequence unconformably overlying Archean rocks that has undergone deformation and a medium to high grade metamorphism as the result of the emplacement of the Elsonian Kiglapait intrusion. Five lithostratigraphic units totaling 239 m in thickness have been recognized: (1) a lower quartz arenite with local arkosic arenites, pelites, conglomerates, and a discontinuous basal conglomerate; (2) a manganiferous silicate iron formation; (3) a marble with associated calcsilicates and quartzites; (4) a sphalerite- and pyrrhotite-bearing quartz-rich, graphitic siltstone; and (5) an upper quartzite. Porphyritic andesite dikes and sills containing numerous subrounded basement xenoliths were emplaced before deformation and metamorphism. Later sills associated with the Elsonian Nain complex are also present. These intrusive rocks collectively have expanded the section to 355 m.

The lower and upper quartzites with their high maturity, festoon and planar crossbedding, ripple marks, graded bedding, and numerous conglomerates were probably deposited in a shallow marine environment under tidal influence. The fine grain size, intraformational conglomerates, small-scale crossbeds, and thin bedding of the intermediate

formations suggest that they were deposited in a quiet, shallow water environment disturbed only by occasional storms. The sedimentary features and thinness but great lateral extent of the lithologies suggest that the Snyder Group is an Aphebian platform assemblage.

Three zones of metamorphic grade are defined by the aluminum silicates: I, andalusite; II, andalusite-sillimanite; III, sillimanite. Anatexis has occurred in zone III. The total width of the aureole is 2-2.5 km. Progressive metamorphic assemblages are:

metapelites:	Ia - and-chl-biot-musc-qz ± Mn gar ± ksp
	Ib - and-cord-biot-qz ± musc ± Mn gar ± ksp
	II - and-sill-cord-biot-qz ± musc ± Mn gar + ksp
	III - sill-cord-biot-qz-ksp
	III - alm-cord-biot-qz-ksp
	III - opx-alm-cord-biot-qz-ksp
metabasites:	I - chl-epid-green hbl-biot-pc-qz ± cpx
	II - cumm-cpx-biot-pc-qz
	III - opx-cpx-brown hbl-pc-qz
marbles:	II - chl-trem-phlog-fo-cc ± spinel
	II - diop-phlog-fo-cc ± spinel
	III - diop-fo-cc ± spinel
	III - periclase-spinel-fo-diop-cc
iron formation:	II - Mn gar-grunerite-qz
	III - Mn gar-inverted Mn pigeonite-qz

Metamorphic conditions, based on aluminum silicate reactions, muscovite + quartz decomposition, experimental cordierite-garnet and pyroxene

pairs, yield a temperature range in the aureole of 350° to 1000°C and a pressure of 4 $\pm$ kb. The irregular nature of dehydration and decarbonization isograds points to a large variation in fluid pressures and compositions.

Snyder Group

Labrador, Canada

0 1 2
km

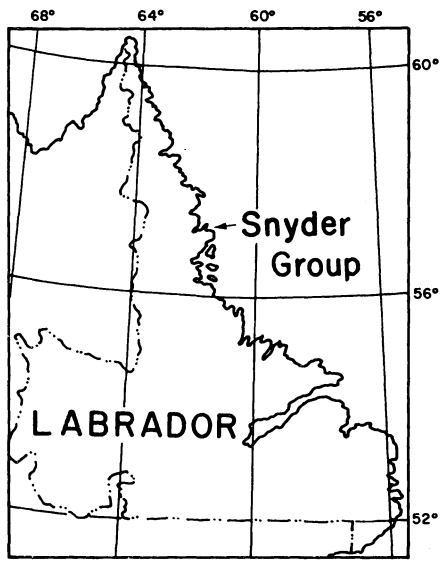

61°45'
61°40'
57°10'
57°05'

A
Snyder Bay
Snyder Island
Cold Comfort Bay
Middle Bay
OBZ
KI
Avakutakh River
Kiglapait Tessialua
N
B
B'
C
C'
D
D'
E
E'
50
45
23
40
28
32
22
25
0
28

Legend

Proterozoic

Post-metamorphic Intrusive Rocks

- Koghukulluk dike
- Border breccias
- KI — Kiglapait intrusion with marginal rocks (OBZ)

Pre-metamorphic Intrusive Rocks

- ultramafic rocks
- Hill 1100 gabbro
- Hill 1300 amphibolite

Snyder Group

- Upper Quartzite
- Sulfide Hornfels, Quartz Marble, and Iron Formation
- Lower Quartzite

Archean

- A — Basement complex

Symbols

- geologic contact, dashed where inferred
- 32 — bedding
- 23 — foliation
- fault

JAS 75

Snyder Bay

Locality Map

517
518
102
460
5 16
515
101
523
522
217
521
218
219
220
214
215
216
280
221
228
279
229
213
230
482
212
226
227
225
211
206
66
16
489
70
15
64
488
16
65
509
510
424
69
66
427
425
68
67
17
542
63
426
59
60
512
210
55
18
486
62
208
209
485
61
56
57
207
444
487
26
511
58
541
540
446
445
41
19
48
447
46
45
44
43
42
33
47
32
237
442
471a
448
459
26a
449
458
450
37
457
472
451
456
455
454
238
452
453
532
481
100
99
480
98
471
28
441
31
470
239
535
467
466
469
240
30
468
465
472
29
439
534
97
533
241
440
464
96
463
462
242
461
243
479
95
94
93
490
244
476
82
477
245
91
473
474
90
89
92
246
88
478
475
87,491
82
86
83
84
492
85
278
277
276
247
248
71
72
249
250
275
73
74
251
273
469
274
253
252
254
493
255
272
256
271
257
258
494
75
270
259
269
495
260
268
76
267
77
78
261
266
265
262
264
263
503n
506
81
79
404
80
405
406
503
407
504
505
408
409
1 km
JAS 75

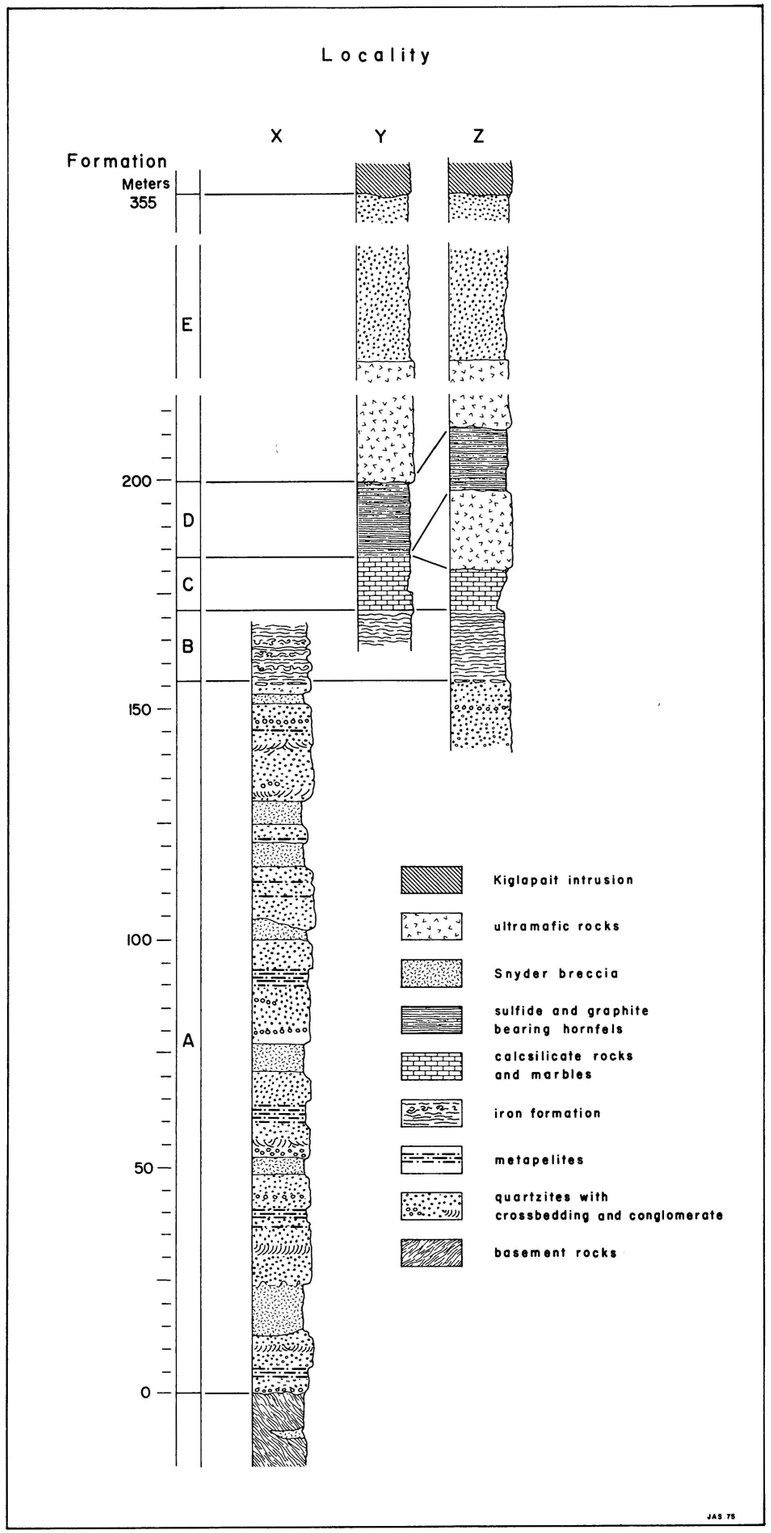
Locality
X
Y
Z
Formation
Meters
355
200
150
100
50
0
E
D
C
B
A
Kiglapait intrusion
ultramafic rocks
Snyder breccia
sulfide and graphite bearing hornfels
calcsilicate rocks and marbles
iron formation
metapelites
quartzites with crossbedding and conglomerate
basement rocks
JAS 75

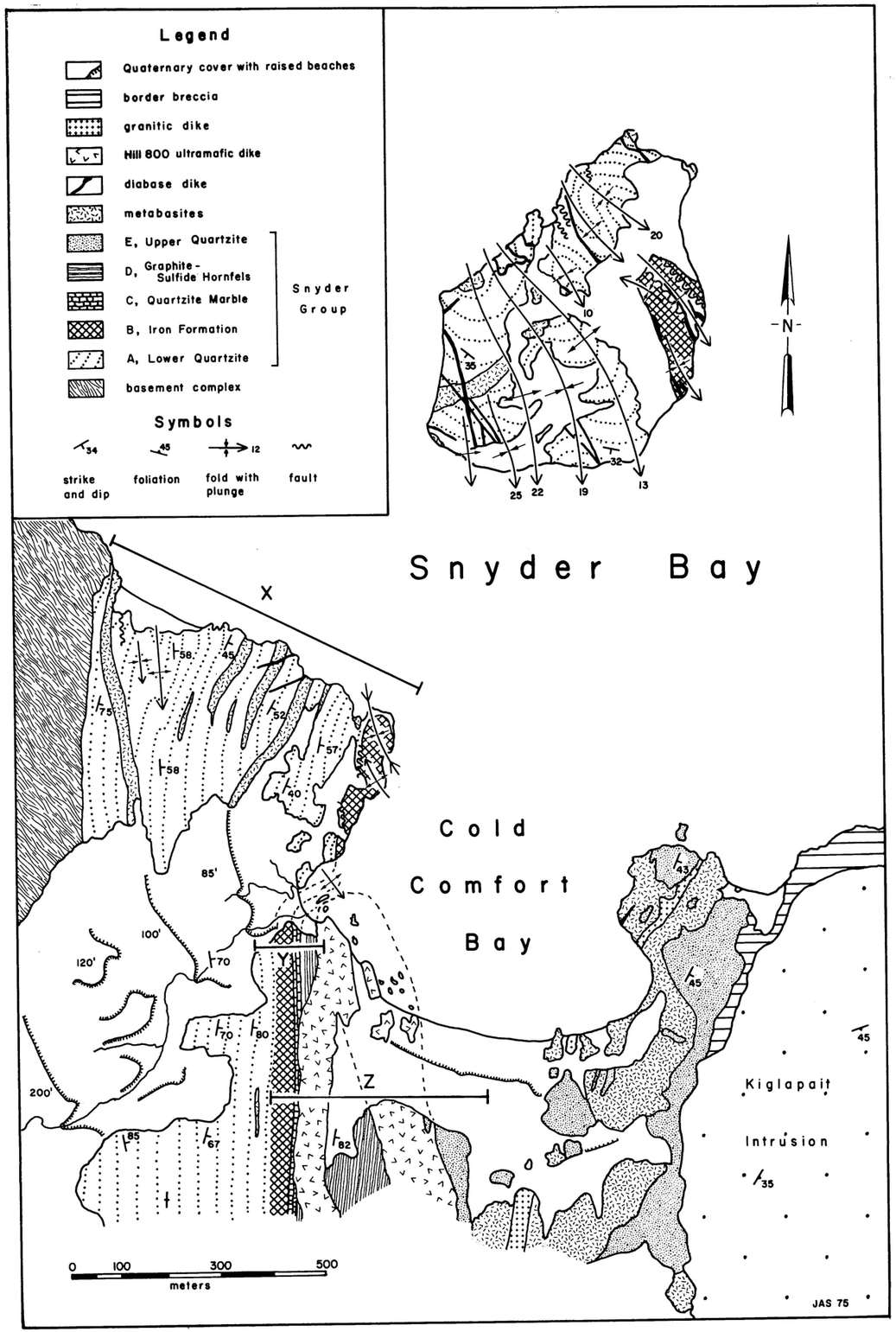
Legend
Quaternary cover with raised beaches
border breccia
granitic dike
Hill 800 ultramafic dike
diabase dike
metabasites
E, Upper Quartzite
D, Graphite - Sulfide Hornfels
C, Quartzite Marble
B, Iron Formation
A, Lower Quartzite
Snyder Group
basement complex
Symbols
strike and dip
foliation
fold with plunge
fault
N
Snyder Bay
X
Y
Z
Cold Comfort Bay
Kiglapait Intrusion
0 100 300 500
meters
JAS 75

Locality Map